IS-T-542

SURFACE SUPERCONDUCTIVITY IN NIOBIUM AND NIOBIUM-TANTALUM ALLOYS

Ph. D. Thesis Submitted to Iowa State University,
August, 1972

J. R. Hopkins

Ames Laboratory, USAEC
Iowa State University
Ames, Iowa 50010

Date of Manuscript: August, 1972

PREPARED FOR THE U. S. ATOMIC ENERGY COMMISSION
DIVISION OF RESEARCH UNDER CONTRACT NO. W-7405-eng-82.

DISCLAIMER

Available from: National Technical Information Service
Department A
Springfield, VA 22151

Price: Microfiche $0.95

Surface superconductivity in niobium and niobium-tantalum alloys

by

John Raymond Hopkins

A Dissertation Submitted to the
Graduate Faculty in Partial Fulfillment of
The Requirements for the Degree of
DOCTOR OF PHILOSOPHY

Department: Physics

Major: Solid State Physics

Approved:

D. K. Finnemore
In Charge of Major Work

R. G. Barnes
For the Major Department

For the Graduate College

Iowa State University
Ames, Iowa

1972

TABLE OF CONTENTS

Surface superconductivity in niobium and niobium-tantalum alloys

John Raymond Hopkins

Under the supervision of D. K. Finnemore
From the Department of Physics
Iowa State University of Science and Technology

The ratio of H_{c3}, the critical field for the surface sheath, to H_{c2}, the upper critical field for the bulk material, niobium, has been measured as a function of temperature and mean free path. At temperatures below $T/T_c = 0.85$, the pure Nb sample shows H_{c3}/H_{c2} values well above 1.695 as predicted by Hu and Korenman for the limit of long electronic mean-free-path. As the mean-free-path decreases, there is a regular depression of H_{c3}/H_{c2} toward 1.695. At temperatures above $T/T_c = 0.85$, the values of H_{c3}/H_{c2} appear to approach 1.0 rather than 1.695. According to Hu, this behavior might be explained by a depressed interaction strength near the surface. Calculations from the data show that the changes in the interaction strengths are between 0.1 and 2 percent. Changes in H_{c3} with frequency and anodization of the sample were determined for pure Nb.

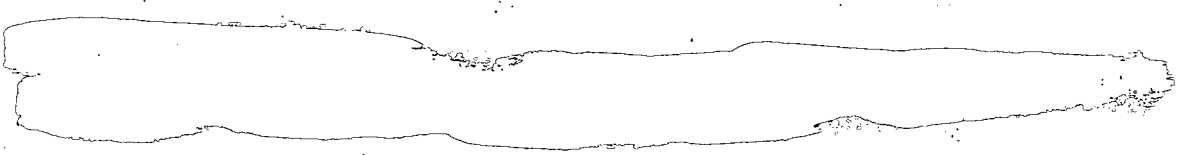

INTRODUCTION

In 1908, Kamerlingh Onnes first succeeded in liquifying helium and proceeded to study a number of phenomena in the temperature interval 1 K to 14 K (1). In 1911, while investigating the electrical resistivity, ρ, to check the Drude-Lorentz theory, which predicted that ρ should vary as $T^{1/2}$ (2), Onnes discovered that the electrical resistance of a mercury wire fell abruptly to zero at about 4 K. This phenomenon was naturally called superconductivity. Since Onnes' historic experiment, many materials have been found which have zero resistance below some critical temperature T_c. The vanishing of electrical resistance, however, is not the only basic property superconductors have. Onnes also discovered that a magnetic field in excess of a certain value H_c forced the superconductors into the normal state. Indeed one can map out a H-T phase boundary which separates the superconducting and normal regions in a manner completely analagous to melting curves for ordinary liquid-solid transitions. There was, however, an element of doubt concerning the applicability of thermodynamics to the transition because the zero resistance phenomenon alone does not predict a reversible transition (3). It was not until 1933 that Meissner and Ochsenfeld (4) discovered the so-called Meissner effect which demonstrated the reversible nature of the transition. This phenomenon is the complete expulsion of flux from the interior of a solid cylinder situated in a uniform applied field $H_a < H_c$ as the cylinder is cooled toward T = 0 K and it cannot be explained solely on the basis of zero resistivity (3,5) but represents a whole new aspect of superconductivity. The Meissner effect

showed that a superconductor behaves as a perfect diamagnet and proved that the superconducting state is a stable thermodynamic state. Hence, the Meissner effect led to a thermodynamic description of pure superconductors by Gorter and Casimir (5) and made possible a phenomenological theory, proposed by F. and H. London (6), of the electromagnetic properties of superconductors. The London theory predicts that the magnetic induction B does not disappear at the surface of a superconductor, but falls off exponentially with distance into the metal with a characteristic length λ_L, the London penetration depth. Within this theory λ_L is related to other fundamental parameters by

$$\lambda_L = [m\ c^2/4\pi\ n_s\ e^2]^{1/2} \qquad (1)$$

where m and e are the mass and charge of an electron and n_s is the number of electrons per unit volume in the superconducting state. The magnetic induction penetration was first confirmed experimentally by Shoenberg (7) in 1940.

The basic equations of the London theory are "local" in the sense that they relate the current density and the electromagnetic potential at the same point in space. Pippard (8) in 1953, however, concluded from surface impedance measurements that the current density at a given point in space depends upon the electromagnetic potentials within a region ξ, the Pippard coherence length, about the point in question. Hence, there are at least two fundamental lengths in a superconductor. The penetration depth determines the static magnetic field variations and the coherence distance determines the degree of locality in the electromagnetic response and the

degree of locality of the ground state wave function.

The existence of the coherence length ξ and the penetration depth λ leads to a natural classification of superconductors into two types in which the primary distinction between the two classes is based on magnetic behavior and the relative magnitudes of ξ and λ. If $\xi \gg \lambda$, the magnetic transition is that of an "ideal" superconductor (shown by the dashed line in Figure 1) and this class of superconductors is called type-I. If $\xi \ll \lambda$, on the other hand, the samples exhibit a broad magnetic transition as shown by the solid line in Figure 1 and this class of superconductors is called type-II. Reversible or ideal type-II behavior is difficult to obtain experimentally, because reversibility is especially sensitive to defects and unwanted impurities.

Type-I superconductors are described by the nonlocal Pippard theory and are usually characterized by $\lambda \ll \xi$. In this class are the physically soft (hence, the term "soft superconductors") low melting point materials such as lead, tin, indium, mercury and most of the other pure metal superconductors, and low concentration alloys with long electronic mean free paths. From the microscopic point of view, the properties of type-I superconductors are well explained by the theory of Bardeen, Cooper, and Schrieffer (9), the BCS theory, in its original form. The BCS theory was able to account for the specific heat, the acoustic attenuation, the infrared absorption, the tunneling effects, etc.

Type-II superconductors in the short mean free path limit are described by the London theory in small magnetic fields and are usually characterized by $\lambda \gg \xi$. In this category are most chemical compounds such as Nb_3Sn,

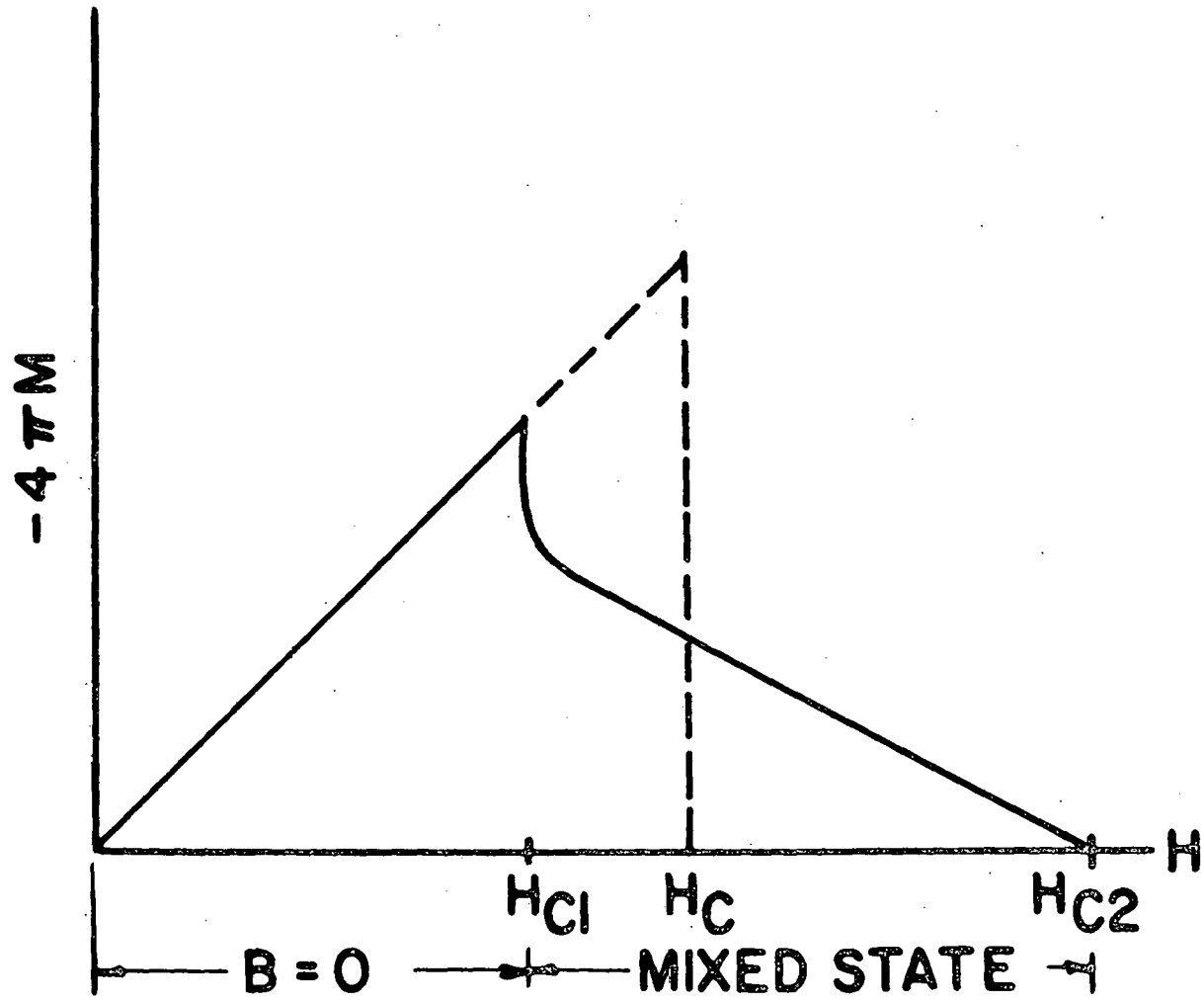

Figure 1. Magnetization curve for an ideal type-II superconductor.

V_3Ga, Nb(Ta) and the pure metals niobium and vanadium[1] which are physically hard (hence, the term "hard superconductors"), and have high melting points. This class of superconductors was first investigated by Shubnikov et al. (11) in 1937 and has become increasingly important in the past few years. Because the present work is concerned with the magnetic properties of niobium and niobium-tantalum alloys, the next few paragraphs will be devoted to a short review of some of the essential magnetic properties of type-II superconductors.

A macroscopic cylinder of an ideal type-II superconductor placed in a field H parallel to its axis exhibits the bulk properties shown in Figures 1 and 2. There are four regions of interest depending on the value of the external field. For $H < H_{c1}$, there is complete exclusion of the magnetic induction from the sample (the Meissner effect). For $H_{c1} < H < H_{c2}$ flux penetrates the sample, but the magnetic induction remains smaller than the applied field. In this region a new state appears in which a triangular lattice of quantized flux-enclosing supercurrent vortices (or filaments) is formed (12,13). This state is commonly called the "mixed state," the "vortex state," or the "Shubnikov state." For $H_{c2} < H < H_{c3}$ the bulk of the specimen becomes normal, but a superconducting sheath of thickness ξ exists on the surface of the metal. The existence of this state was first postulated in 1963 by Saint-James and de Gennes (14) and verified experimentally by Hempstead and Kim (15). For $H > H_{c3}$ the entire sample is in the normal state.

[1] The impurity levels in the available La and Tc have been too high to conclusively show that La and Tc are also intrinsic type-II superconductors (10).

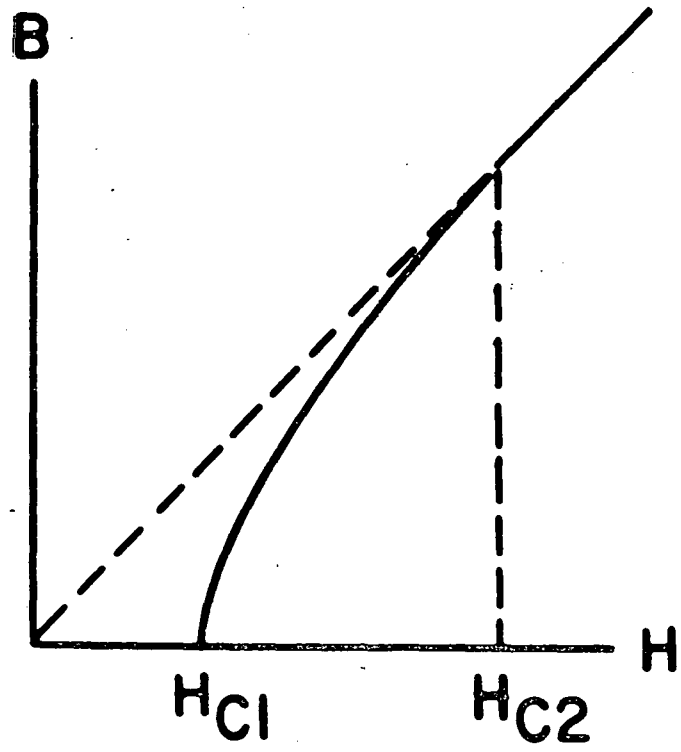

Figure 2. Schematic variation of the induction B versus the applied field H in a type-II superconductor.

In 1950 Ginzburg and Landau (16) proposed a phenomenological extension of the London theory to take account of the spatial variation of the density of superconducting electrons n_s which occurs in the mixed state. Their theory was based on three fundamental assumptions: 1) There exists an order parameter ψ which is a measure of the density of ground state electrons n_s and which goes to zero at the transition. 2) The free energy may be expanded in powers of $|\psi|^2$, at least near T_c, where $|\psi|^2$ is proportional to n_s. 3) The coefficients of the expansion are regular functions of T. Ginzburg and Landau assumed that ψ was an "effective wave function" describing the condensed electrons (electrons in the superconducting state). In order to allow for spatial variations of n_s they assumed that there would be an extra term in the free energy proportional to $|\text{grad}\psi|^2$, or, in the presence of a magnetic field, $|\frac{\hbar}{i}\text{grad}\psi + \frac{e}{c}\underset{\sim}{A}\psi|^2$ corresponding to the usual kinetic energy term in the Hamiltonian. This theory has had considerable success in describing boundary situations in the intermediate state, where n_s varies smoothly from the value n_{s0} appropriate to the field-free situation right down to zero in the normal regions. Its principal defects lie in the fact that its electrodynamics are entirely local and do not allow for the nonlocal effects which Pippard showed must be present as materials become more pure (as the coherence distance becomes longer).

Within the Ginzburg-Landau treatment one starts by assuming that the free energy difference f per unit volume between superconducting and normal states can be expanded in terms of the order parameter; that is,

$$f = f_n + \alpha(T)|\psi|^2 + \frac{\beta(T)}{2}|\psi|^4 + \cdots . \qquad (2)$$

For a normal metal $\psi = 0$ and for an ideal superconductor $\psi = \psi_o$. At thermodynamic equilibrium f is a minimum so

$$\frac{\partial f}{\partial |\psi|^2} = 0 \tag{3}$$

which yields

$$|\psi_o|^2 = -\frac{\alpha(T)}{\beta(T)} . \tag{4}$$

The corresponding free energy is then

$$f(T) = -\frac{\alpha^2}{2\beta} \tag{5}$$

which must be (from thermodynamics) $-\frac{H_c^2}{8\pi}$. Hence,

$$\frac{\alpha^2}{2\beta} = \frac{H_c^2}{8\pi} . \tag{6}$$

If ψ is allowed to have a slow spatial variation, then the first significant terms will be of the form

$$\left[\frac{\partial \psi}{\partial x}\right]^2 ; \left[\frac{\partial \psi}{\partial x}\right]\left[\frac{\partial \psi}{\partial y}\right] ; \text{ etc.} \tag{7}$$

For cubic symmetry one obtains

$$f(T) = \alpha|\psi|^2 + \frac{\beta}{2}|\psi|^4 + \gamma|\underset{\sim}{\nabla}\psi|^2. \tag{8}$$

This equation would not have been of great help if Ginzburg and Landau had not proposed an extension of Equation 8 to describe the superconductor in the presence of a magnetic field. In order to insure gauge invariance they wrote

$$f = \alpha|\psi|^2 + \frac{\beta}{2}|\psi|^4 + \frac{1}{2m^*}\left|\left(-i\hbar\nabla - \frac{e^*\underset{\sim}{A}}{c}\right)\psi\right|^2 + \frac{h^2}{8\pi} \tag{9}$$

where

$$\underset{\sim}{h} = \text{curl } \underset{\sim}{A}\,, \tag{10}$$

$\frac{h^2}{8\pi}$ is the magnetic energy per unit volume in free space, and ψ is a macroscopic version of a "wave function" for a "particle" of charge e^* and mass m^*. This is the form for the free energy proposed by Ginzburg and Landau well before the development of the microscopic theory.

In order to obtain the equilibrium equations we must minimize the free energy $F = \int f d\underset{\sim}{r}$ with respect to both the order parameter ψ and the magnetic field $\underset{\sim}{h}$, therefore $\underset{\sim}{A}$. If we vary ψ by $\delta\psi$ and $\underset{\sim}{A}$ by $\delta\underset{\sim}{A}$, we obtain the variation in the free energy which, after an integration by parts, becomes

$$\delta F = \int d^3r\{\delta\psi^+[\alpha\psi + \beta|\psi|^2\psi + \frac{1}{2m^*}\left(-i\hbar\nabla - \frac{2e^*\underset{\sim}{A}}{c}\right)\psi]$$

$$+ \text{c.c.}\} + \int d^3r\{\delta\underset{\sim}{A}\cdot[\frac{1}{8\pi}\,\text{curl } \underset{\sim}{h} - \frac{e^*}{m^*c}\psi^*\left(-i\hbar\nabla - \frac{e^*}{c}\underset{\sim}{A}\right)\psi$$

$$+ \text{c.c.}]\} \tag{11}$$

where c.c. means the complex conjugate quantity. For F to be a minimum $\delta F = 0$ so Equation 11 yields the two equations called the Ginzburg-Landau equations:

$$\frac{1}{2m^*}\left[-i\hbar\nabla - \frac{e^*}{c}\underset{\sim}{A}\right]\psi + \alpha\psi + \beta\psi|\psi|^2 = 0 \tag{12}$$

$$\frac{\text{curl } \underset{\sim}{h}}{4\pi} = \underset{\sim}{j} = \frac{e^* \hbar}{2im^* c}(\psi^* \underset{\sim}{\nabla}\psi - \psi \underset{\sim}{\nabla}\psi^*) - \frac{e^{*2}}{m^* c^2} \psi^* \psi \underset{\sim}{A} . \tag{13}$$

The first equation, Equation 12, allows the order parameter ψ to be calculated in the presence of the field, while Equation 13 gives the distribution of the currents and thus the diamagnetic response of the superconductor.

In their original paper Ginzburg and Landau found no reason to consider e^* as different from the electronic charge. Consequently, they set $e^* = e$ and $m^* = m$. Actually, Gor'kov (17,18) was able to derive Equations 12 and 14 from the BCS microscopic theory (9). In the convention used by Gor'kov where m and e are the electronic mass and charge the Ginzburg-Landau equations take the form

$$\frac{1}{2m}\left[-i\hbar \underset{\sim}{\nabla} - \frac{2e\underset{\sim}{A}}{c}\right]\psi + \alpha\psi + \beta|\psi|^2| = 0 \tag{14}$$

$$\frac{\text{curl } \underset{\sim}{h}}{4\pi} = \frac{\underset{\sim}{j}}{c} = \frac{e\hbar}{imc}(\psi^* \underset{\sim}{\nabla}\psi - \psi \underset{\sim}{\nabla}\psi^*) - \frac{4e^2}{mc^2}|\psi|^2 \underset{\sim}{A} . \tag{15}$$

Gor'kov determined α and β from the microscopic theory. For pure materials, those with long electronic mean free path,

$$\alpha = \frac{1.83\hbar^2}{2m} \frac{1}{\xi_o^2} \left[\frac{T - T_c}{T_c}\right] \tag{16}$$

$$\beta = \frac{0.35}{N(0)} \left[\frac{\hbar^2}{2m} \frac{1}{\xi_o^2}\right]^2 \left[\frac{1}{k_B T_c}\right]^2 \tag{17}$$

where $N(0)$ is the density of states at the Fermi level.

In order to define the problem completely, it is necessary to add a boundary condition to Equations 12 and 13. For example, the current flowing through the surface of the sample can be taken to be zero. Equation 15 shows that this condition is equivalent to

$$\left[-i\hbar\underset{\sim}{\nabla} - \frac{2e\underset{\sim}{A}}{c}\right]_n \psi = i\gamma\psi \tag{18}$$

where n indicates the component normal to the surface and γ is a regular function of T. Ginzburg and Landau set $\gamma = 0$. De Gennes (19) has shown that Equation 18 holds with $\gamma = 0$ for a superconductor-insulator interface and Equation 18 with $\gamma \neq 0$ holds for a superconductor-normal metal interface. We shall see later that Equation 18 has important implications in the onset of surface superconductivity.

Now let us investigate the origin of the two characteristic lengths $\xi(T)$ and $\lambda(T)$ in the Ginzburg-Landau scheme. In Equation 14 we replace ψ by $g\psi_o$ where ψ_o is the order parameter for no currents or magnetic fields and g is some function describing the spatial variation of ψ. We then obtain

$$\frac{-\hbar^2}{2m}\nabla^2 g + \alpha g - \alpha g^3 = 0 \ . \tag{19}$$

It is then natural to introduce the length $\xi(T)$, such that

$$\xi^2(T) = \frac{-\hbar^2}{2m\alpha} \ , \tag{20}$$

which yields, from Equation 19,

$$-\xi^2(T)\nabla^2 g - g + g^3 = 0 \ . \tag{21}$$

Thus $\xi(T)$ is the unit of length for the variation of g or ψ. This characteristic length is called the temperature-dependent coherence length.

The second characteristic length is the penetration depth $\lambda(T)$, which determines the range of variation of the magnetic field. Consider the equation for the current, Equation 15. To first order in $\underset{\sim}{h}$, $|\psi|^2$ may be replaced by ψ_o^2, the value of $|\psi|^2$ in the absence of a field; hence,

$$\underset{\sim}{j} = \frac{e\hbar}{im}(\psi^* \underset{\sim}{\nabla}\psi - \psi \underset{\sim}{\nabla}\psi^*) - \frac{4e^2}{mc} \psi_o^2 \underset{\sim}{A} . \tag{22}$$

Taking the curl of $\underset{\sim}{j}$, we obtain

$$\text{curl } \underset{\sim}{j} = - \frac{4e^2}{mc} \psi_o^2 \underset{\sim}{h} , \tag{23}$$

which is equivalent to the London equation with the penetration depth

$$\lambda(T) = \left[\frac{mc^2}{16\pi e^2 \psi_o^2}\right]^{1/2} . \tag{24}$$

For a pure metal we obtain from the microscopic picture (9)

$$\xi(T) = 0.74\, \xi_o \left[\frac{T_c}{T_c - T}\right]^{1/2} \tag{25}$$

$$\lambda(T) = \frac{1}{\sqrt{2}} \lambda_L(0) \left[\frac{T_c}{T_c - T}\right]^{1/2} . \tag{26}$$

The Ginzburg-Landau hypothesis has led us to a local relation between the current and vector potential, Equation 15. From the microscopic analysis in the case where $|\psi|$ is constant and $\underset{\sim}{h}$ is small, the exact relation is nonlocal; that is, the current density $\underset{\sim}{j}(\underset{\sim}{r})$ depends on $\underset{\sim}{A}(\underset{\sim}{r}')$

for $|\underset{\sim}{r} - \underset{\sim}{r}'| \lesssim \xi_o$ in a pure metal. In order for the local approximation to be valid, it is necessary that $\underset{\sim}{A}$ or the current have a slow variation on the scale of ξ_o, thus

$$\xi(T) \gg \xi_o \tag{27}$$

and

$$\lambda(T) \gg \xi_o \, . \tag{28}$$

Equation 27 is equivalent to

$$\frac{T_c - T}{T_c} \ll 1 \, , \tag{29}$$

and Equation 28 is equivalent to

$$\frac{T_c - T}{T_c} \ll \left[\frac{\lambda_L(0)}{\xi_o}\right]^2 \, . \tag{30}$$

For a pure metal, these conditions will be satisfied if T is sufficiently close to T_c.

Although $\lambda(T)$ and $\xi(T)$ both diverge as T approaches T_c, their ratio

$$\kappa(T) = \frac{\lambda(T)}{\xi(T)} \tag{31}$$

remains finite for all T and it is this ratio which largely determines the behavior of the material. This dimensionless parameter, called the Ginzburg-Landau parameter, may be related to the critical field $H_c(T)$ using Equations 4, 6, 20, and 24. It is easily found that

$$\kappa(T) = 2\sqrt{2}\ \frac{e}{\hbar c}\ \lambda^2(T)\ H_c(T)\ . \tag{32}$$

Using the values of Gor'kov for $\lambda(T)$ and $\xi(T)$ from the microscopic theory,

$$\kappa(T) = 0.96\ \frac{\lambda_L(0)}{\xi_0}\ . \tag{33}$$

We now look at situations where $|\psi|^2$ varies spatially, that is, nucleation in the bulk. Consider a superconducting metal in a high magnetic field. For sufficiently high fields, superconductivity is destroyed and the magnetic induction is uniform in the sample. At $H = H_{c2}$ the superconducting regions begin to nucleate spontaneously. In the regions where the nucleations occur, superconductivity is just beginning to appear and therefore $|\psi|$ is small. The Ginzburg-Landau equation then can be linearized to give

$$\frac{1}{2m}\left[-i\hbar\underset{\sim}{\nabla} - \frac{2e\underset{\sim}{A}}{c}\right]^2\psi = -\alpha\psi\ . \tag{34}$$

Since the supercurrents are proportional to $(\psi\underset{\sim}{\nabla}\psi^* - \psi^*\underset{\sim}{\nabla}\psi)$ the corrections to the field are negligible in the linear approximation and

$$\text{curl}\ \underset{\sim}{A} = \underset{\sim}{H}\ . \tag{35}$$

Therefore, Equation 34 is identical to the Schrödinger equation for a particle of charge 2e and mass m in a uniform magnetic field. In an infinite medium the particle has a constant velocity v_z along the field and moves in a circle in the x-y plane with frequency $\omega_c = \frac{2eH}{mc}$. It has bound state energies

$$\frac{1}{2}mv_z^2 + (n + \frac{1}{2})\hbar\omega_c \cdot \tag{36}$$

The lowest energy level occurs for $v_z = 0 = n$, the corresponding eigenvalue $-\alpha$ is

$$-\alpha = \frac{e\hbar H}{mc}, \tag{37}$$

and the nucleation field thus obtained is H_{c2}. With a little algebra one obtains

$$H_{c2} = \sqrt{2}\,\kappa\, H_c \cdot \tag{38}$$

From this equation we can distinguish between type-I and type-II superconductors. For $\kappa > \sqrt{1/2}$, superconductivity appears at a field $H_{c2} > H_c$. These superconductors are type-II. For $\kappa < \sqrt{1/2}$, the specimen may remain normal, in decreasing fields, down to a field $H_{c2} < H_c$ (a metastable state) at which a complete Meissner effect takes place. These superconductors are type-I. The condition $\kappa = \sqrt{1/2}$ was first used as the dividing line between type-I and type-II superconductors in the theory of Abrikosov (20).

We now look at the nucleation of superconductivity at the sample surface. The surface is assumed to be a plane (radius of curvature $\gg \xi(T)$) and the boundary separates the superconductor from either an insulator or a vacuum such that $j_n = 0$. Consider two cases:

(1) H perpendicular to the surface of the sample,

(2) and H parallel to the surface of the sample.

In the first case, the function ψ corresponding to the lowest energy level

of Equation 34 is also an eigenfunction of $\pi_z = -i\hbar \frac{\partial}{\partial z} - \frac{2eA_z}{c}$ with eigenvalue zero. Therefore, $j_n = 0$ is automatically satisfied and the surface does not modify the nucleation field. In the second case, $\underset{\sim}{H}$ is directed along the z-axis and the surface is in the y-z plane. We select the gauge $\underset{\sim}{A} = \hat{e}_y Hx$ and look for solutions of the form $\psi = e^{iky} g(x)$. Equation 34 becomes

$$-\frac{\hbar^2}{2m} \frac{d^2g}{dx^2} + \frac{1}{2m}\left(\hbar k - \frac{2eHx}{c}\right)^2 g = -\alpha g \tag{39}$$

and the boundary condition is

$$\left.\frac{dg}{dx}\right|_{x=0} = 0 \, . \tag{40}$$

Equation 39 is analogous to the Schrödinger equation of a harmonic oscillator of frequency $\omega = \frac{2eH}{mc}$ with the equilibrium position being the point $x_o = \frac{\hbar kc}{2eH}$. If $x_o \approx \xi(T)$, the lowest eigenvalue is lower than that given in Equation 37. Hence, nucleation is favored by the presence of a surface (14,21,22). A detailed calculation shows that the optimum value of x_o is $0.590\ \xi(T)$ and that the corresponding eigenvalue is

$$-\alpha = 0.590 \frac{e\hbar H}{mc} \tag{41}$$

where the field thus obtained is H_{c3}. The nucleation field H_{c3} may be written as

$$H_{c3} = \frac{\sqrt{2}\,\kappa\, H_c}{0.590} = \frac{H_{c2}}{0.590} \, , \tag{42}$$

or, as more commonly written,

$$H_{c3} = 1.695\ H_{c2}. \tag{43}$$

The order parameter varies over a distance of the order of $\sqrt{0.590}\ \xi(T) = 0.77\ \xi(T)$ from the surface (Figure 3). Hence, superconductivity is not entirely destroyed for fields greater than H_{c2}. The bulk of the material is normal, but a superconducting sheath exists within about one coherence length from the surface.

Many experiments have been performed to detect the surface sheath and to determine the ratio H_{c3}/H_{c2}. Serin (23) has compiled a summary of experimental results on the limiting field for surface superconductivity for experiments conducted prior to 1964.

Saint-James and de Gennes (14) were the first to predict the possible existence of the surface sheath but their value of H_{c3}/H_{c2} (1.695) was independent of many properties of the samples used. Ebneth and Tewordt (24) and Lüders (25) extended this work to just below the Ginzburg-Landau region and found

$$\frac{H_{c3}}{H_{c2}} = 1.695 + 1.041\ \epsilon \tag{44}$$

where

$$\epsilon = 1 - T/T_c \tag{45}$$

for a sample with a specular surface. Hu and Korenman (26,27) then showed that the expansion parameter near T_c is actually $\epsilon^{1/2}$ and found

$$\frac{H_{c3}}{H_{c2}} = 1.695 + 1.041\ \epsilon - 0.978\ \epsilon^{3/2}. \tag{46}$$

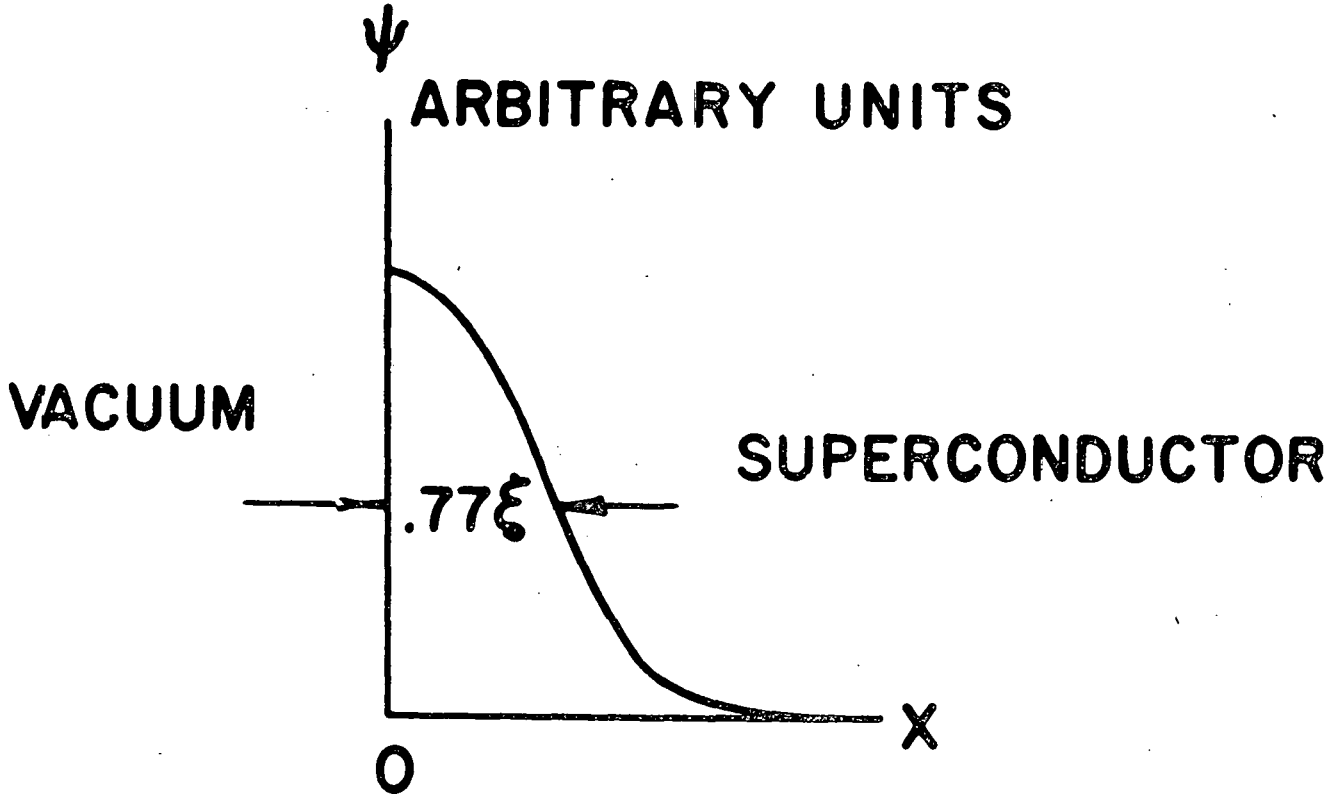

Figure 3. Variation of the order parameter close to the surface.

They were also able to expand the theory to lower temperatures and found H_{c3}/H_{c2} approached a value nearly equal to 1.925 with vanishing slope as T approached absolute zero. The following interpolation formula was proposed to cover the entire temperature range below T_c:

$$\frac{H_{c3}(T)}{H_{c2}(T)} = 1.695[1 + 0.614\,\epsilon - 0.577\,\epsilon^{3/2} - 0.007\,\epsilon^{2} + 0.106\,\epsilon^{5/2}]. \quad (47)$$

Ostenson and Finnemore (28) have studied surface superconductivity of pure Nb. For temperatures below 8.5 K, the pure Nb showed H_{c3} values well above 1.695 as predicted by Hu and Korenman for the limit of long electronic mean-free-path. For temperatures above 8.5 K, the values of H_{c3}/H_{c2} broke away from the theory and approached 1.0 rather than 1.695. In 1969 Hu (29) proposed a mean-field-theoretical model to explain deviations of the experimental data from Equation 47. In this model the pure ($\ell \gg \xi_o$) superconducting system is considered to occupy the semi-infinite region $x > 0$. The superconductor is characterized by a space-dependent interaction $V(x)$ which is the energy associated with the electron-phonon-electron interaction (9). It is this electron-phonon-electron interaction which causes the electrons to fall into the lower, superconducting, energy state (9,30). Hu considered the particular case where $V(x) = V_o + V_1\,\Theta\,(D - x)$ where $\Theta(y)$ is the unit step function. V_o is the interaction strength in the bulk of the sample and was assumed to be less than zero so that the main bulk of the sample could become superconducting. $|V_1|$ was assumed to be much less than $|V_o|$ so that only first order effects needed to be considered. In Hu's model the width L of the surface sheath was larger or smaller than D, the width over which the interaction constant

is changed, depending on the sample temperature since L is proportional to $\xi_o \epsilon^{-1/2}$. The temperature range $0 < T < T_c$ was divided into three regions: region A, in which the surface sheath lies entirely within the surface layer, that is, $D > \xi_o(1 - T/T_c)^{-1/2}$; region B, in which the surface sheath extends beyond the weak-interaction layer into the bulk, that is, $D < \xi_o(1-T/T_c)^{-1/2}$; and region C, in which the layer may be treated as a perturbation, i.e. $D \ll \xi_o(1 - T/T_c)^{-1/2}$. A different temperature dependence for H_{c3}/H_{c2} is found in each region, but the overall curve gives a continuous decrease of H_{c3}/H_{c2} below the value expected for a homogenous system, and dropping to unity at $T = T_c$.

The physics of the problem, according to Hu (29), is as follows: Near T_c, H_{c3} and H_{c2} plotted with respect to T give two nearly straight lines which normally intersect the abscissa at the same point, the transition temperature T_c. By slightly suppressing the interaction strength near the surface of the sample, one can produce a small parallel displacement of the H_{c3} line to the left of the H_{c2} line. This effect, where we have now assumed T_c of the surface is less than T_c of the bulk, then would explain why H_{c3}/H_{c2} falls so far below the value of 1.695 as T approaches T_c for niobium (28). However, such a picture is not correct very close to T_c. When the width of the pair wave function becomes much larger than D, it becomes energetically favorable for the pair wave function to respond as if the interaction constant depression at the surface was a perturbation. This ought to result in a reduction of the effect of the pair wave function responding to a mean perturbed interaction which occurs at lower temperatures. Thus the critical field ratio does not drop to negative infinity

as is predicted from the simple consideration which assumes that the nucleation processes are determined by the mean interaction strength over the region where the nucleations take place. Hence, using simple perturbation theory very close to T_c, Hu concludes that H_{c3}/H_{c2} drops to unity at $T = T_c$. With the help of this theory, it is possible to determine, from experimental curves of H_{c3}/H_{c2} versus T/T_c, the change in interaction strength near the surface. Ostenson et al. (31) interpreted $H_{c3}(T)/H_{c2}(T)$ data for pure Nb using Hu's theory and concluded that to explain the Nb data, a 2% shift in interaction constant near the surface is needed over a distance of less than two coherence lengths. Hence rather small changes in the interaction constant near the surface can cause very large changes in the surface superconductivity.

The present work is a series of experiments in which surface superconductivity was used as a tool to investigate the superconducting interaction strength in the region of a vacuum-metal interface. Physically, there probably is a large change in interaction strength within a few angstroms of the surface but the extent of the Cooper pair wave function, ξ, causes physical measurements of superconducting parameters such as H_{c2} and H_{c3} to respond as if there were a small change in interaction strength over a distance comparable to ξ. The idea of the experiment was to enhance the effect of the changing interaction strength within a few angstroms of the surface by decreasing ξ. For fairly pure materials ξ decreases as

$$\frac{1}{\xi} = \frac{1}{\xi_o} + \frac{1}{\ell} \tag{48}$$

so pure Nb was alloyed with Ta to decrease ℓ and thus ξ. Tantalum was

selected since Nb and Ta have the same valences and form solid solution alloys over the entire range of composition with very small changes in atomic spacings. Hence, the purpose of this work was to systematically study the dependence of H_{c3}/H_{c2} and $|V_1/V|$ on the normal state mean free path.

SAMPLE PREPARATION

Dissolved gases strongly affect the superconducting properties of Nb so an important aspect of this research is the removal of these gases. De Sorbo (32,33,34) has shown, for example, that dissolved oxygen depresses the transition temperature of Nb by 0.93 K per at. percent. In addition to the shift in T_c, the presence of oxygen also broadens the superconducting transitions and it increases the resistivity in the normal state by 5.2 Ω - cm per at. percent. Fortunately, these dissolved gases can be removed (35) from niobium by outgassing in a vacuum of 10^{-9} Torr at a temperature of 2000°C for 8 to 12 h. At this temperature and pressure the absorption rates of N and O are equal to the evaporation rates of the volatile oxides yielding N and O concentrations of a few ppm (36).

After the sample has been cooled to room temperature surface oxidation would occur if the sample were exposed to air. This causes some special problems because large amounts of surface oxides could cause a reduced gap parameter with more normal excitations within a few monolayers of the sample surface. The properties of the surface will also influence measurements of H_{c3} and changes of the gap parameter at the surface can produce anomalous ratios of H_{c3}/H_{c2}. A study of surface oxidation by Hurlen et al. (37) indicates that an exposure of Nb to a pure O_2 atmosphere at 150°C for 30 min will give less than a monolayer of oxide on the surface. Water vapor in the air ordinarily enhances oxidation so ordinary air would probably oxidize the surface more rapidly. A more recent study by Dickey et al. (38) indicates a clean niobium surface, indeed, is

obtained upon heating the sample to 1800°C in agreement with measurements on oxygen removal from bulk niobium (39,40). To avoid all these problems, the samples reported here were never exposed to the air but were sealed under helium gas so the surface contamination should be no greater than that of the bulk.

The niobium metal used in this experiment was obtained from the DuPont Corporation in shot form identified as Lot No. CDH-43-4. The tantalum metal was obtained from the Kawecki Corporation in 0.020 in. wire form (40). Sixty grams of the niobium metal were first arc melted and then electron beam melted into a button about 1.5 in. in diameter (41). This button was cut into pieces and arc melted again with the appropriate amounts of Ta to form the alloyed buttons to be used for the experiment. The buttons were then swaged and drawn into 0.030 in. wires. Segments of each of the alloyed wires were then electropolished in a 2 % sulfuric-methano. mixture at -70°C for five minutes and cut into lengths of 1.5 in. ("samples"). Near one end of the sample, a 0.25 in. segment was rolled and cut into a ribbon approximately 0.006 in. thick and 0.030 in. wide. The purpose of this thin section was to provide a region where the sample could be melted easily so that the sample would drop into a capillary. If the section to be melted is not very thin, the force of surface tension is larger than the weight of the sample and the wire melts into a ball rather than dropping into the capillary.

Outgassing of the samples was accomplished with the aid of the electron bombardment assembly shown in Figure 4. The flattened end, the ribbon, of the sample was spot welded onto electrode 2 (the electrodes

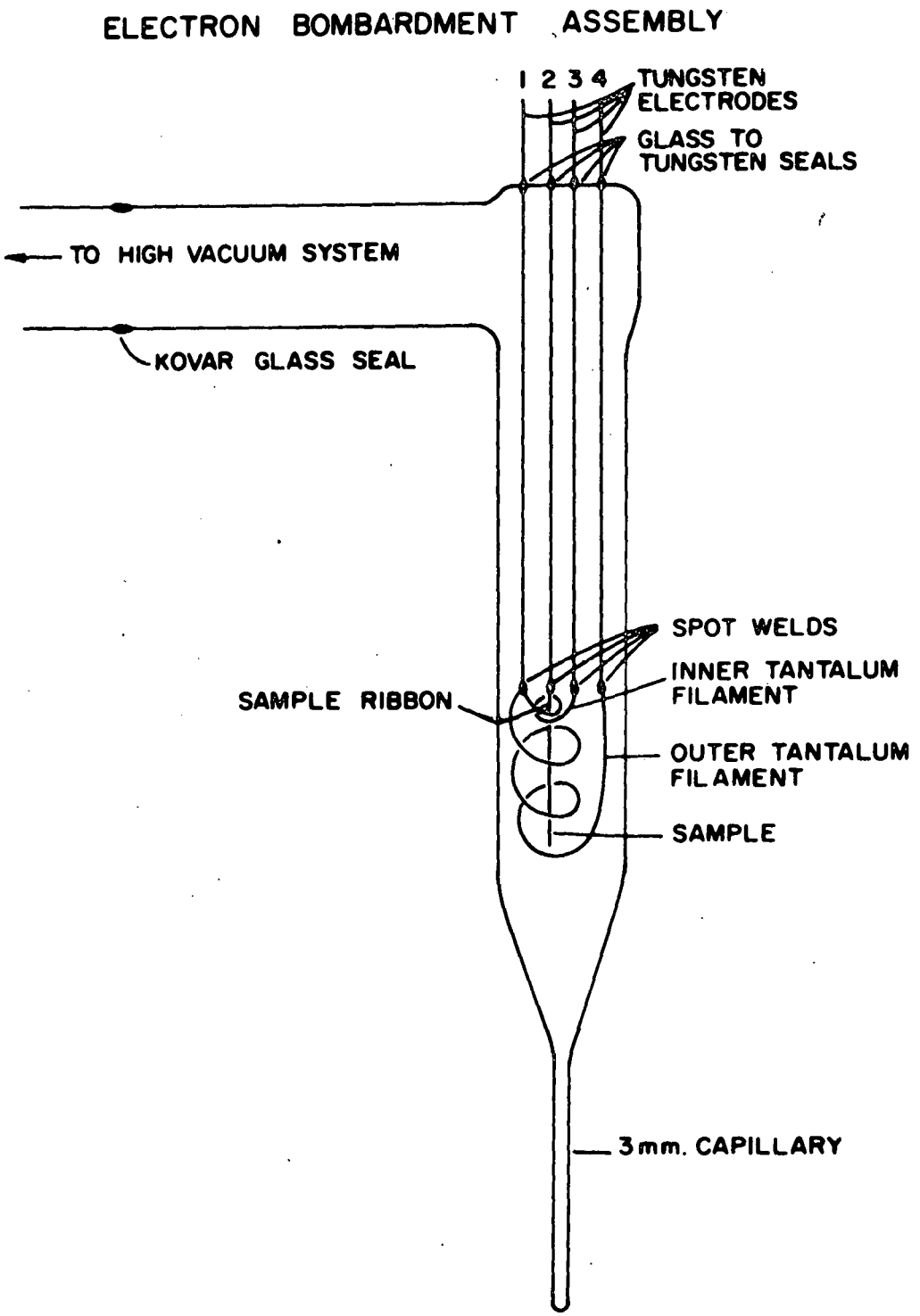

Figure 4. Electron bombardment assembly.

were 0.06 in. tungsten rods) and a filament (the inner filament) of 0.010 in. tantalum wire was closely wound around the ribbon about 0.1 in. below the end of electrode 2. Another filament (the outer filament) was spiraled around the sample with a pitch of two turns per inch. The sample and filament assembly then was sealed onto a high vacuum system (39) and evacuated to a pressure of 15 microns with a Welch 1405 mechanical vacuum pump. A portion of the pumping line was immersed in liquid nitrogen to trap vapors from the pump before they entered the high vacuum system. An Ultek absorption pump, using Linde 5A pellets, then was used to obtain a pressure of less than one micron. The final pumping unit, an Ultek ion pump, evacuated the system to a pressure of 5×10^{-8} Torr. At that time, the entire system was baked for 12 hours with heating tapes wound close to the ion pump and an oven placed over the top of the system. The oven was maintained at a temperature of 250°C during the baking period. When the system had cooled to room temperature, the pressure was noted as 9×10^{-10} Torr.

Before outgassing the sample, the tantalum filaments were outgassed by passing a 5.5 A current through them for 3 or 5 h. The sample was heated by electron bombardment; that is, the sample was maintained at 1000 V while a current of 4.5 A was passed through the filaments causing energetic electrons to leave the filaments and "bombard" the sample. The power (emission current times sample voltage) fed to the sample was set at 60 W and held there for nearly 24 h. This kept the temperature of the sample close to 2000°C. At the end of the 24 h electron bombardment period, when the pressure was noted as 2×10^{-9} Torr, the power was

quickly lowered to zero and the sample was allowed to cool for 2 or 3 h. A rough calculation, assuming radiation as the only cooling mechanism for energy dissipation, indicates that the sample will cool to less than 500°C (radiation in the visible region ceases for temperatures less than 500°C) in about 2 sec. It was observed that the sample did cease emitting visible radiation about 2 sec after the electron bombardment was stopped.

After the cooling period the sample was cut from its support by melting it in the ribbon region. Only the inner filament around the ribbon was connected to the filament power supply using electrodes 1 and 3. The voltage of the sample was steadily increased at the rate of 300 V/sec, while a current of 5 A was passed through the inner filament, until the sample ribbon melted and the sample dropped off and fell into the capillary. The ion pump then was turned off and helium gas, 99.999 % pure, was allowed to leak into the system until the pressure was slightly less than one atmosphere. The sample was sealed inside the glass capillary by heating the capillary immediately above the sample.

The above procedures should have cleaned the sample and protected it from environmental contamination until the susceptibility measurements were made.

Table I shows the results of analyses made on the samples used for the susceptibility measurements as well as similarly prepared samples. The tantalum and tungsten contents were determined to better than 10 % by neutron activation. Nitrogen, oxygen, and hydrogen impurity levels were determined to within 10 % by mass fusion. The amounts of iron, tungsten,

Table I. Results of the chemical analyses for several samples.

Sample	Ta	O	N	H	Fe	W
H-7, Nb	43	13	<1	<1	5	
H-9, Nb[a]	110					48
H-26, Nb[a]						
H-15, Nb-1000 ppm Ta	730	<1	<1	<1	10	44
H-19, Nb-1000 ppm Ta[a]	1150					
H-13, Nb-5000 ppm Ta[a]	5590					
H-21, Nb-5000 ppm Ta	6320	5	<1	<1	5	48
H-10, Nb-10000 ppm Ta	10300	60	<1	<1	1	48
H-11, Nb-10000 ppm Ta[a]	10600					
H-23, Nb-20000 ppm Ta[a]	22100					
H-27, Nb-20000 ppm Ta	25100	6	<1	<1	10	43

[a]Samples used for ac susceptibility measurements.

and other trace elements were determined to within a factor of two or three by mass spectroscopy. The latter measurements indicated that all the trace elements constituted an impurity level of less than 50 at. ppm in each sample. A reasonable determination (within a factor of 2 or 3) of the carbon content could not be carried out because none of the samples were massive enough for the chemical processes used for a determination of the carbon content. However, previous work by Finnemore et al. (35,39) indicates that the carbon content is less than 100 at. ppm.

The purpose of alloying the niobium with various amounts of tantalum was to create samples with varying electronic mean free paths without drastically different superconducting magnetic properties. Decreasing the mean free path of the electrons decreases the resistivity ratio ($R_{300\ K}/R_{4.2\ K}$) and the transition temperature. The effect of decreasing the mean free path in the samples studied here as well as the results of Ikushima and Mizusaki (42) is shown in Figure 5. The large difference between the two sets of data could be due to anomalously high resistivity ratios for the data of Ikushima and Mizusaki if the residual resistivities at 4.2 K were measured without completely destroying the superconducting surface sheath with the application of a magnetic field greater than H_{c3} (4.2 K).

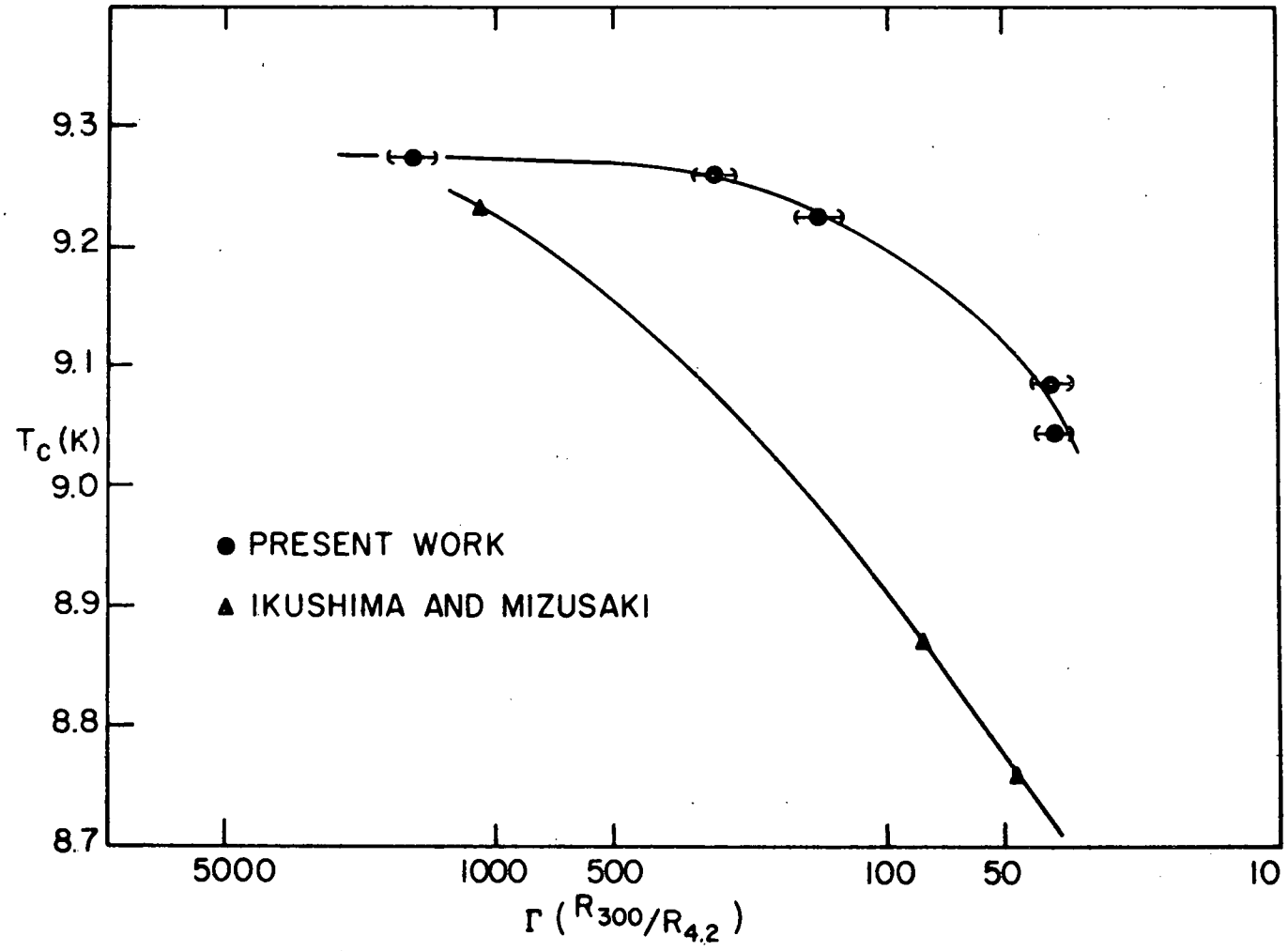

Figure 5. Plot of the superconducting transition temperature, T_c, versus the resistivity ratio, Γ.

EXPERIMENTAL SYSTEMS

The dewar system (Figure 6) used in this experiment is a standard design for work in a magnetic field at temperatures between one and twenty Kelvin. Both the liquid nitrogen and liquid helium dewars were metal dewars built in the Ames Laboratory shops. Magnetic fields were generated by a 7500 Oe liquid nitrogen cooled compensated solenoid which surrounded the tail of the helium dewar. The solenoid was constructed from No. 14, square, pure-annealed, copper wire insulated to withstand temperatures of 150°C. The layers were separated by 0.13 in. wide teflon strips 0.02 in. thick to allow liquid nitrogen to penetrate and cool the windings. Additional windings were put on each end so that the field would be uniform near the center of the magnet. The magnetic field homogeneity was checked using a Bell 240 Incremental Gaussmeter which utilizes the Hall Effect to measure fields. The magnetic field was found to be homogeneous to within 0.3 % over a volume of six cubic inches near the center of the solenoid. The magnitude of the field (as a function of current in the solenoid) was determined by nuclear magnetic resonance. The proton resonance in glycerine was measured and yielded a value of $152.45 \pm .02$ Oe/A for six fields between 1700 Oe and 3300 Oe. The solenoid was powered by a Spectromagnetic current regulated power supply which can deliver 50 A in a 1 Ω load with a stability of one part in 10^5 over an 8 h period. The dc resistance of the solenoid was 0.94 Ω at 78 K. The current in the solenoid was determined by the voltage drop across a Rubicon 0.01 Ω, 100 A shunt using a Keithley Instruments 662 guarded differential voltmeter.

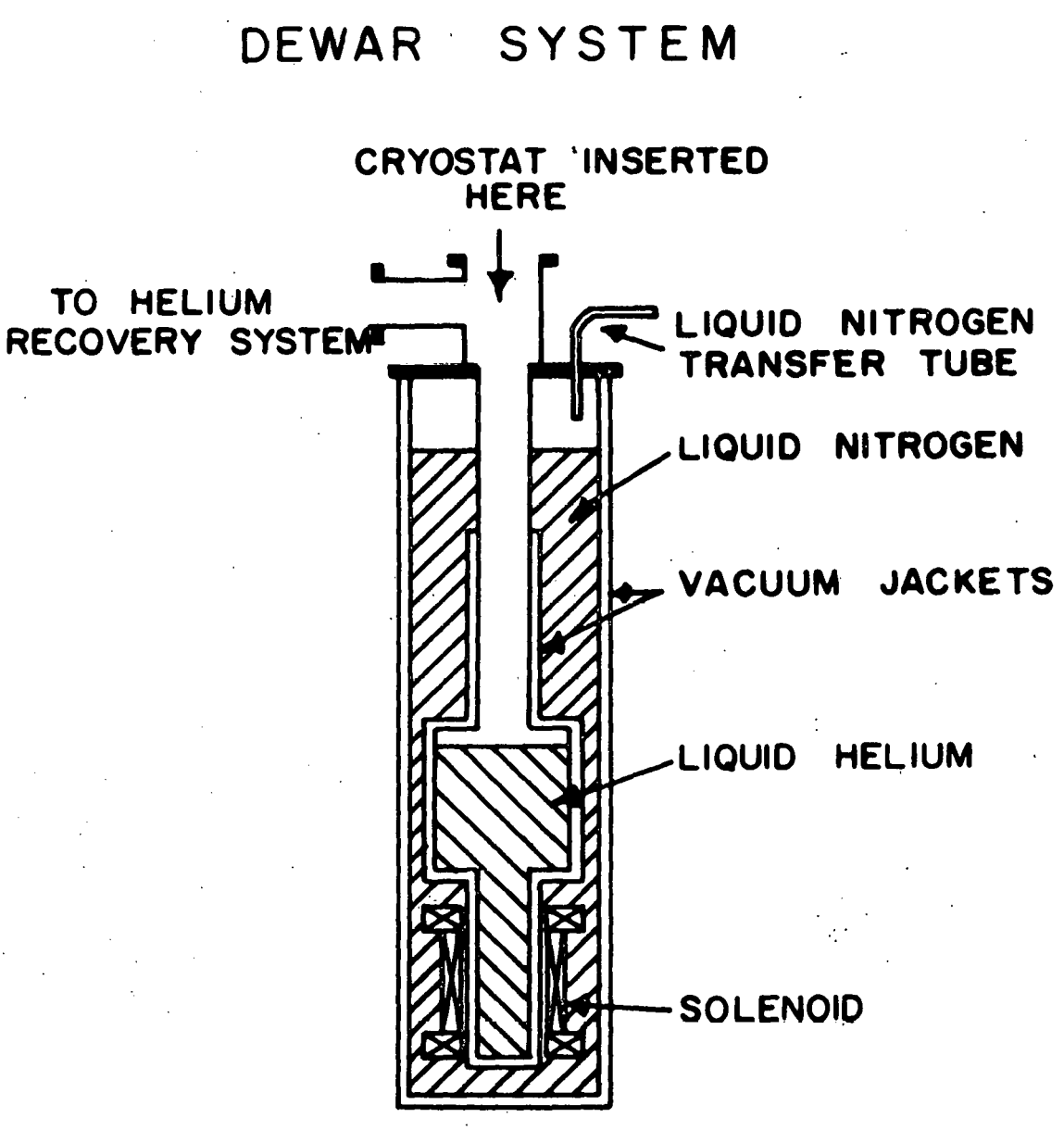

Figure 6. The dewar system.

The earth's magnetic field was compensated to approximately 0.01 Oe by a pair of Helmholtz coils. The currents required in each coil to cancel the horizontal and vertical components of the earth's field in the sample region of the cryostat were determined using the Bell 240 Incremental Gaussmeter.

The cryostat consists of two brass cans (Figure 7) surrounding a sample space containing the essential components (Figure 8) of the experiment.

Temperature control for temperatures between 5 K and 10 K in the sample region was accomplished in the following manner. The heat leak chamber vacuum space was evacuated to a pressure of less than 10^{-3} Torr and the sample chamber was sealed at a pressure of less than 0.2 Torr with the temperature of the sample space equal to 4.2 K. This pressure was chosen for the sample space since higher pressures led to convection currents and substantially lower pressures gave rise to poor thermal equilibrium. In order to control the temperature of the sample space at some constant temperature, an equilibrium was established between the amount of heat generated by an astatically wound 1000 Ω manganin heater, mounted at the top of the sample space (Figure 7), and the amount of heat leaking from the sample space to the liquid helium bath. The temperature control element, a 492.2 Ω Allen Bradley carbon resistor, was mounted close to the sample coil. The resistance of this element was monitored using a Wheatstone bridge (Figure 9) with the off balance of the bridge being fed into a Fluke 845 AB High Impedance Voltmeter-Null Detector which amplified the signal so that it could be

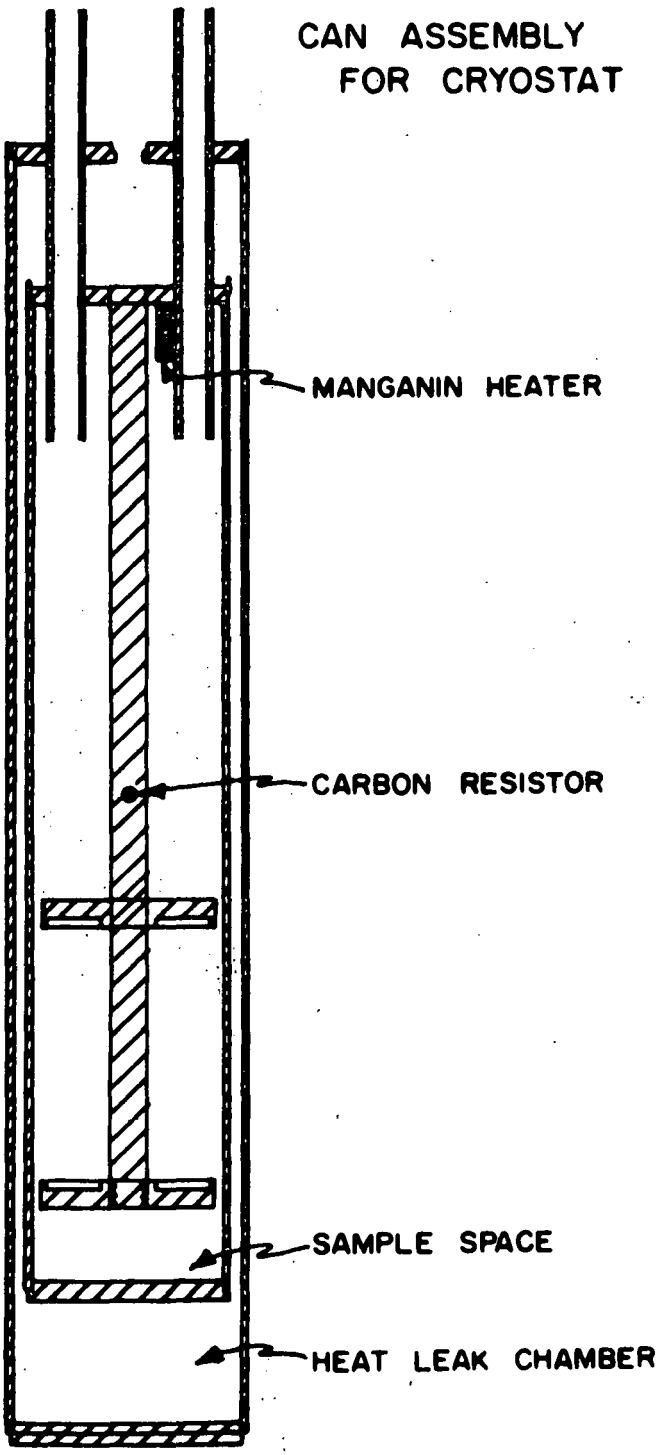

Figure 7. Double can assembly for cryostat.

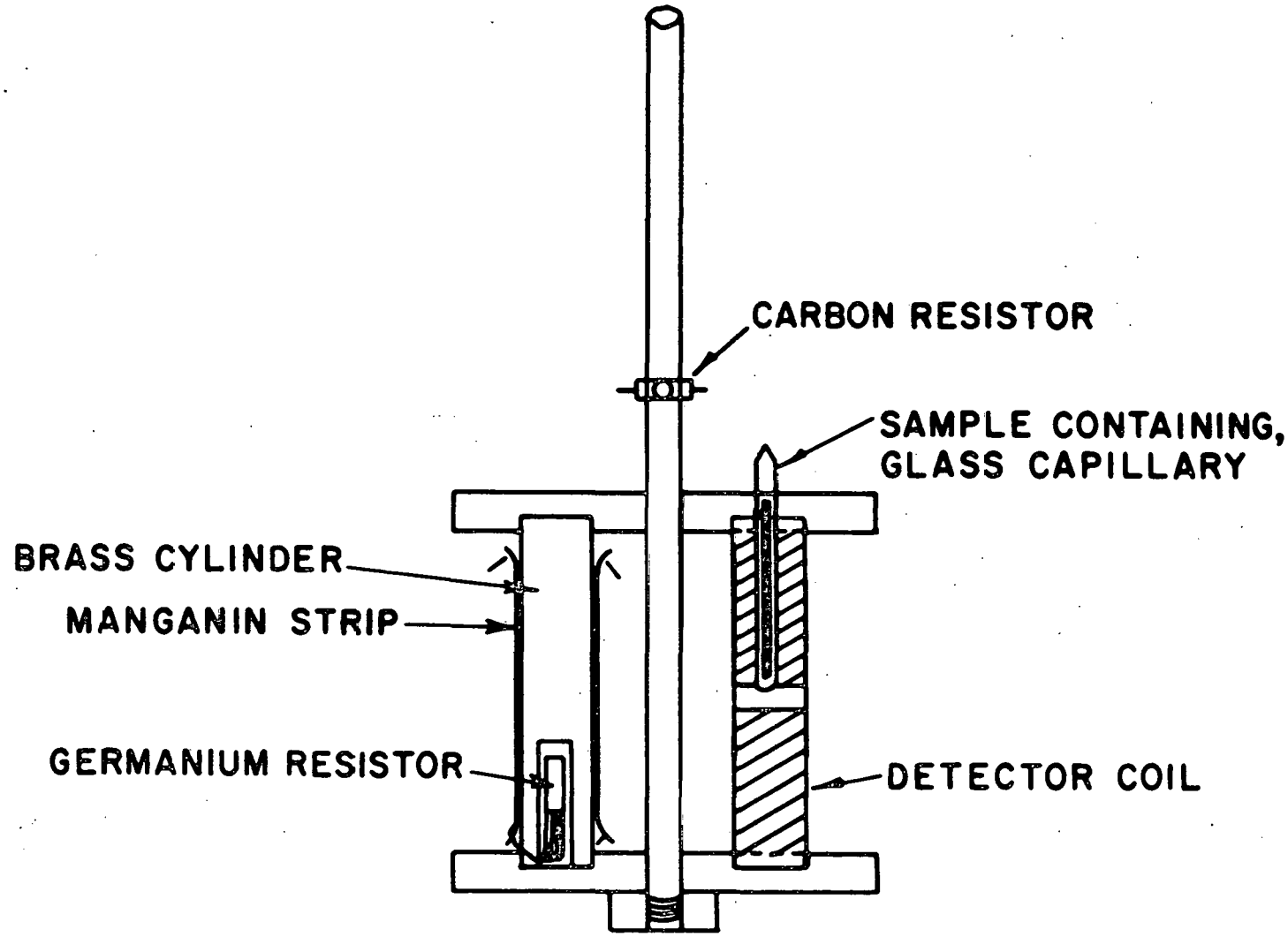

Figure 8. Essential components of the cryostat.

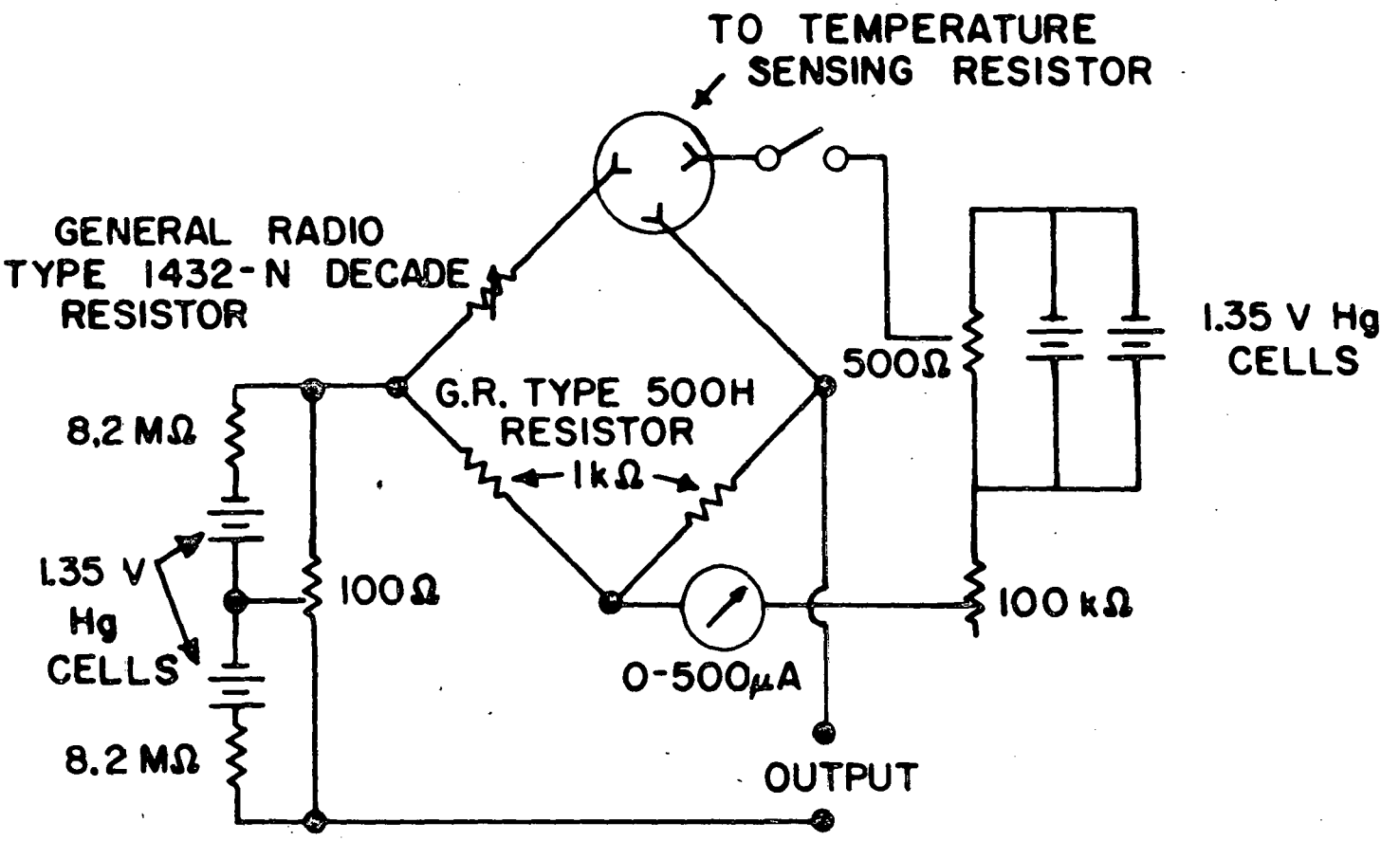

Figure 9. Wheatstone bridge used for temperature control.

displayed on a Bristol 2 mV chart recorder. On the recorder was mounted a cam and microswitch combination which was used to switch the current incrementally (Figure 10) in the manganin heater at a given set point on the recorder. With the above temperature controlling equipment it was possible to maintain temperature stability to 0.001 K for periods of two hours or longer (the time required for a run), and temperature stability of 0.0001 K was possible for periods of 5 min.

Data were taken to determine the effect of the carbon resistor's magnetoresistance on its ability to control the temperature. The carbon resistor in this experiment closely obeys the magnetoresistance relation

$$\frac{\Delta R}{R} = -H \left(\frac{1.2}{T} + 0.14\right) \times 10^{-6}$$

found by Carlson (43) where H is in Oersteds and T is in Kelvin. For $T \approx 8$ K, the effect of the magnetic field on the carbon resistor can be shown to produce a temperature shift of one millikelvin. However, for $T \approx 5$ K, the fields used to drive the sample normal cause a shift in temperature of nearly 0.020 K. This effect at 5 K gives only a 3 % shift in H_{c3}/H_{c2}. The region of interest for the samples measured was between 6 K and 9.3 K so most of the data was unaffected by the magnetoresistance of the temperature controlling carbon resistor.

The thermometer in this experiment was the same single crystal germanium resistor (GR 99) used by Finnemore, Stromberg, and Swenson (35) in the previous work on pure Nb. The calibration of this resistor was carried out using a constant volume gas thermometer to measure the temperature. The precision in this experiment was $\pm$ 0.001 K but the accuracy

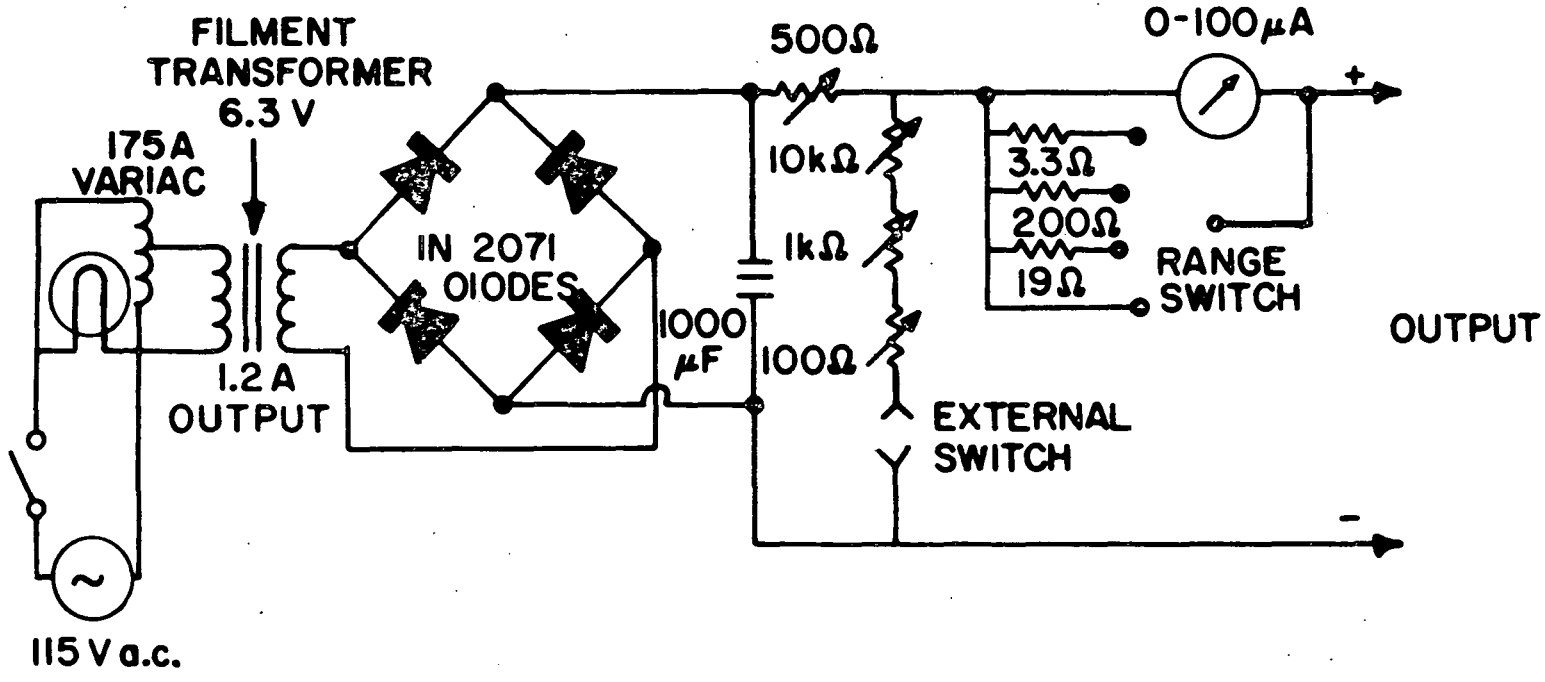

Figure 10. Current supply for the heater used for temperature control.

was limited by the accuracy of the calibration, $\pm$ 0.010 K. The resistance of the germanium resistor was measured using a Leeds and Northrup K-3 potentiometer in a standard 4 probe dc technique. This bridge could measure resistances of 1000.00 Ω to $\pm$ .01 Ω. The germanium resistor was inserted into a close fitting hole in a 0.375 in. brass cylinder (Figure 8). Apiezon "N" grease was used to give thermal contact between the brass cylinder and the resistor. The leads of the thermometer were connected to manganin strips held in place with GE 7031 varnish to provide thermal contact between the leads and the brass cylinder. Nylon mesh cut from an ordinary nylon stocking was used for electrical insulation between the brass cylinder and the manganin strips.

The sample coils (Figure 11) were wound on a nylon form using No. 38 Isonel insulated, copper wire. The 1000 turn primaries were layer wound nonastatically, and had a room temperature resistance of 125 Ω and a self inductance of 1.88 mH. The 5000 turn secondaries were scatter wound astatically on the primary coils and had a room temperature resistance of 850 Ω and a self inductance of 72.5 mH. No special attempt was made to make the measuring coils exactly astatic.

Changes in the output of the measuring coils due to the sample transition from the normal state to the superconducting state were measured using a mutual inductance comparison bridge (Figure 12). The output voltage of the secondaries should be zero for astatically wound coils if the sample is normal. However, voltages are induced in the detection circuit due to eddy current losses for a normal sample, non-ideal inductors in the circuit, the coils not being astatic, and perhaps

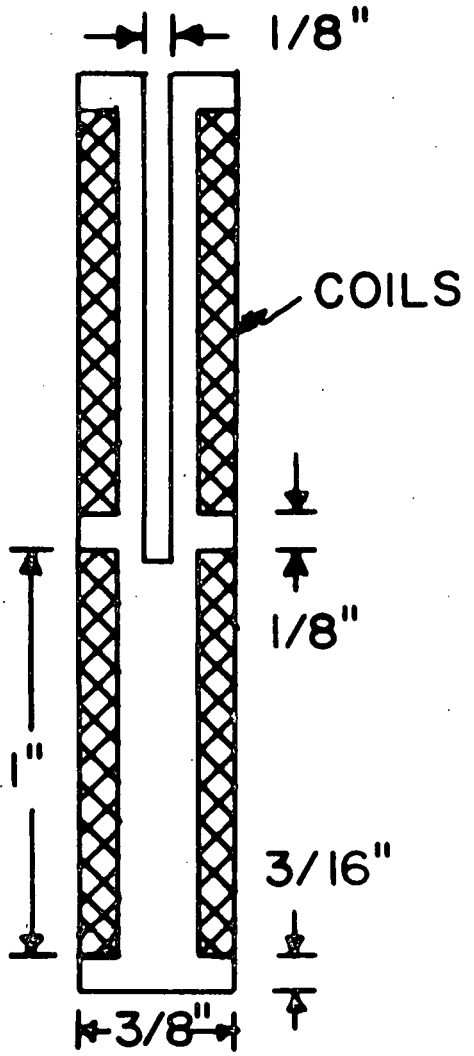

Figure 11. Measuring coils.

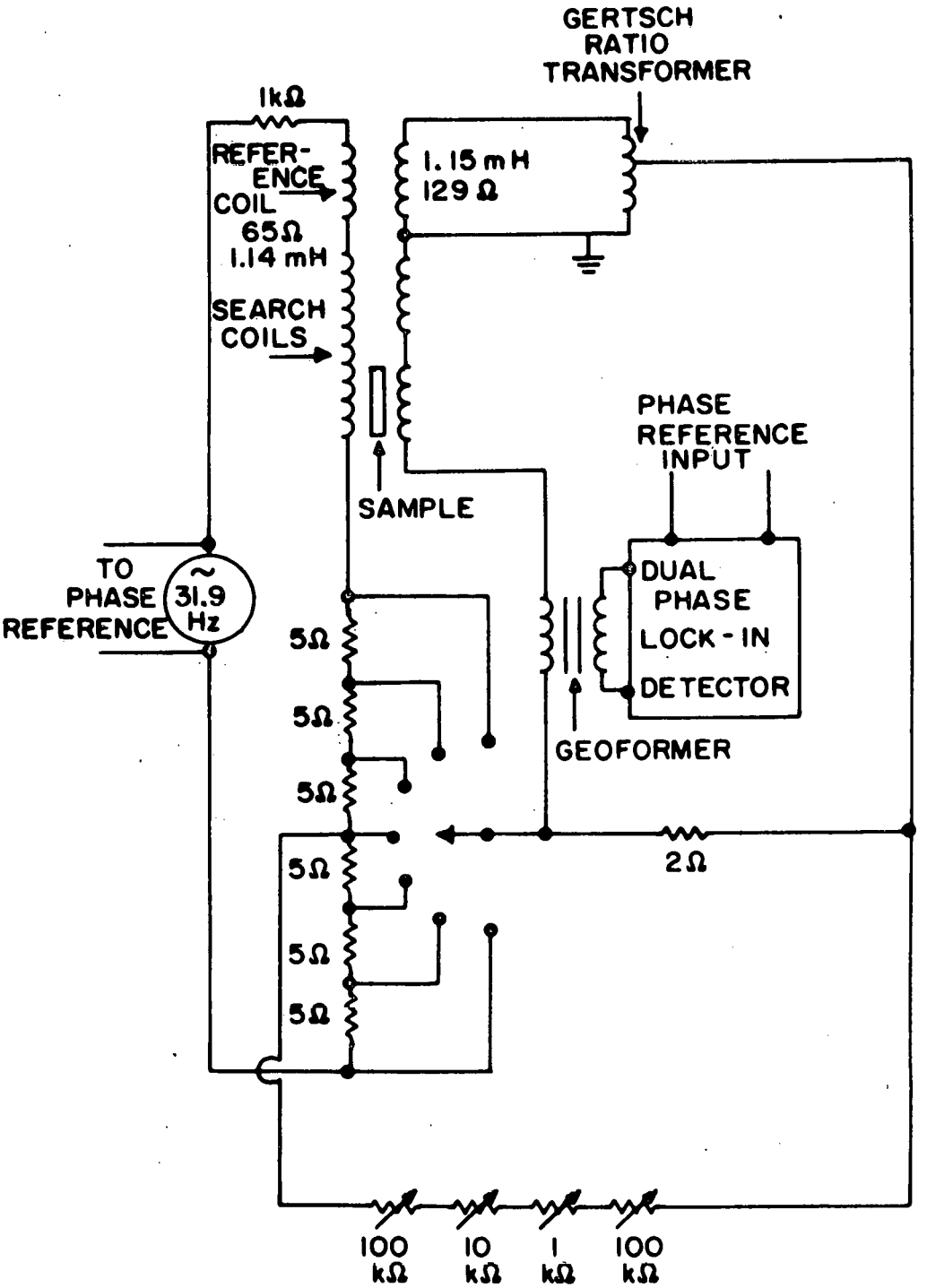

Figure 12. Circuit diagram of the mutual inductance comparison bridge.

the mutual inductance of materials in the area of the measuring coils. The resistive voltage from the secondaries is balanced by a voltage generated across a 2 Ω resistor in the detection portion of the bridge which is driven by a resistive network which picks off the necessary voltage from the primary circuit. The voltage introduced into the detection circuit is proportional to $1/(11,110,000 - R)$ where R is the setting of the variable resistors. The inductive component of the voltage from the secondaries is balanced by a voltage generated across a fixed reference coil. The voltage introduced into the detection circuit is proportional to M, the setting on the Gertsch Ratio Transformer which divides the output of the fixed reference coil.

For those portions of the experiment which were done at 31.9 Hz, a fixed frequency phase sensitive lock-in detector, locally built, was coupled to the circuit through a geoformer. A convenient feature of this detector was that both phases of an off balance signal could be displayed on twin output meters. When the detector was properly phased changes in inductive and resistive voltages were independent of each other as long as the meters were on scale. Full scale deflection for the inductive component meter on the most sensitive scale used corresponded to about 10 % of the change from the completely superconducting state to the completely normal state. The detector was tuned to operate at 31.9 Hz and the oscillator was tuned to the precise ($1:10^4$) frequency of the detector. In the frequency dependent studies a variable frequency Princeton Applied Research HR-8 lock-in amplifier was used for the detector and the precisely tuned oscillator was replaced by a Hewlett-Packard 200 CD oscillator.

EXPERIMENTAL TECHNIQUES AND BASIC MEASUREMENTS

The critical fields, H_{c1}, H_{c2}, and H_{c3}, were determined from isothermal ac susceptibility measurements from zero field to a field significantly above H_{c3}. At each field setting the mutual inductance bridge was balanced for both the inductive and resistive components μ' and μ'' respectively. No attempt was made to determine the absolute magnitudes of μ' and μ''. μ' was proportional to the setting of the Gertsch Ratio Transformer (Figure 12) in the inductive network of the bridge and μ'' was proportional to $1/(11,110,000 - R)$ where R was the setting of the variable resistors (Figure 12) in the resistive network of the bridge. For temperatures between 0.6 T_c and 0.9 T_c the bridge could be balanced with a sensitivity of better than 0.1 % of the total change from the completely superconducting state to the completely normal state. For temperatures below 0.6 T_c the measurements of H_{c3} were difficult because the magnetic fields were too high for quiet operation of the liquid nitrogen cooled solenoid. The liquid nitrogen boiled rapidly for currents larger than 20 A and this seemed to introduce a time varying thermal contact between the liquid nitrogen and the wires of the solenoid. This may have caused rapid and random changes in the resistance of the solenoid which the regulated power supply could not follow. Hence, stray signals were fed into the bridge making it impossible to take H_{c3} data for reduced temperatures much lower than 0.6. For temperatures higher than 0.99 T_c the instability of the power supply and temperature fluctuations caused the precision of the bridge to diminish to about 1 % of the total change from the completely superconducting state to the completely normal state. In this range the

susceptibility becomes more sensitive to changes in magnetic field and temperature for temperatures close to T_c. However, the curves were still well defined even at temperatures of 0.998 T_c.

A fairly thorough investigation of the dependence of the critical fields on the measuring field, h_o, was made. For $T/T_c \leq 0.9$, h_o was less than 10^{-4} H_{c2} (0.19 Oe) but became of the order of 10^{-2} H_{c2} as the temperature was increased to 0.995 T_c. No significant changes in the critical fields were noted as h_o was varied as long as the breaks in μ' and μ'' were well defined. Several runs were made on samples H-9, Nb and H-23, Nb-20000 ppm Ta at a reduced temperature of 0.9 for measuring fields between 0.05 Oe and 1.5 Oe. For very large measuring fields, greater than 1.5 Oe, the determination of H_{c3} became uncertain because the slopes of the μ' and μ'' versus H curves between H_{c2} and H_{c3} become smaller as h_o is increased. Superimposed plots which were copied from the original data of runs for h_o = 0.37 Oe and h_o = 0.05 Oe are shown in Figure 13 for the pure Nb sample H-9. These measurements were obtained using a locally built ramp generator to sweep the applied field and a Moseley 7001 AR x-y recorder to plot the off balance voltages of the inductive and resistive networks of the bridge versus the applied field.

In order to determine if there were any contributions due to changing susceptibilities of materials (other than the sample) near the measuring coils, runs (plots of μ' and μ'' versus H_a at fixed temperatures) were made with no sample in the coils at various temperatures and various measuring fields h_o. For temperatures between 4 and 9 K the change in susceptibility was less than 0.1 % of the change in susceptibility with

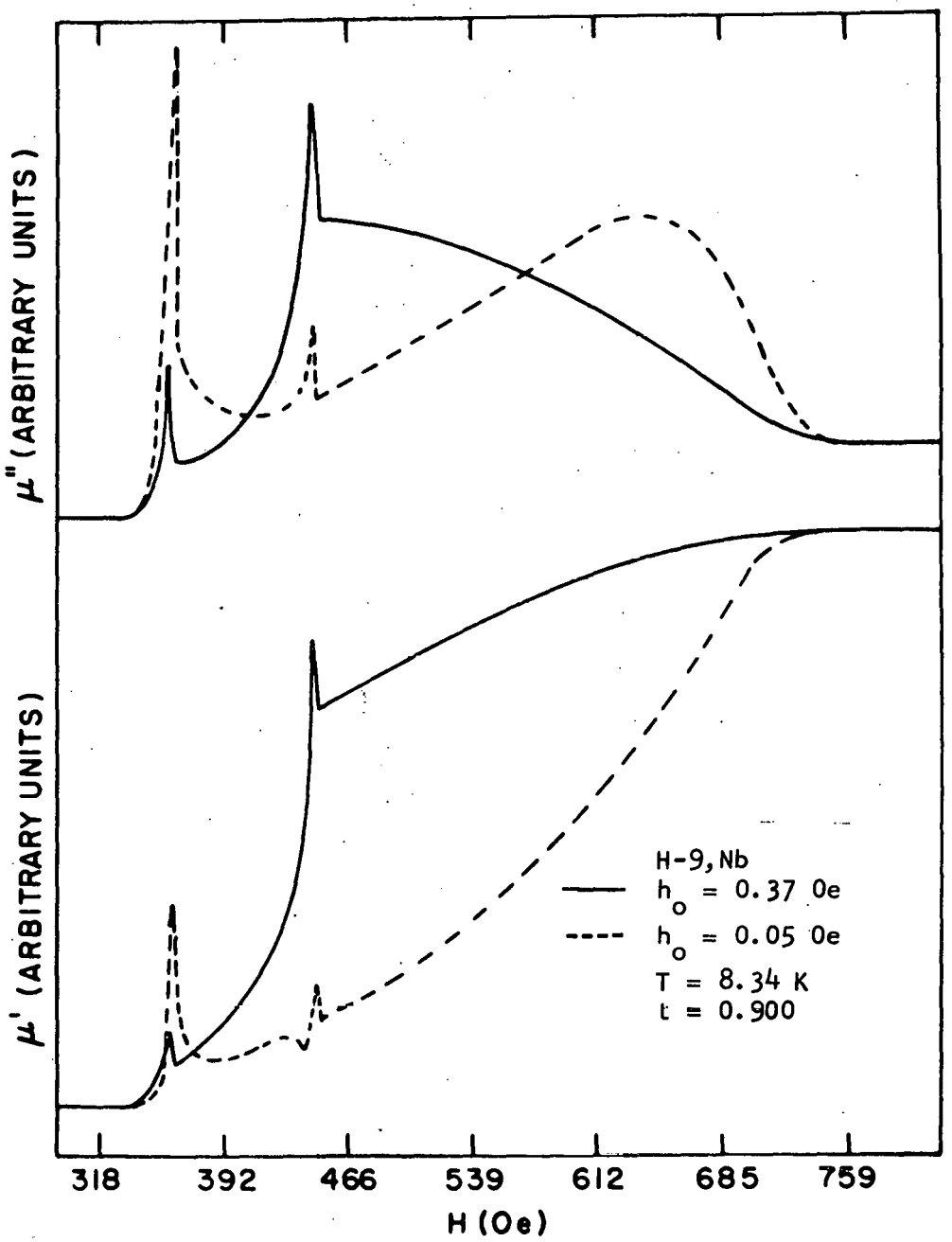

Figure 13. Plots of $\mu'(H)$ and $\mu''(H)$ for h_o = 0.05 Oe and 0.37 Oe at T/T_c = 0.900 for pure niobium.

a sample present going from a completely normal state to a completely superconducting state.

Misalignment of the sample axis with the applied field axis might be another factor which could affect the critical field measurements. Rollins and Silcox (44) have reported that in the case of Pb - 2% In a misalignment of 1^{o} causes a decrease of nearly 40 % in the critical current density of the superconducting sheath but decreases the value of H_{c3} by less than 1 %. Runs were made with the field axis purposely misaligned from the sample axis by approximately 3^{o} at H_{c3} using Helmholtz coils to produce a small field in the horizontal plane (Figure 14). The μ'' curve changed shape as the field axis was changed due to the fact that the critical current is sensitive to misalignment but the values of H_{c3} and H_{c2} remained unchanged as long as the samples were warmed above their transition temperatures and cooled in zero magnetic field (virgin samples). In spite of the fact that the runs in Figure 14 were not for virgin samples, H_{c3}/H_{c2} remained unchanged as the field alignment was varied. Figure 15 shows that H_{c3} for a virgin sample remained unchanged for small changes in misalignment.

In general, all the samples gave hysteretic susceptibility curves (Figure 16), but no detailed study was made of this effect because the hysteresis did not alter H_{c2} or H_{c3} values. This hysteresis was most marked in the H_{c1} region as reported by Finnemore, Stromberg, and Swenson (35) for magnetization measurements on pure bulk niobium.

H_{c1} was defined from the susceptibility data as the half-height of the first peak in μ' as shown in Figure 17. The corresponding point in

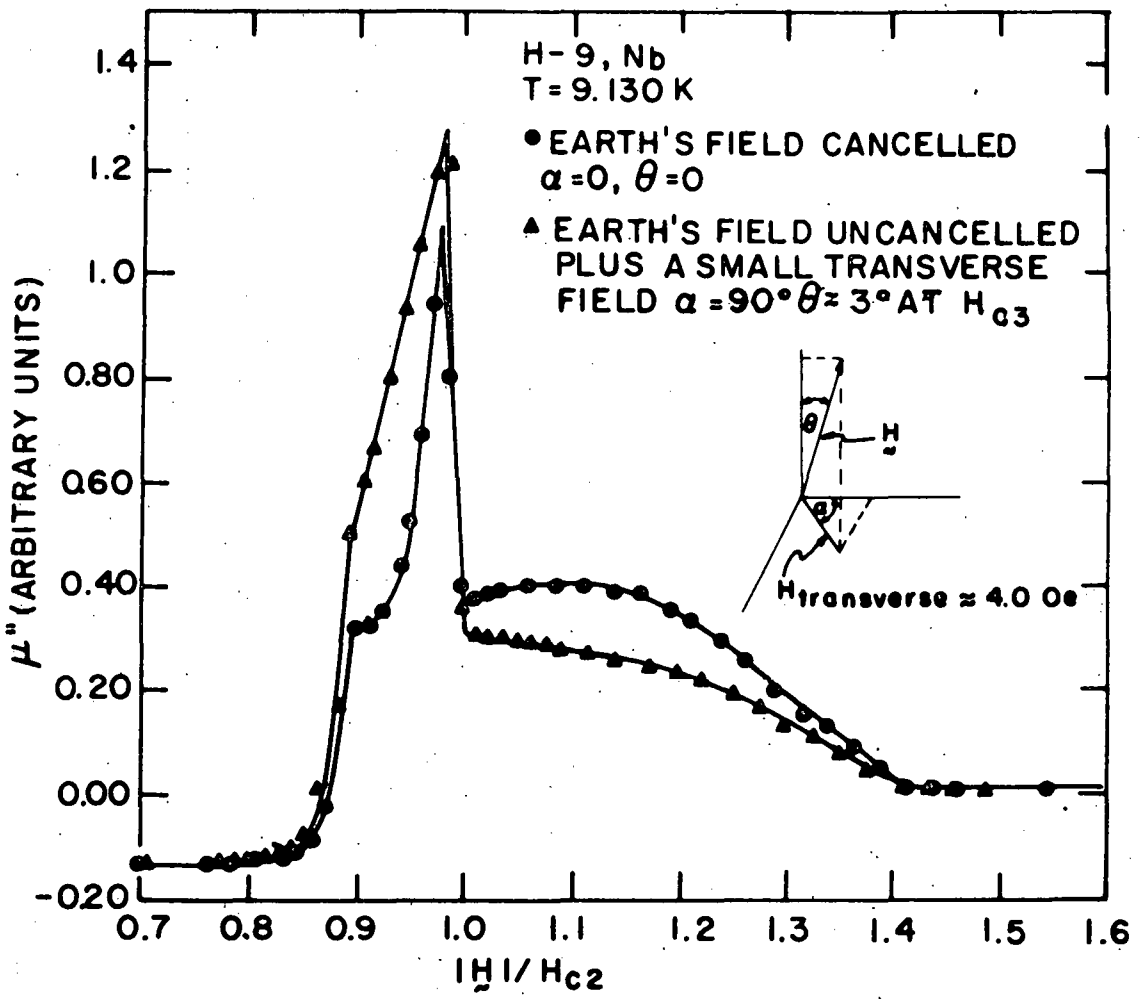

Figure 14. $\mu''(H)$ for a normal run (solid dots) and $\mu''(H)$ with a small transverse field applied (solid triangles).

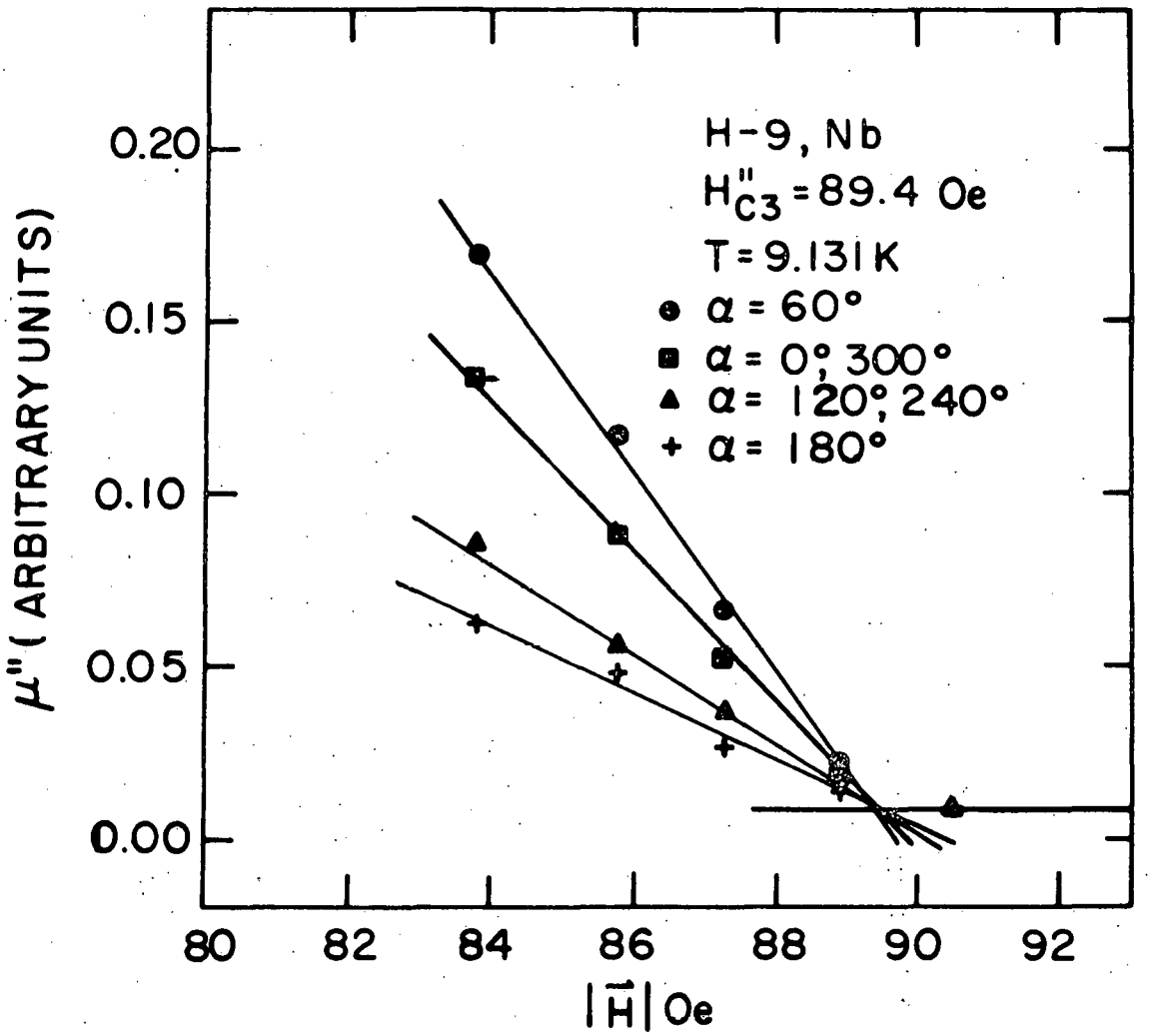

Figure 15. Proof that H_{c3} remains unchanged for a virgin sample as the field misalignment is changed slightly.

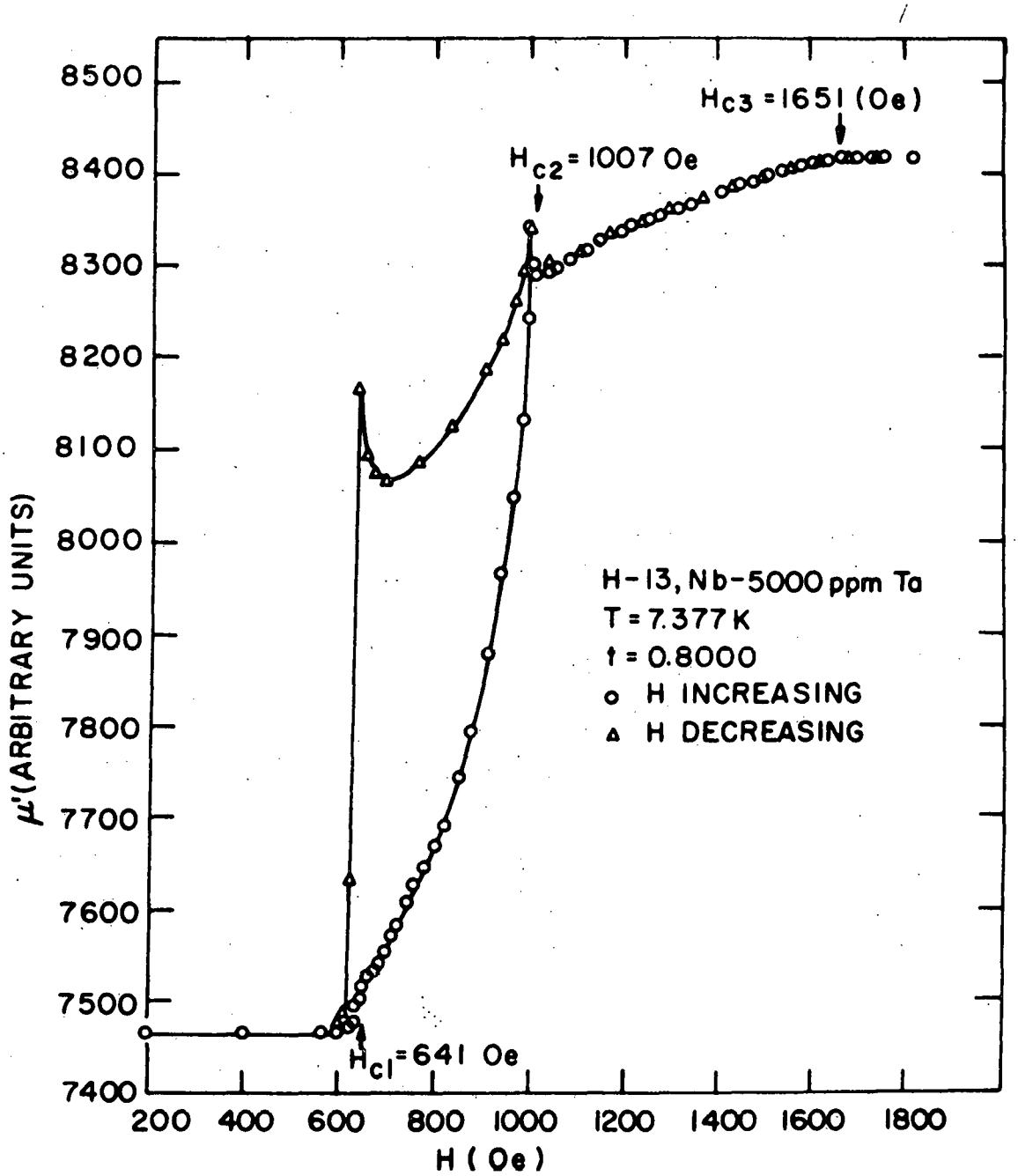

Figure 16. A typical $\mu'(H)$ curve demonstrating hysteresis in sample H-13.

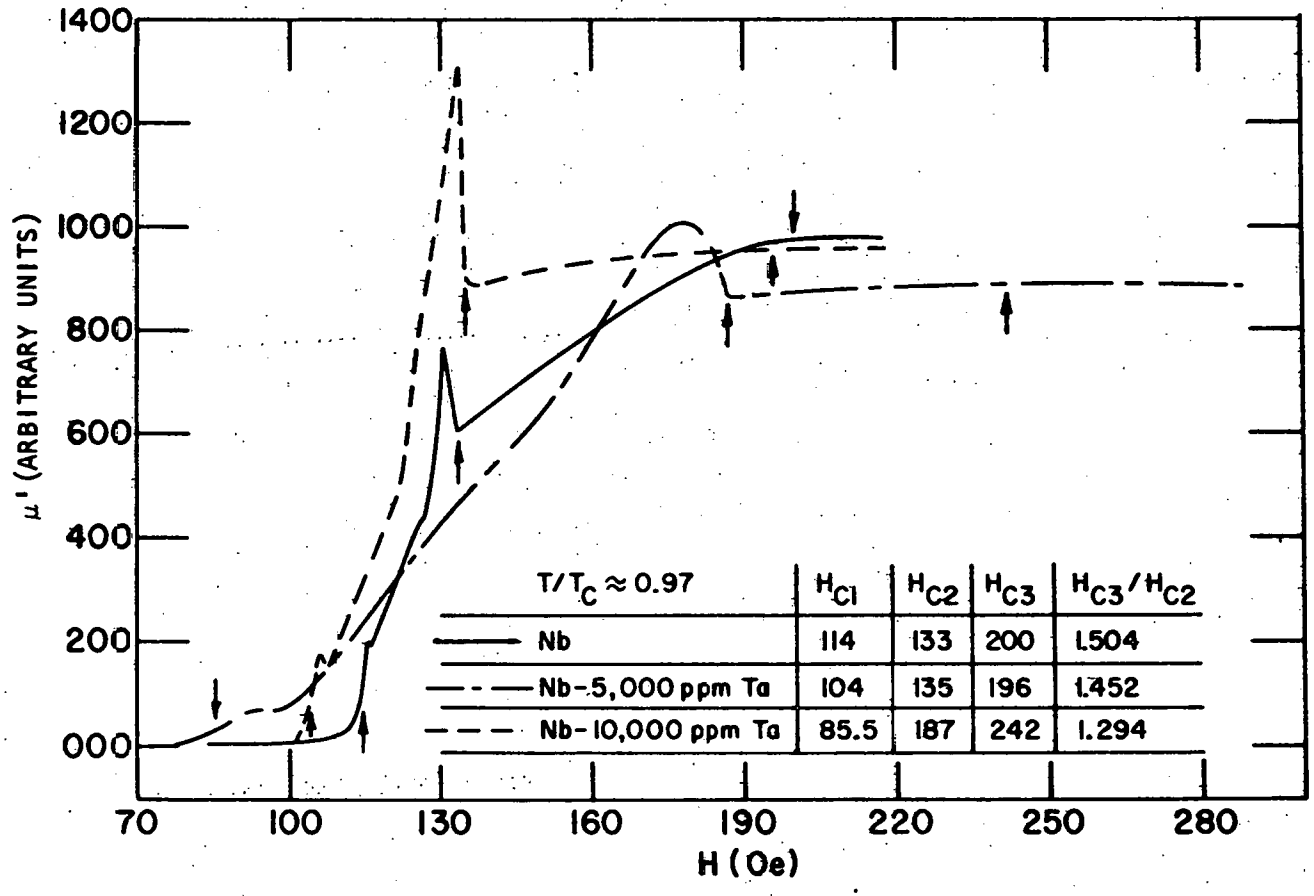

Figure 17. Typical plots of $\mu'(H)$ at $T/T_c \approx 0.97$ for samples H-9, H-13, and H-11.

μ'' gave the same value for H_{c1} although it was not as easily identified throughout the data. H_{c2} was identified as the shoulder of the second peak (Figure 18) which was about midway between the completely normal and completely superconducting values of μ''. The corresponding point in μ' gave the same value for H_{c2}. These definitions of H_{c1} and H_{c2} differ by about 2 % from the definitions used by Ostenson and Finnemore (28). More will be said about these definitions later. However, using the above definitions for H_{c1} and H_{c2} gives good agreement between the bulk magnetization measurements and the ac susceptibility values for pure niobium (Figures 19 and 20). This very good agreement between the different methods gives credibility to the characteristic points chosen as the critical field points. The value of H_{c3} could be taken as that dc field at which either μ'' approaches zero or μ' approaches 1. However, the values of H_{c3} obtained from the μ' curves are consistently lower than those obtained from the μ'' curves by about 2 % and were not as well defined. The critical current model of the surface sheath (44) suggests that μ'' gives a more sensitive measurement of H_{c3} and hence the best value of H_{c3} is determined from the μ'' curve. H_{c3} was taken as the value of the field at the point of intersection of the extrapolation of the μ'' curve above and below H_{c3}.

In the studies of the frequency dependence of H_{c2} and H_{c3}, the off balance voltages of both the inductive and resistive networks of the bridge were plotted as a function of the applied field using the Moseley x-y recorder, the ramp generator, the PAR lock-in detector, and the Hewlett-Packard oscillator as described in the previous section. However, the

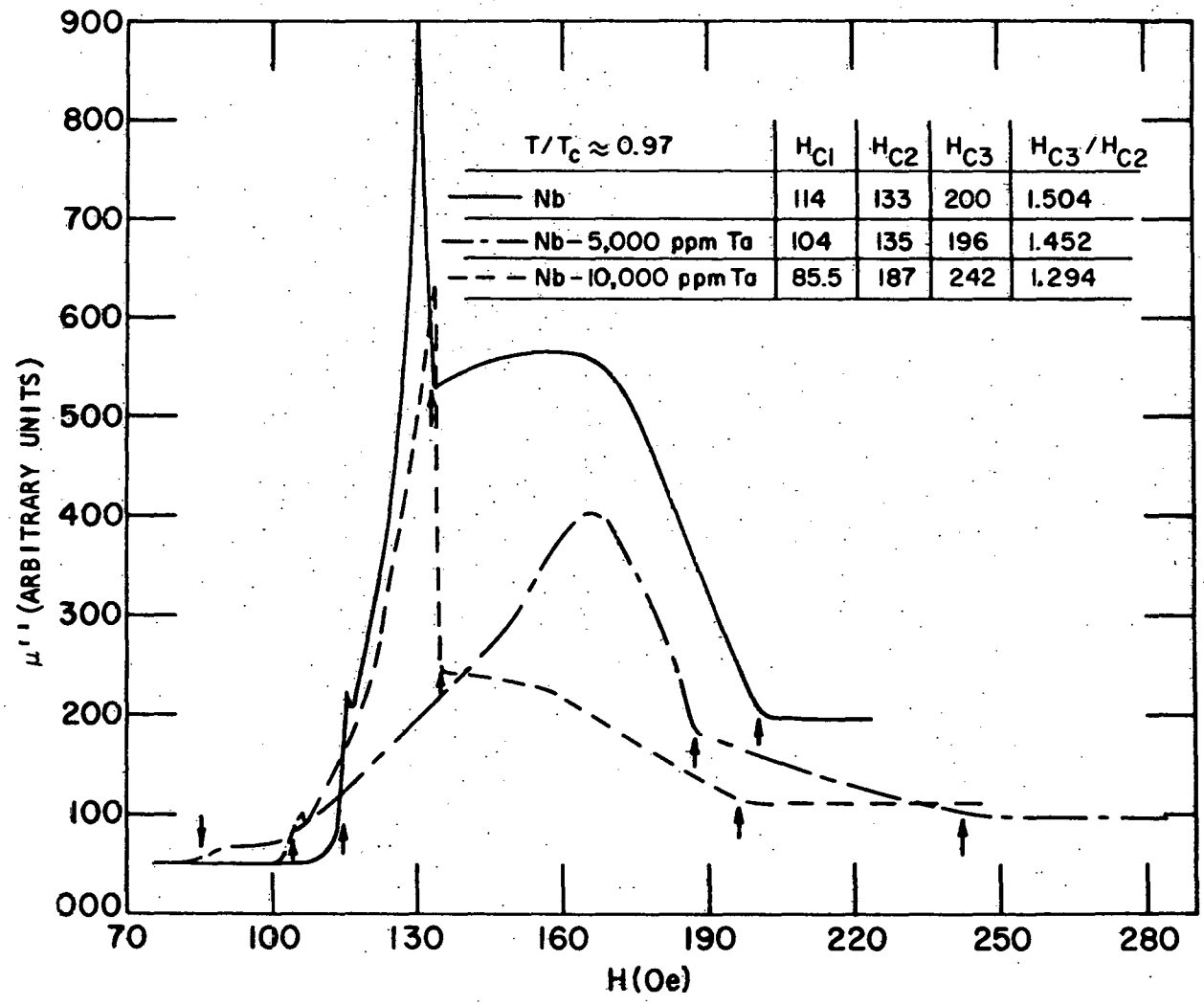

Figure 18. Typical $\mu''(H)$ plots at $T/T_c \approx 0.97$ for samples H-9, H-13, and H-11.

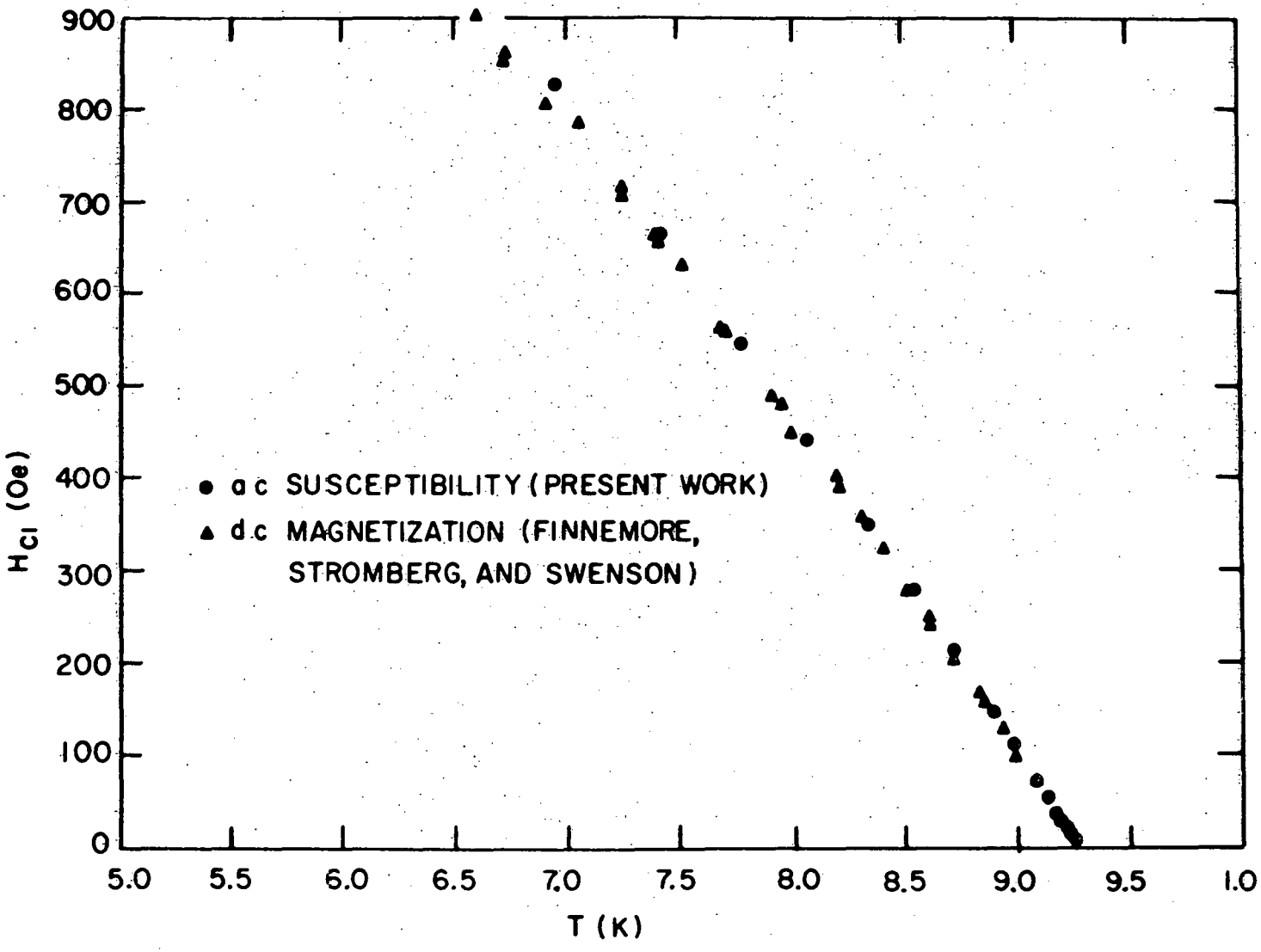

Figure 19. Comparison of $H_{c1}(T)$ for the present work and the work of Finnemore, Stromberg, and Swenson (35).

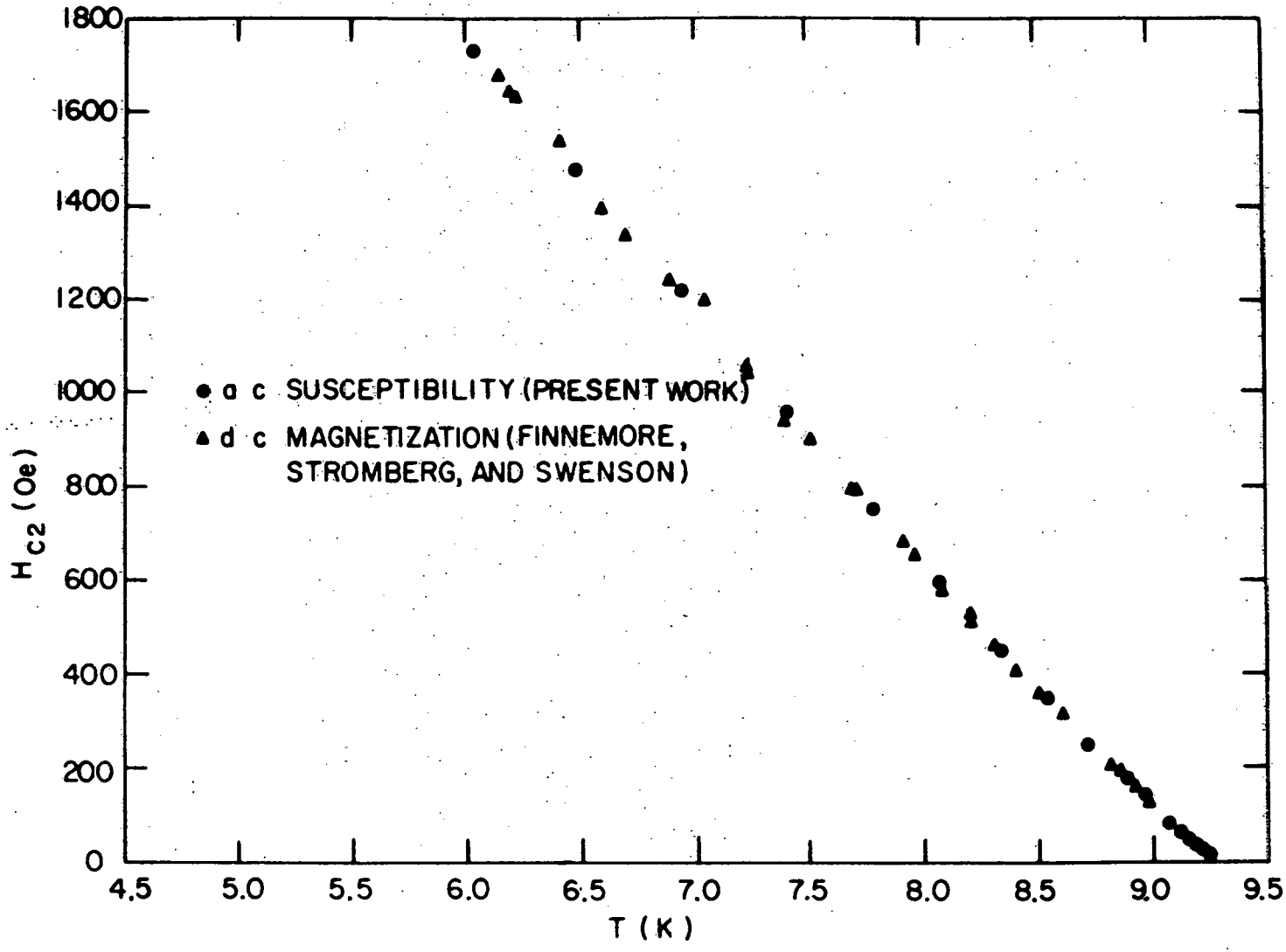

Figure 20. Comparison of $H_{c2}(T)$ for the present work and the work of Finnemore, Stromberg, and Swenson (35).

value of H_{c3} used here was obtained from the μ' curves since the frequencies used (11 cps < f < 11000 cps) gave large variations in the shapes of the μ'' curves due to eddy current effects.

RESULTS AND DISCUSSION

The real and imaginary components of the isothermal susceptibility for the pure niobium and niobium-tantalum alloys studied here are shown in Figures 21-29. Each set of curves ($\mu'(H)$ and $\mu''(H)$) can be used to determine a value of H_{c1}, H_{c2}, and H_{c3} at any particular temperature for the sample under investigation. These critical field values were independent of the amplitude of the measuring field. The detailed shapes of the curves also are relevant and yield information about the flux pinning properties of the sample (45) but for this aspect of the data our comments will be qualitative because there are so many variables in the pinning problem.

Critical Field Curves

The temperature dependence for the lower critical field, H_{c1}, is shown in Figure 30. For the pure niobium sample H-9 (Figure 19), H_{c1} was in excellent agreement with the data obtained by Finnemore, Stromberg, and Swenson (35,39). As the Ta content increased in the alloyed samples $H_{c1}(t)$ decreased as expected theoretically. For the Nb-1000 ppm Ta sample, $H_{c1}(T)$ was not much different from the curve for the pure Nb sample but for the Nb-10000 ppm Ta sample the decrease in $H_{c1}(T)$ from the pure Nb values was quite observable, and, for example, amounted to about a 20 % decrease at $T = 7$ K. At present the temperature dependence of H_{c1} is not well understood theoretically because the Ginzburg-Landau theory does not strictly apply when the order parameter is large. For the samples studied here $H_{c1}(t)/H_{c1}(t=0.7)$ was the same for all samples (Figure 31) indicating that $H_{c1}(t)$ had the same temperature dependence for all the samples.

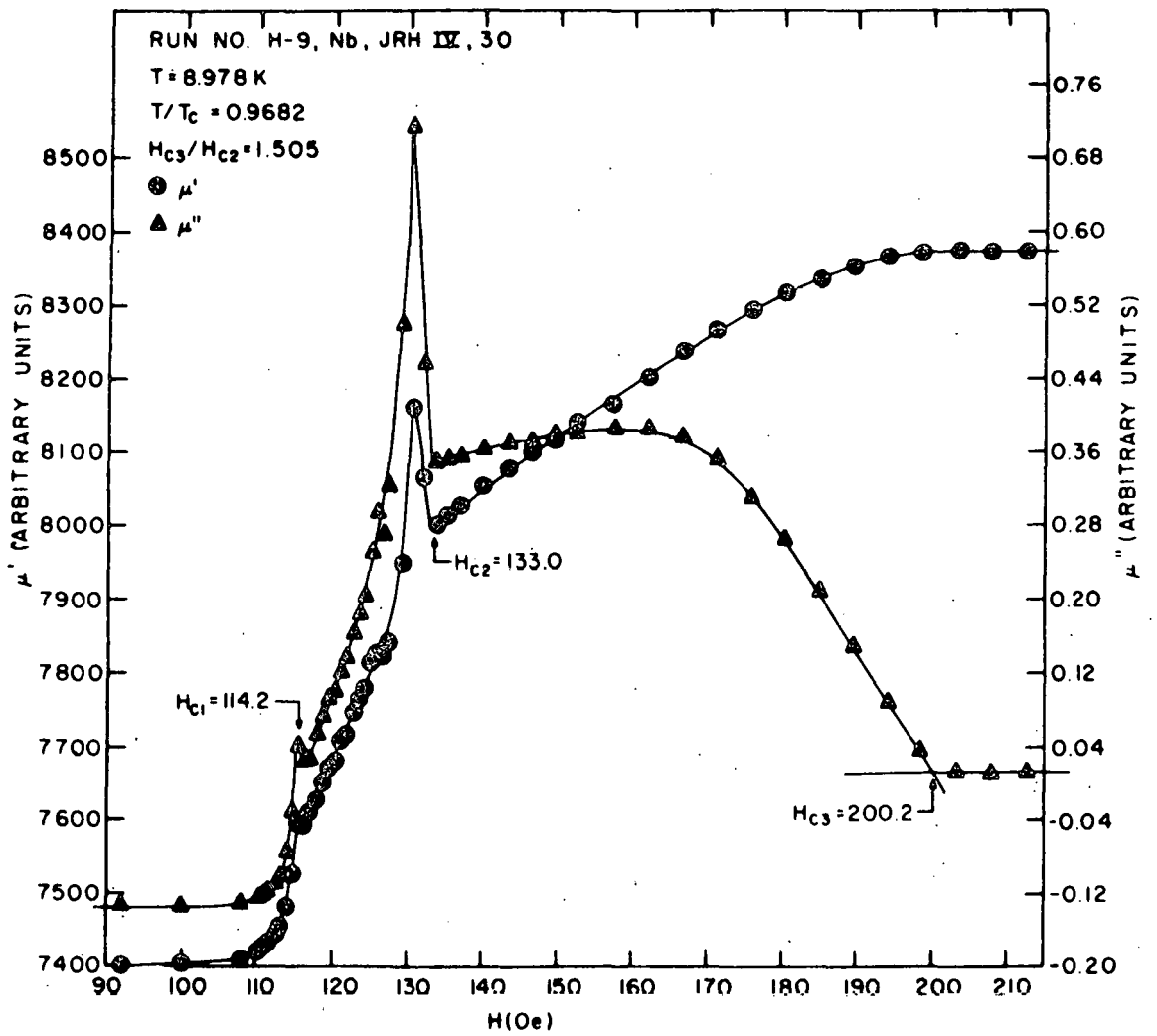

Figure 21. $\mu'(H)$ and $\mu''(H)$ at $T/T_c = 0.968$ for sample H-9.

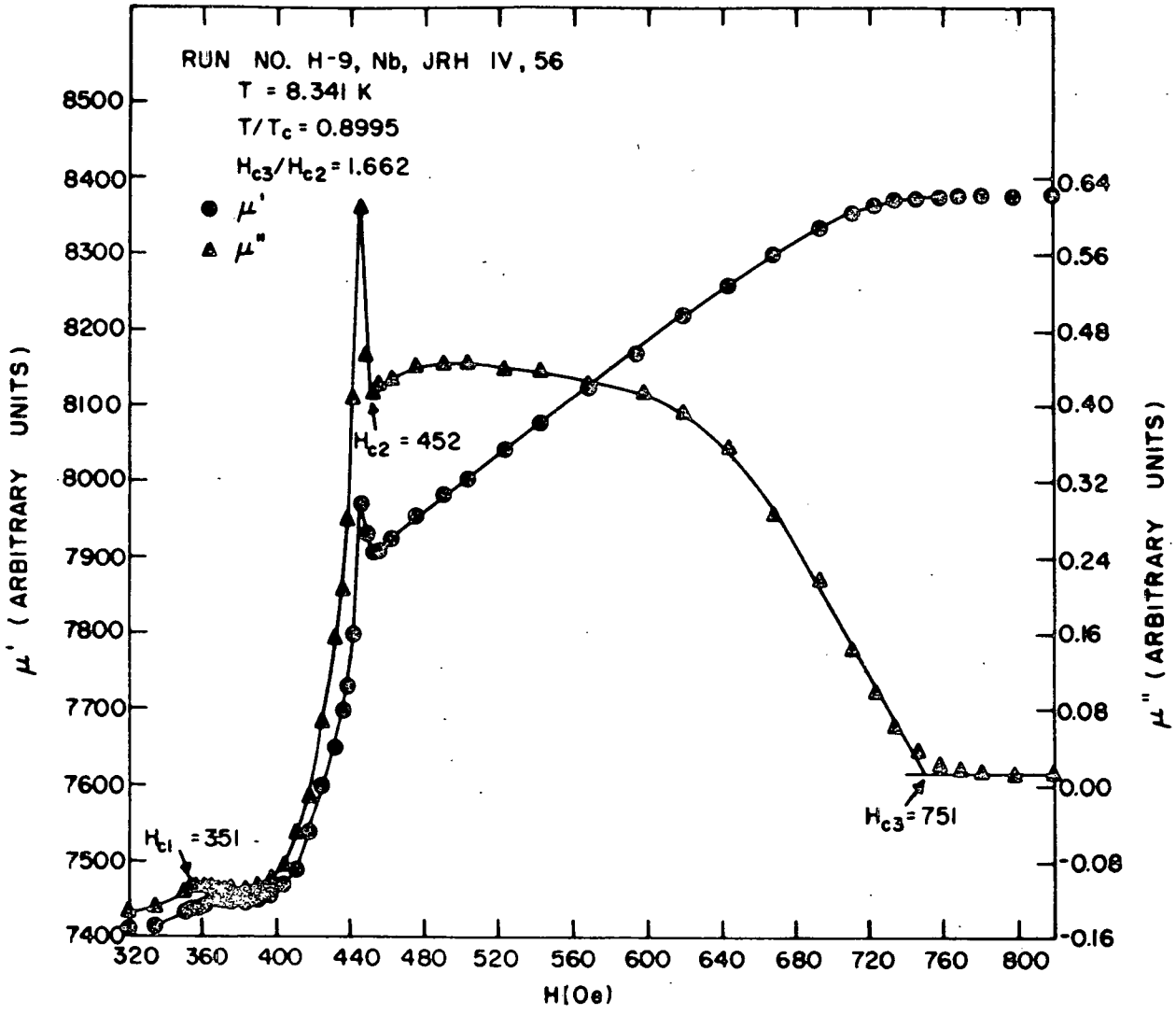

Figure 22. $\mu'(H)$ and $\mu''(H)$ at $T/T_c = 0.900$ for sample H-9.

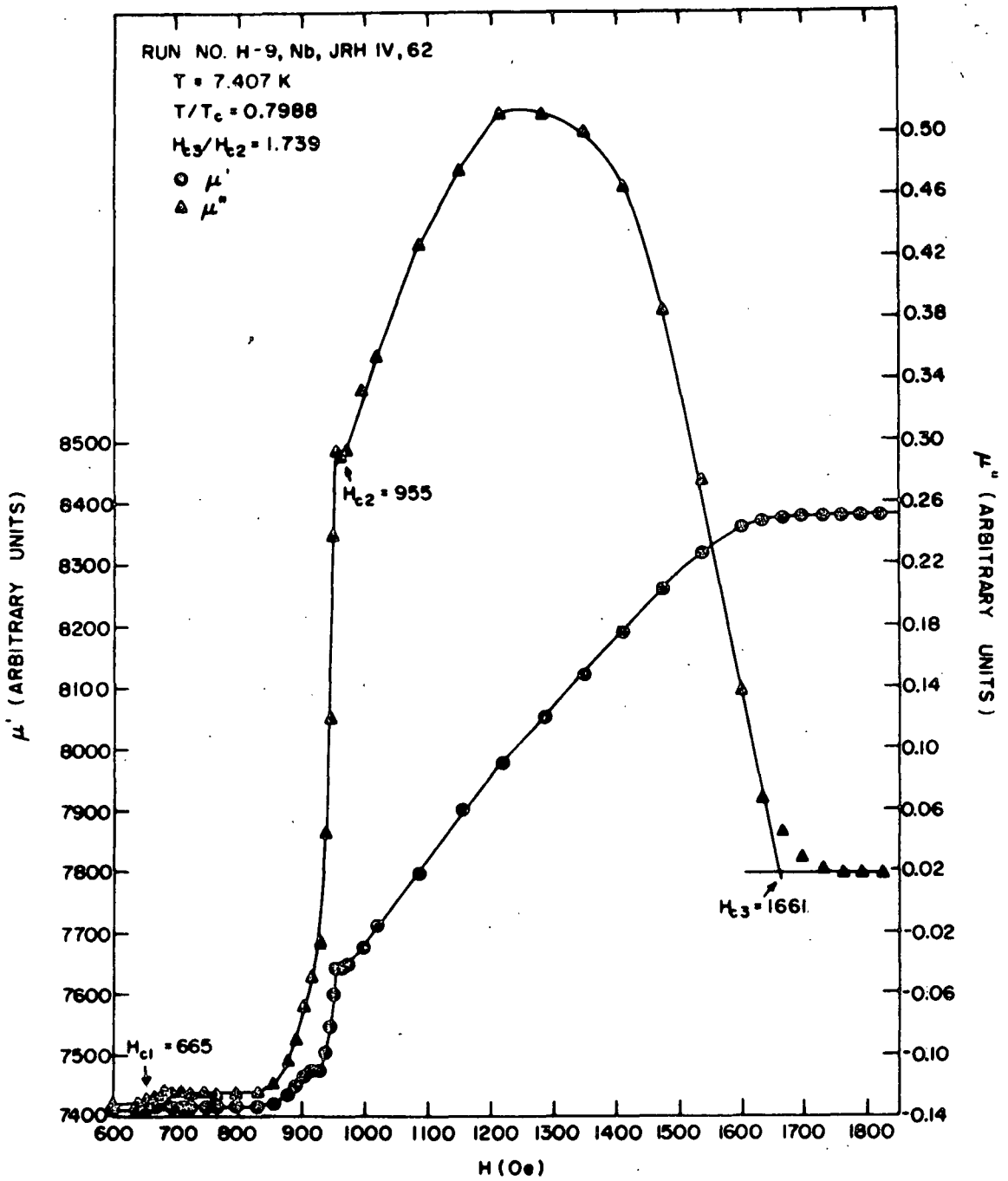

Figure 23. $\mu'(H)$ and $\mu''(H)$ at $T/T_c = 0.799$ for sample H-9.

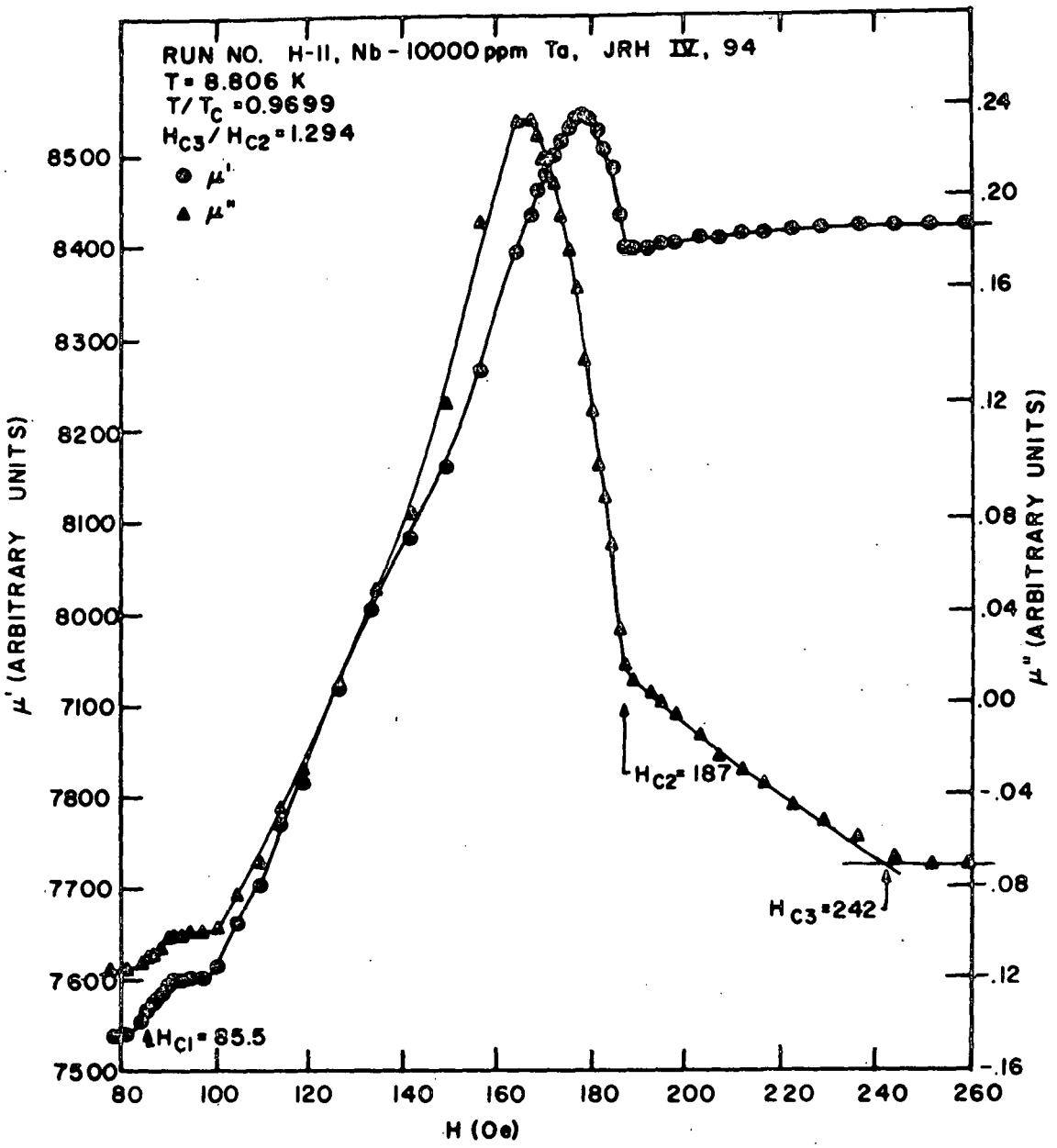

Figure 24. $\mu'(H)$ and $\mu''(H)$ at $T/T_c = 0.970$ for sample H-11.

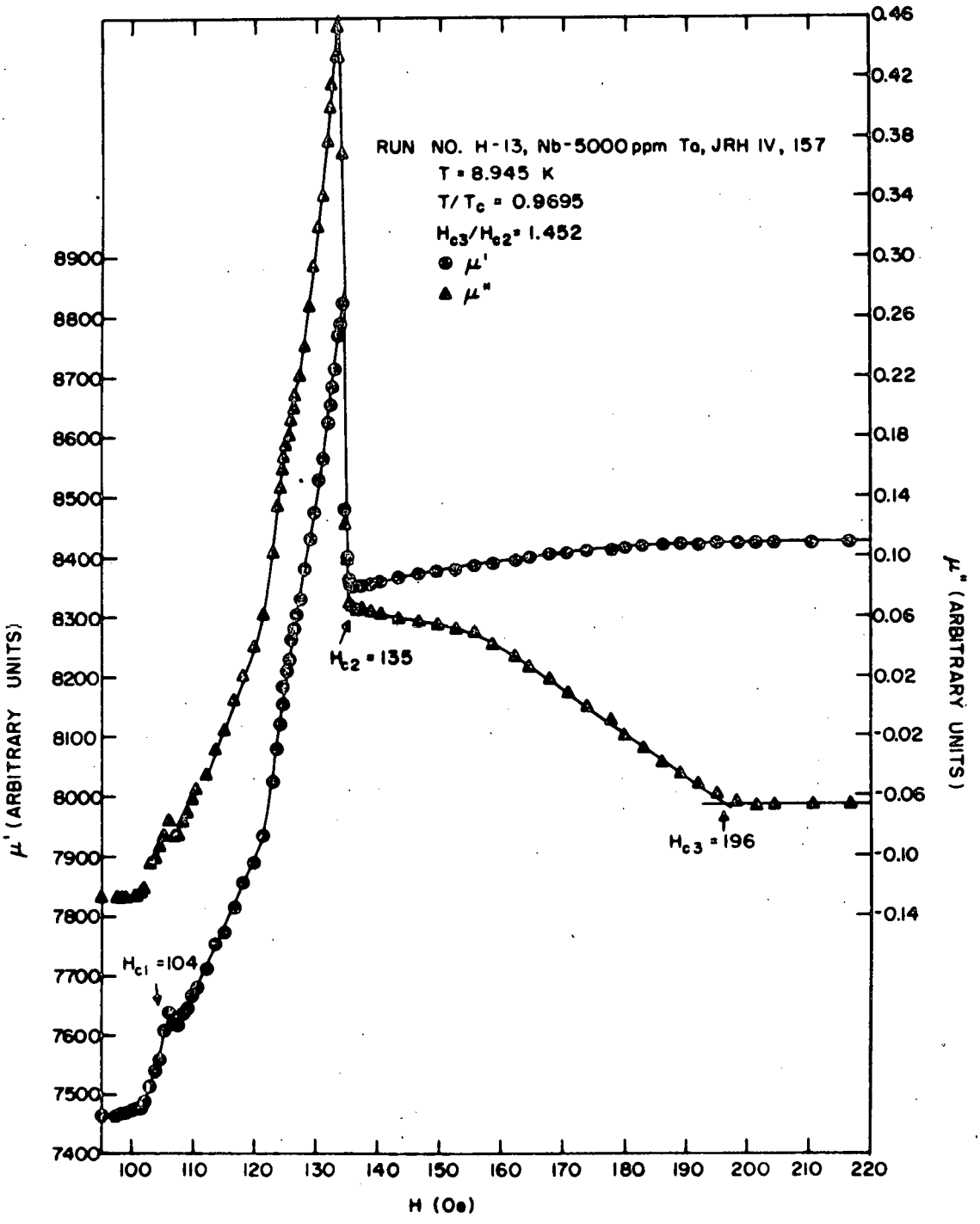

Figure 25. $\mu'(H)$ and $\mu''(H)$ at $T/T_c = 0.970$ for sample H-13.

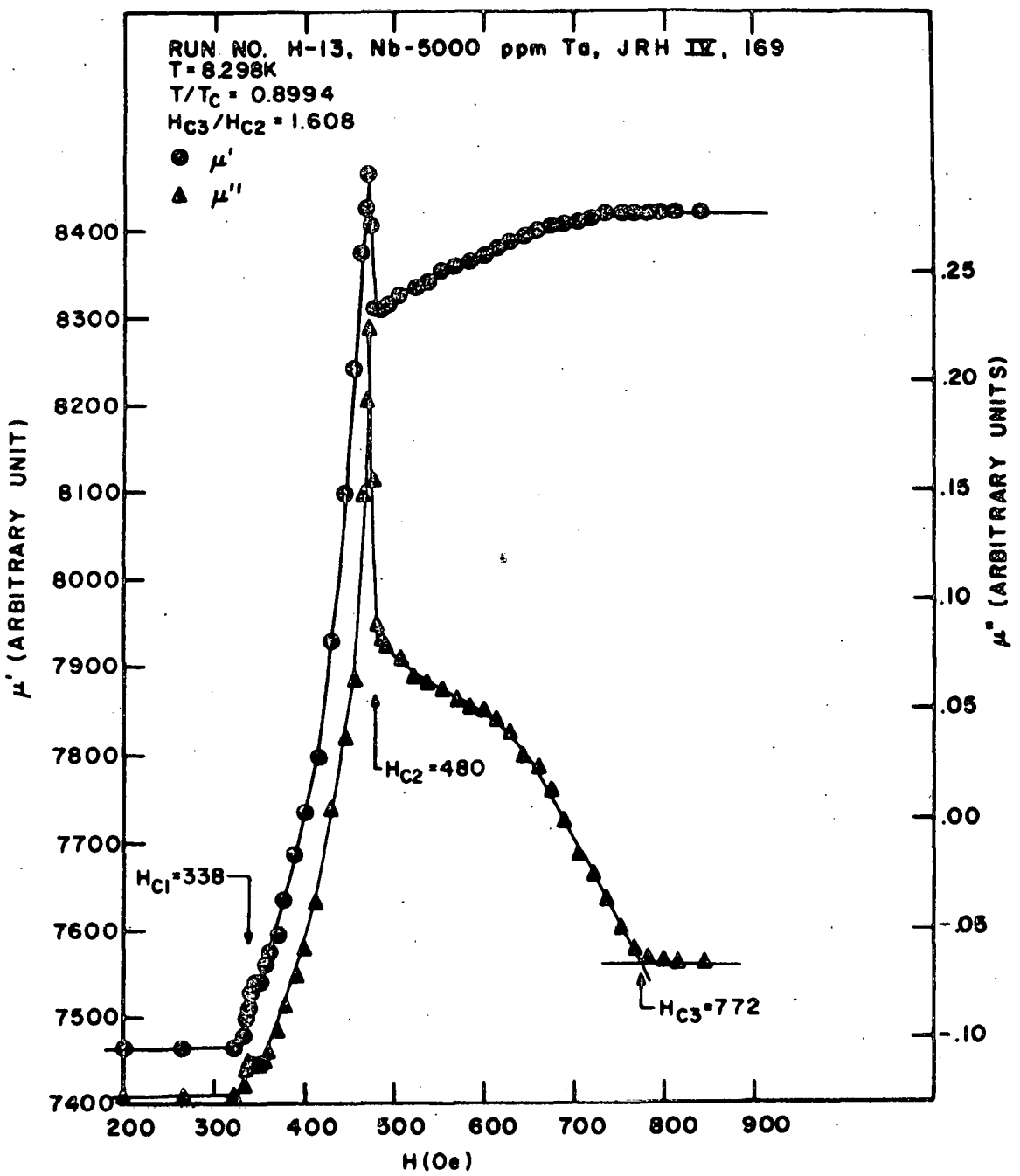

Figure 26. $\mu'(H)$ and $\mu''(H)$ at $T/T_c = 0.899$ for sample H-13.

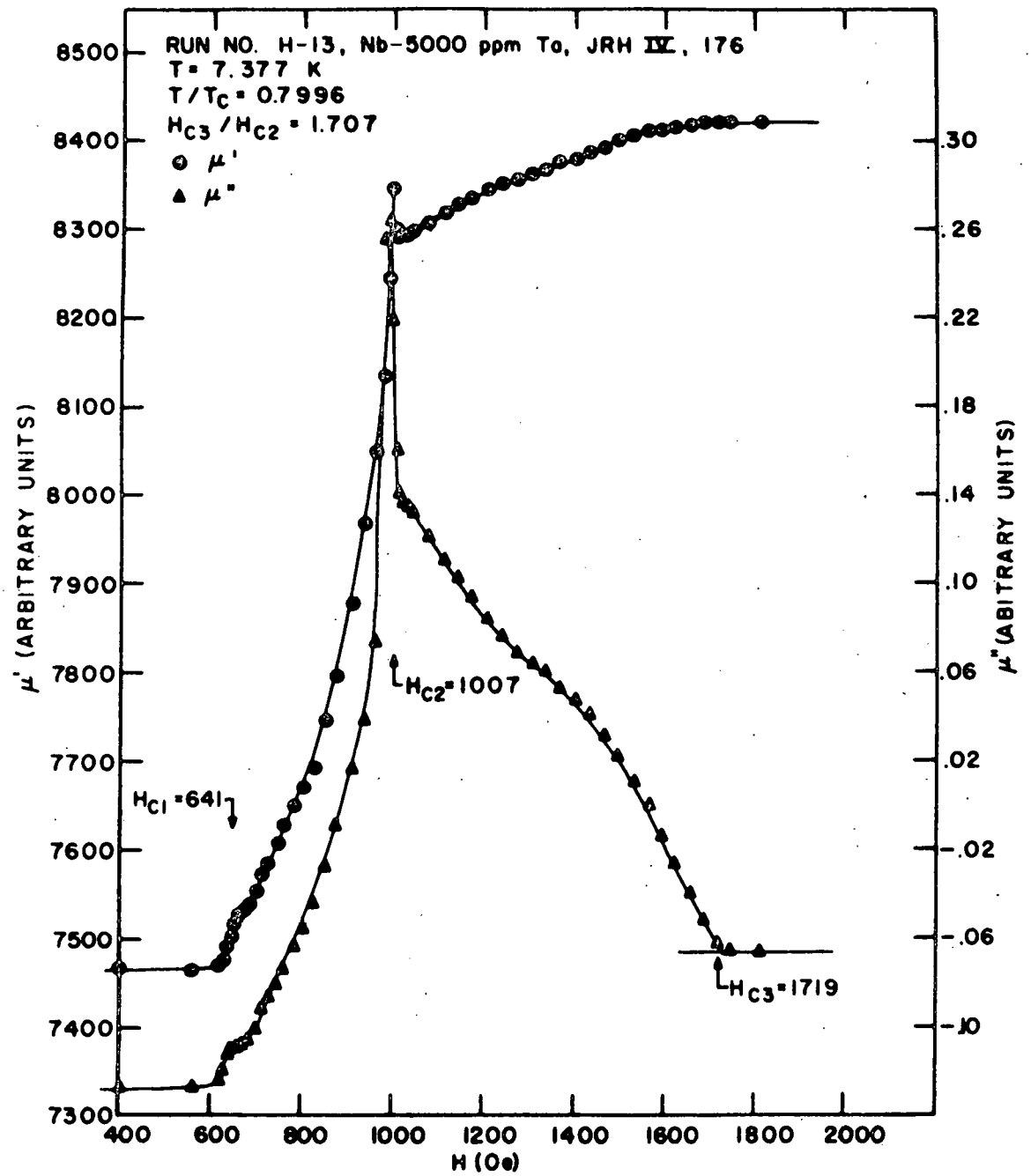

Figure 27. $\mu'(H)$ and $\mu''(H)$ at $T/T_c = 0.800$ for sample H-13.

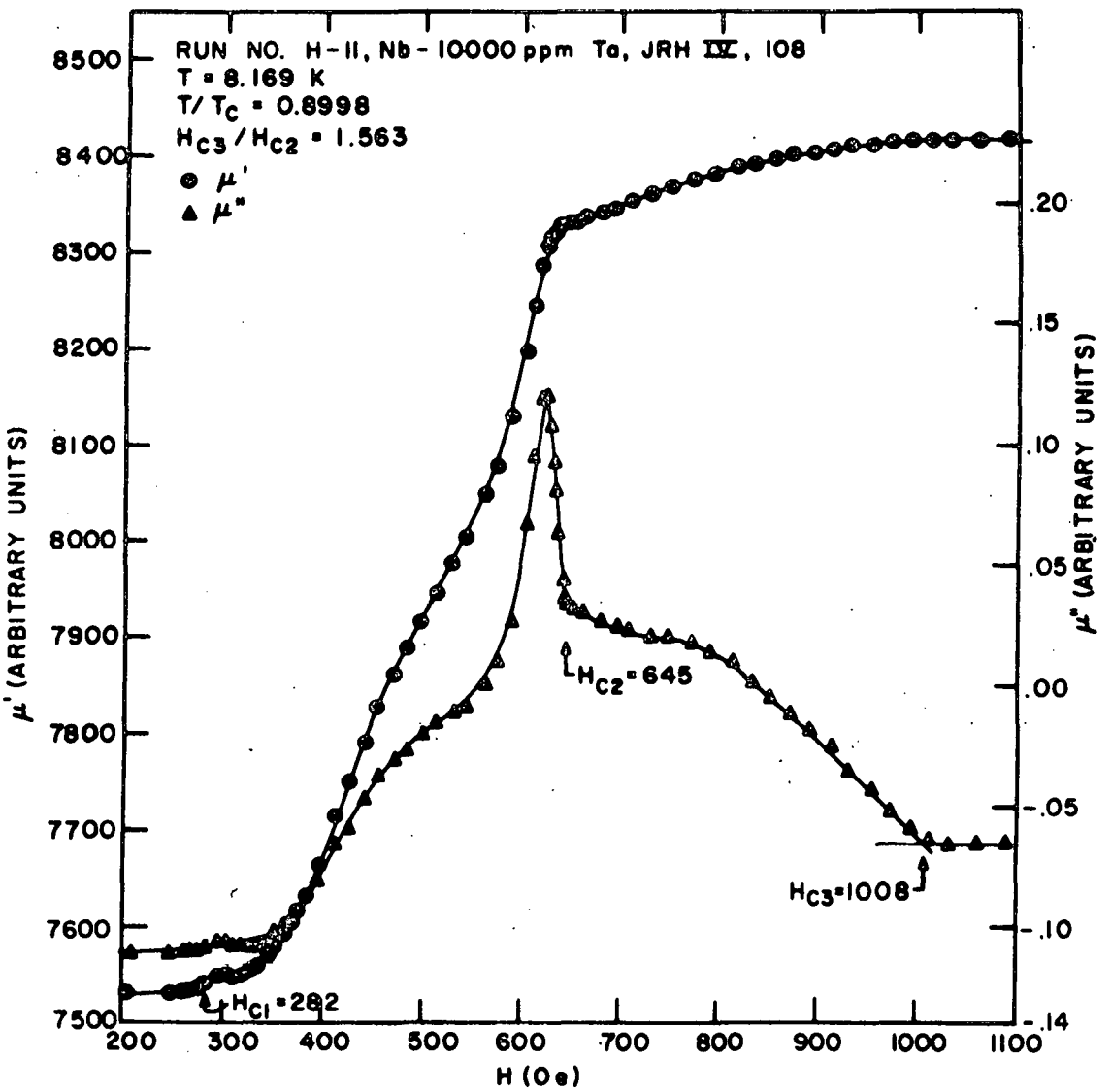

Figure 28. $\mu'(H)$ and $\mu''(H)$ at $T/T_c = 0.900$ for sample H-11.

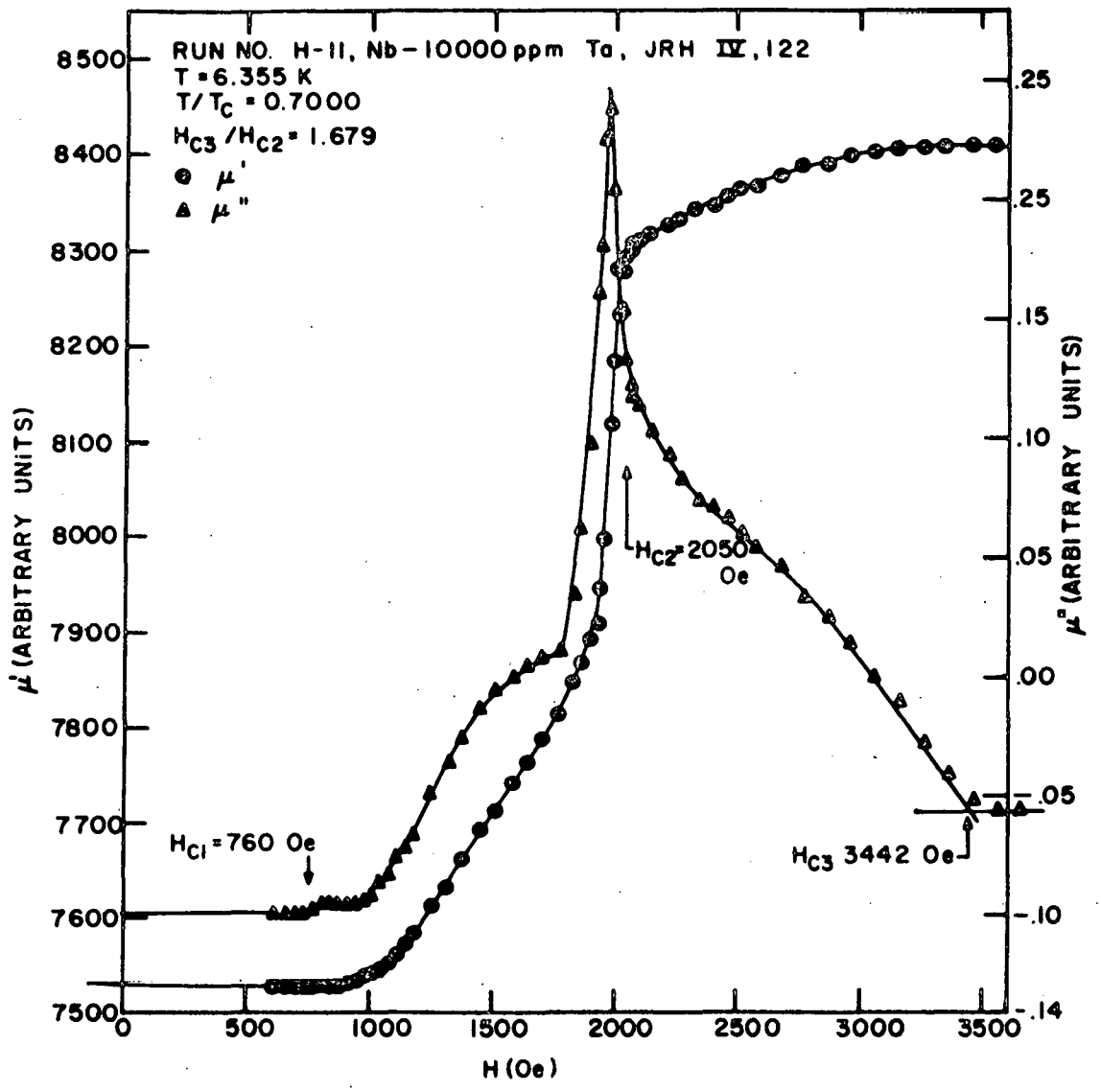

Figure 29. $\mu'(H)$ and $\mu''(H)$ at $T/T_c = 0.700$ for sample H-11.

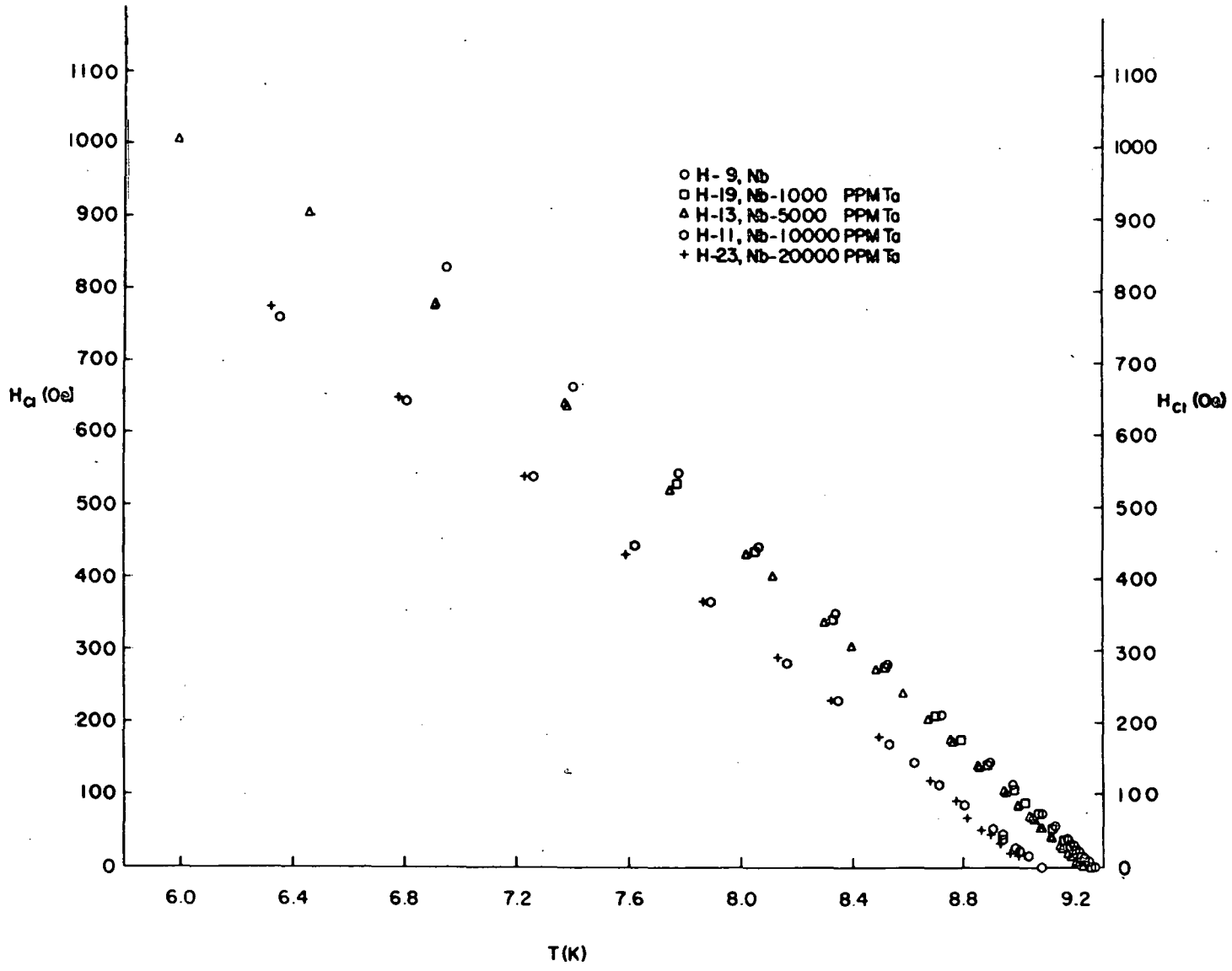

Figure 30. H_{c1} versus T for the niobium and niobium-tantalum samples studied here.

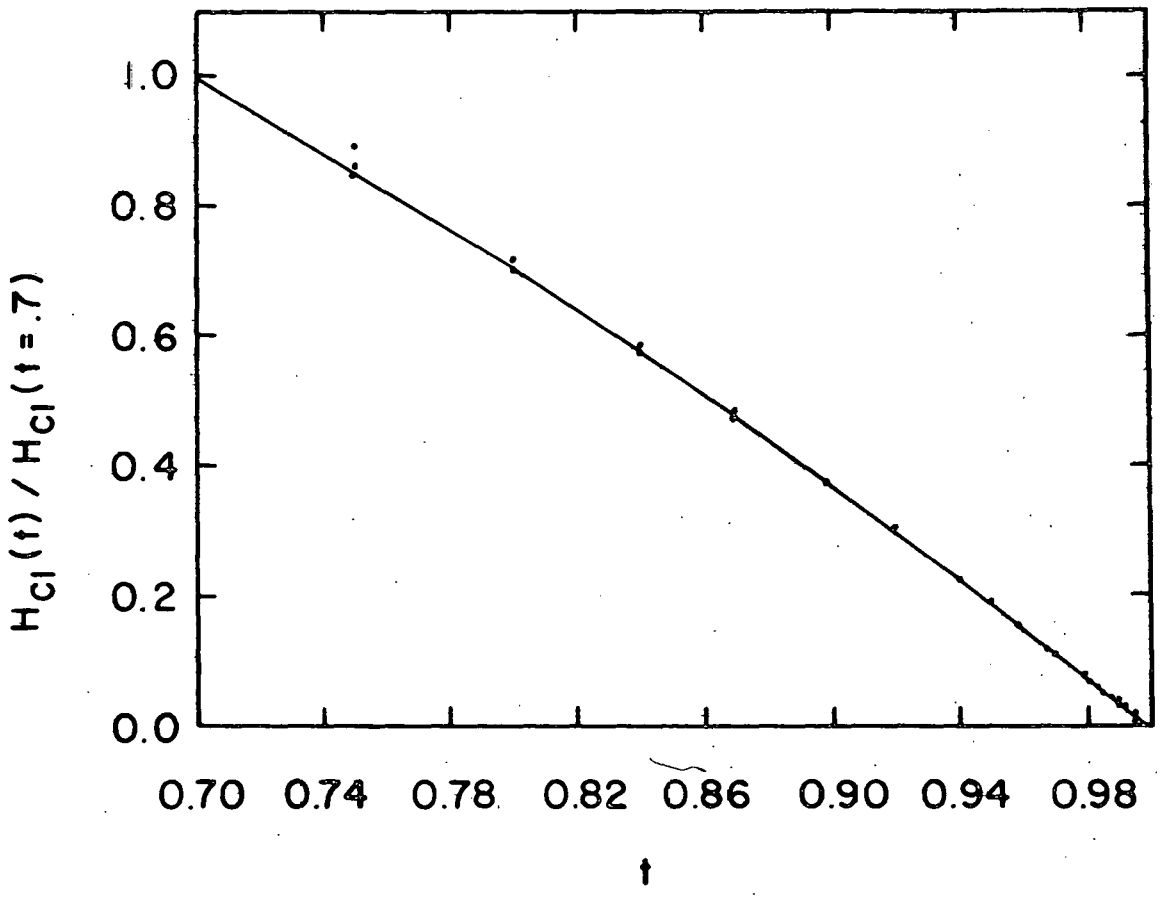

Figure 31. A plot indicating that $H_{c1}(t)$ has the same temperature dependence for all the samples.

The magnetic phase boundaries for the upper bulk critical field, H_{c2}, are shown in Figure 32. $H_{c2}(T)$ for the pure niobium sample H-9 (Figure 20) was in excellent agreement with the data obtained by Finnemore, Stromberg, and Swenson (35,39) using dc magnetization techniques. $H_{c2}(t)$ increased as the Ta content increased. This was a direct consequence of the fact that κ was increasing with increasing Ta content. The bulk properties of pure niobium and Nb(Ta) alloys have been studied in detail elsewhere (35,39, 42, 46) so details need not be repeated here.

The magnetic phase boundaries for the surface critical field, H_{c3}, are shown in Figure 33. The data for $H_{c3}/H_{c2}(t)$ of the pure niobium sample, H-9, agree well with the data obtained earlier by Ostenson and Finnemore (28) and again show large deviations from the theories (14,24, 25,26,27,47) near T_c. As expected from the Ginzburg-Landau and Saint-James-de Gennes theories, the slope of the critical field curves increases with decreasing ℓ and increasing κ. To illustrate the systematic changes with mean free path, the ratio of H_{c3}/H_{c2} is plotted for all the samples in Figure 34. The addition of Ta broadens the temperature region in which there are large deviations from the simple picture theory of Hu. This can be seen more clearly on a plot of H_{c3}/H_{c2} versus log(1-t) as shown in Figure 35. The large deviations from the basic theories are interpreted in terms of variations of the interaction constant at the surface.

To evaluate these results in more detail it is helpful to determine λ, ξ, and κ for each sample. The values of κ for the Nb(Ta) alloys were determined using the pure niobium κ value and the resistivity ratios. Following the theories of Gor'kov (17,18) and Goodman (48),

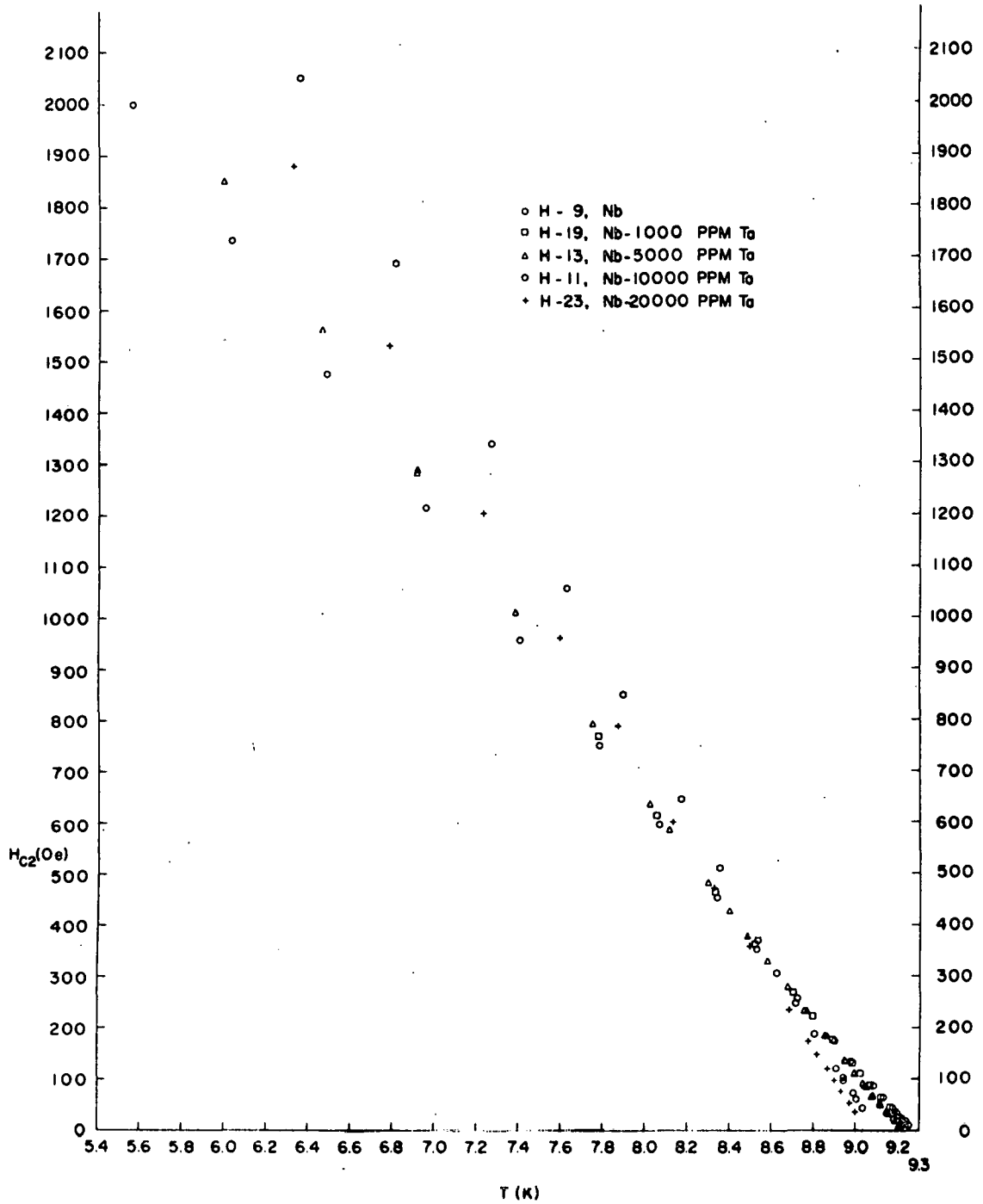

Figure 32. H_{c2} versus T for the niobium and niobium-tantalum samples studied here.

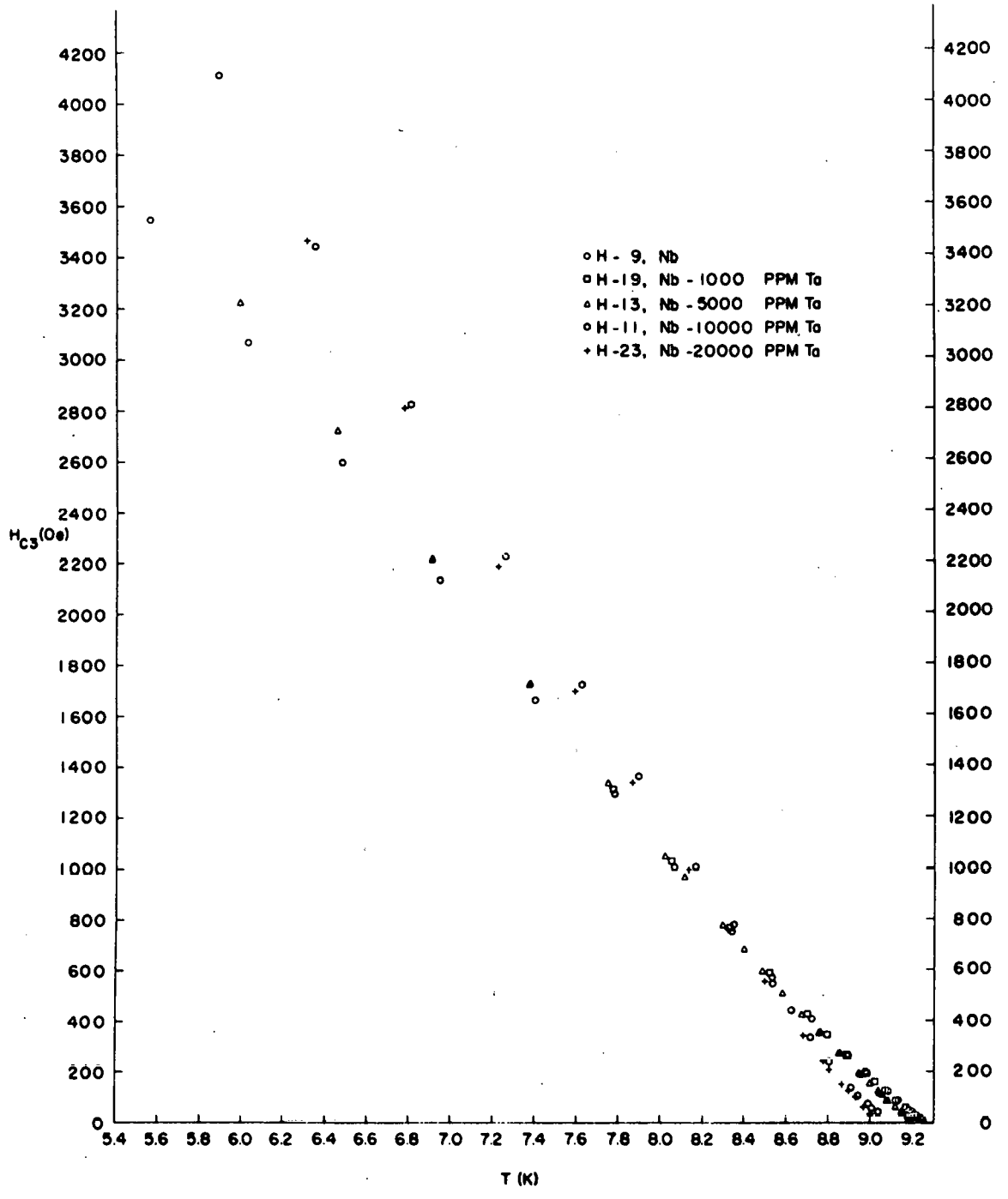

Figure 33. H_{c3} versus T for the niobium and niobium-tantalum samples studied here.

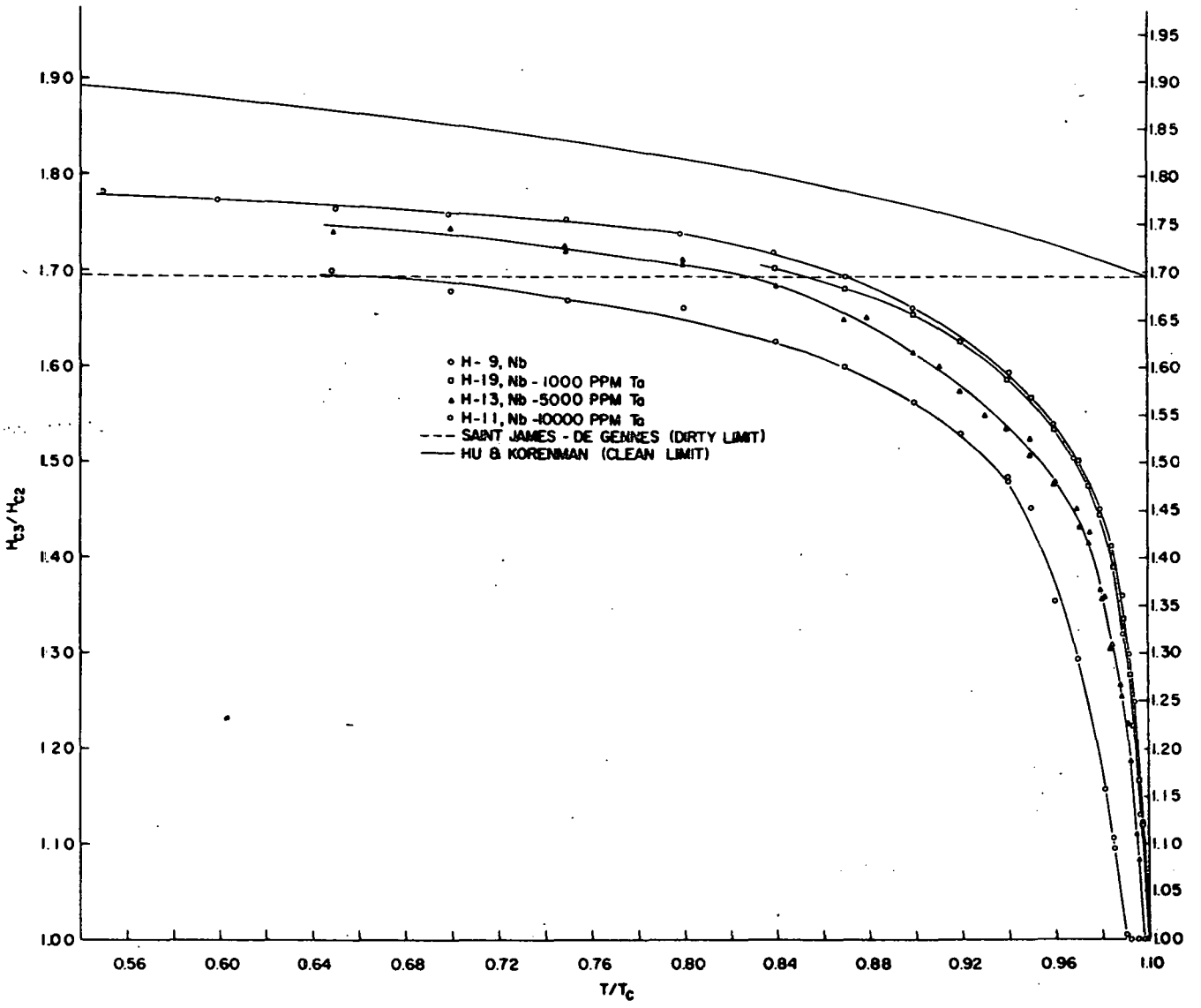

Figure 34. H_{c3}/H_{c2} versus T/T_c for samples H-9, H-19, H-13, and H-11.

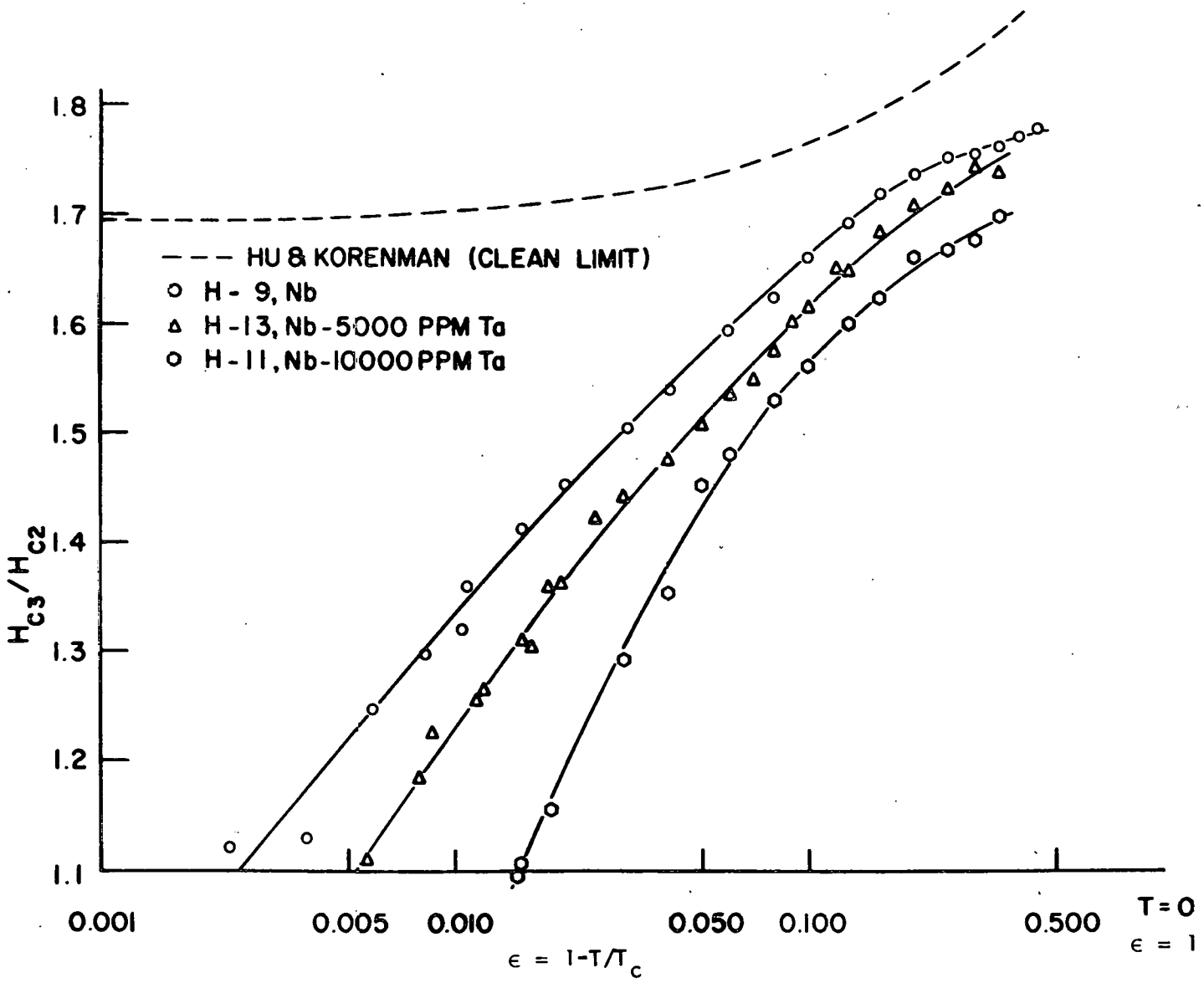

Figure 35. H_{c3}/H_{c2} versus ϵ, plotted on a logarithmic scale, for samples H-9, H-13, and H-11.

$$\kappa = \kappa_o + 7.53 \times 10^3 \rho_n \gamma^{1/2} \tag{49}$$

where $\kappa_o = 0.96\ \lambda_L(0)/\xi_o$, γ is the electronic specific heat in ergs/cm^{3}K^2, and ρ_n is the residual resistivity at 4.2 K in Ω·cm. Using the data of Stromberg (39) in

$$\kappa_1(t) = \frac{H_{c2}(t)}{\sqrt{2}\ H_c(t)},$$

$\kappa_1(1)$ was found to be 0.78. Near T_c, $\kappa \approx \kappa_1 \approx \kappa_3$; hence, κ_o was determined to be 0.76 using $\rho_n(4.2\ K) = 1.04 \times 10^{-8}\ \Omega$·cm and $\gamma = 7 \times 10^4$ ergs/cm^{3}K^2. The thermodynamic critical fields, H_c, for pure Nb (39) then were used in

$$\kappa_3 = 4.3 \times 10^7\ H_c(\text{Oe})\lambda^2(\text{cm}) \tag{50}$$

to determine $\lambda(t)$. Using the pure limit relationship

$$\lambda(t) = \frac{\lambda_L(0)}{\sqrt{2}\sqrt{1-t}} \tag{51}$$

$\lambda_L(0)$ was found to be 330 Å. The temperature independent coherence length, ξ_o, was then determined to be 414 Å from κ_o. The κ values of the Ta doped samples (Table II) were found from Equation 49 using the resistivity ratios (Table II) and the assumptions that ρ_n (300 K) and γ were constant and respectively equal to 14.5 $\mu\ \Omega$·cm and 7.0×10^4 ergs/cm^{3}K^2. The values of the temperature independent coherence lengths, ξ_x, of the Nb(Ta) alloys were determined (Table II) from

$$\frac{1}{\xi_x} = \frac{1}{\xi_o} + \frac{1}{\ell} \tag{52}$$

which is valid in the case $\ell > \xi_o$, where ℓ is the electronic mean free path. The mean free paths were determined (Table II) within the free

Table II. Γ, κ, ℓ, and ξ for the niobium and niobium-tantalum alloys studied here

Sample	Γ	κ	ℓ (Å)	ξ_x (Å)	x
H-9	1600	0.78	121,600	414	0
H-19	276	0.88	20,980	406	1 K
H-13	150	0.98	11,400	399	5 K
H-11	38	1.64	2,890	362	10 K
H-23	37	1.66	2,810	361	20 K

electron model using

$$\ell = \frac{h}{n_s e^2 \rho} \left[\frac{3n_s}{\pi} \right]^{1/3} \tag{53}$$

where $n_s = 1.11 \times 10^{23}$ cm^{-3} and is the density of superconducting electrons (40% of the free electron density). Note that this value of n_s in

$$\lambda_L(0) = \left[\frac{mc^2}{4\pi n_s e^2} \right]^{1/2} \tag{54}$$

yields $\lambda_L(0) = 350$ Å in comparison to the value of 330 Å determined from the data. The resistivities used in Equation 53 were determined by assuming $\rho_x(4.2\ K) = \rho_o(4.2\ K)\ \Gamma_o/\Gamma_x$ where Γ is the resistivity ratio, $R_{300}/R_{4.2}$, of the sample (Table II).

Analysis of H_{c3}/H_{c2} Data

One straightforward way to understand the large deviations from the basic theory is to cast the results in terms of the theory according to

Hu (29). Within this model the deviations from the clean limit theory of Hu and Korenman (26,27) arise because the interaction constant has a spatial dependence near the surface. To analyze the data in terms of this model it is necessary to divide the range of temperatures from 0 to T_c into three regions: (1) Region A, the low temperature region, was defined by $D > \xi(0)\epsilon^{-1/2}$. (2) Region B was defined by $D < \xi(0)\epsilon^{-1/2}$ but not $\ll \xi(0)\epsilon^{-1/2}$. (3) Region C, the temperatures in the extreme neighborhood of T_c, was defined by $D \ll \xi(0)\epsilon^{-1/2}$. In each of these regions the deviation of the H_{c3}/H_{c2} data from the clean limit ($\ell > \xi(0)$) curve (Equation 47),

$$\delta h = \left.\frac{H_{c3}}{H_{c2}}\right|_{\text{THEORY}} - \left.\frac{H_{c3}}{H_{c2}}\right|_{\text{DATA}} , \tag{55}$$

can be related to the spatial dependence of the interaction constant. At T=0, of Region A

$$\delta h(T=0) = \frac{(-V_1/V)\times 3.85}{N(0)V} . \tag{56}$$

Hence, $(-V_1/V)$ could be evaluated directly if data existed at T=0. Unfortunately the H_{c3}/H_{c2} data here extends only to reduced temperatures of 0.6 for technical reasons and extrapolating the data to T=0 is not very reliable. Region A is bounded above by $D \gtrsim \xi(0)\epsilon^{-1/2}$. In Region B δh is expected to vary as

$$\delta h = Z' \epsilon^{-1/2}, \tag{57}$$

where

$$Z' = \frac{2.009}{N(0)V}\left[\frac{-V_1}{V}\right]\left[\frac{D}{\xi(0)}\right] . \qquad (58)$$

Hence, plotting δh versus $\epsilon^{-1/2}$, the H_{c3}/H_{c2} data yields a Z' for each of the samples as shown in Figure 36. Region B is bounded below by $D \lesssim \xi(0)\epsilon^{-1/2}$. If the value of the reduced temperature which separates Regions A and B can be determined from the data then $D/\xi(0)$ will be known and hence $(-V_1/V)$ may be determined from Z'. Each sample was analyzed by first plotting δh versus $\epsilon^{-1/2}$ to determine Z' as in Figure 36. A distinct minimum occurred, at $\epsilon^{-1/2} \approx 2.3$ for all the samples. This can be taken as the separation of Regions A and B, hence $D/\xi(0) \approx 2.3$. The slope of the straight line portion of the graph (δh versus $\epsilon^{-1/2}$) yields Z' and $-V_1/V$ (Table III). As a check on the procedure, the value of $-V_1/V$ obtained was used in Equation 56 to evaluate $\delta h(T=0)$ and $H_{c3}/H_{c2}(T=0)$ (Table III). These values are reasonable extrapolations of the data to T=0 K.

The results for Z' and $|-V_1/V|$ show that when small amounts of Ta are added to Nb the effective interaction strength perturbation has a stronger effect on surface superconductivity. Notice that $Z'/\kappa \approx$ constant for all the samples measured here and surprisingly even for V (31). This implies that the perturbation of V at the surface, which is just the drop off of V towards zero within 10 Å of the surface on the microscopic scale, has a greater effect on H_{c3}/H_{c2} when κ is larger, or since $\kappa \sim \lambda/\xi$, when ξ is less.

An alternate, but closely related, way to interpret the data is to view the deviations of H_{c3}/H_{c2} from the theory as arising from the

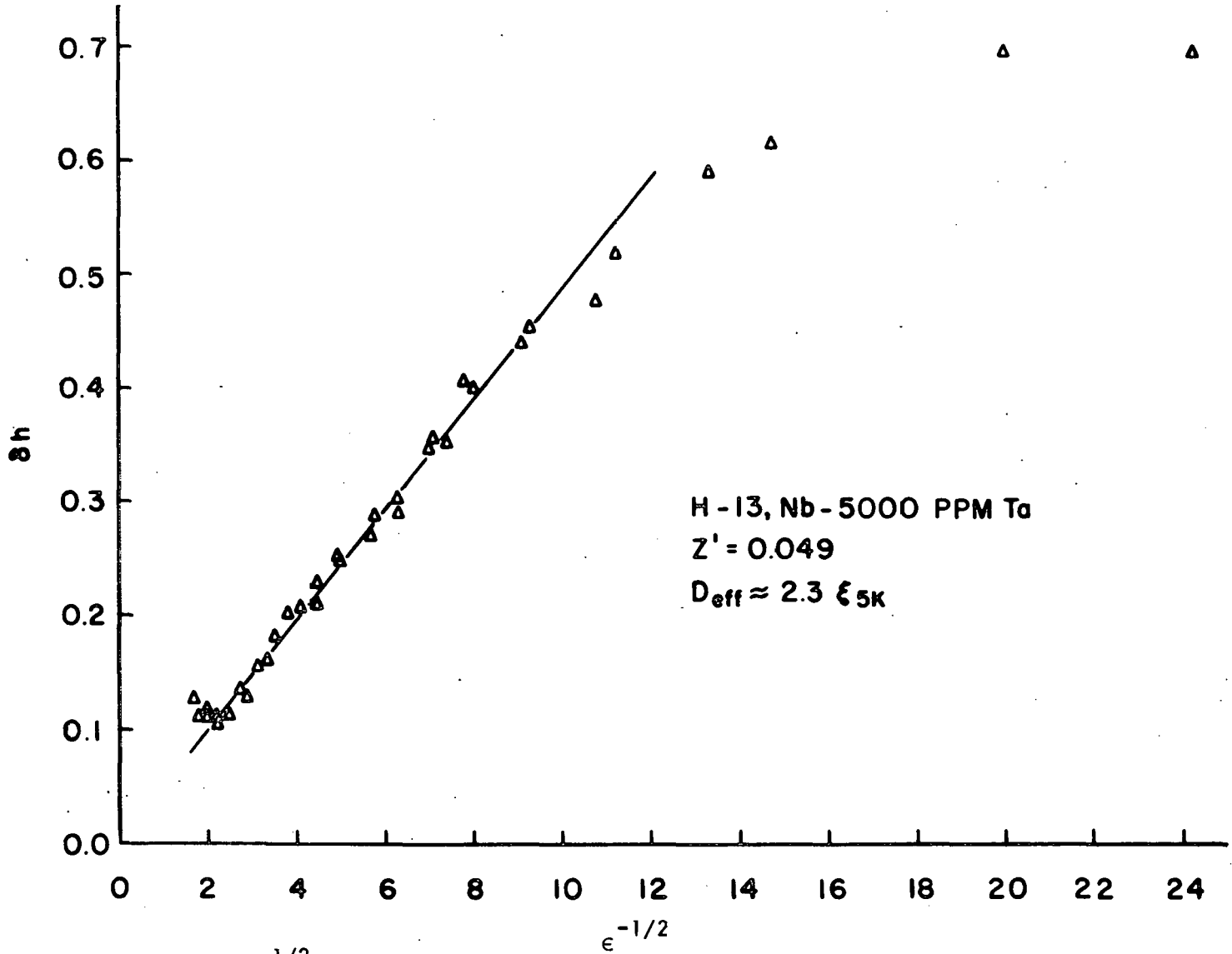

Figure 36. δh versus $\epsilon^{-1/2}$ for sample H-13, Nb-5000 ppm Ta.

Table III. $|V_1/V|$, Z', κ, Z'/κ, $\delta h(T=0)$, and $H_{c3}/H_{c2}(T=0)$ for the niobium and niobium-tantalum alloys studied here and Z', κ, and Z'/κ for V(31)

Sample	Description	Z'	$\lvert V_1/V\rvert$	κ	Z'/κ	$\delta h(T=0)$	$H_{c3}/H_{c2}(T=0)$
H-9	Pure Nb	0.039	0.0076	0.78	0.050	0.038	1.888
H-19	Nb-0.1%Ta	0.040	0.0080	0.88	0.045	0.040	1.886
H-13	Nb-0.5%Ta	0.049	0.0096	0.98	0.050	0.048	1.878
H-11	Nb-1.0%Ta	0.078	0.016	1.64	0.048	0.080	1.846
FRS-20-205	Pure V	0.042	---	0.84	0.050	---	---

failure of the slope of the wave function to be zero at the surface. In the original Saint James-de Gennes calculation the slope of the wave function was assumed to be strictly zero but if there are irregularities at the surface one could easily envisage a nonzero slope at the surface. Hence one can parameterize the H_{c3}/H_{c2} data in terms of an effective slope of the wave function at the surface. Unfortunately no theory exists which yields values of H_{c3}/H_{c2} as a function of ξ/b, where

$$\frac{1}{b} = \frac{\left.\frac{d\psi}{dx}\right|_{x=0}}{\psi(x=0)} , \qquad (59)$$

for the pure limit ($\ell > \xi_o$) but Fink and Joiner (47) have calculated values of b for the dirty limit and we have used these calculations as a guide. To estimate ξ/b for the samples used here we have rather arbitrarily assumed that corrections to the Saint James-de Gennes theory for the mean free path effect, Hu and Korenman, and the corrections for variations in b are independent and additive. This whole procedure is at best a crude approximation. Values of b calculated in this manner (Table IV) indicate that rather small changes in the slope of the wave function can cause the substantial changes in H_{c3}/H_{c2} observed near T_c. As indicated in Table IV the addition of Ta regularly increases the slope. Note that $\frac{\xi(0)/b}{\kappa}$ is a constant ($0.8 < t < 0.95$) implying that the amount of increase of $\frac{\xi(0)}{b}$ is regular with increasing κ and that indeed the samples with the smaller coherence lengths "see" more of the abrupt change of the order parameter at the surface. It should be pointed out that

Table IV. $\frac{\xi(0)}{b}$, b, and $\frac{\xi(0)/b}{\kappa}$ for the niobium and niobium-tantalum alloys studied here

Sample	Description	$\frac{\xi(0)}{b}$	b(Å)	$\frac{\xi(0)/b}{\kappa}$
H-9	Pure Nb	0.019	22,000	0.025
H-19	Nb-1000 ppm Ta	0.022	18,000	0.025
H-13	Nb-5000 ppm Ta	0.029	14,000	0.029
H-11	Nb-10000 ppm Ta	0.044	8,200	0.027

$\frac{\xi(0)}{b}$ was not constant over the entire temperature range studied. This could be due to the assumptions used when analyzing the data or perhaps b is a function of t, in which case no theory exists (49) for the dependence of H_{c3}/H_{c2}.

A detailed understanding of the origin of the perturbation at the surface is not available at the present but reproducible results for a number of pure Nb samples indicate that this perturbation is a basic property of Nb and not an artifact associated with a dirty surface. If the origin of the perturbation is a dirty surface, then it is reproducible dirt. On a macroscopic scale the interaction strength probably is changing abruptly in a region within one or two lattice constants ($\sim$ 10 Å) of the surface where the phonons are soft. The quantities H_{c2} and H_{c3}, however, are average quantities and as such are determined by the electron pairs as a whole. The Cooper pair wave function samples this abrupt change in interaction strength at the surface but averages it out over a distance $\sim \xi$ so that on a macroscopic scale there exists a small perturbation of the interaction strength over a distance comparable to the temperature independent coherence length. If the temperature independent coherence length were shortened (by shortening the electronic mean free path), there should exist an increase in the amount of perturbation observed on the macroscopic scale. This was indeed the result obtained in this experiment.

μ' And μ'' Curve Shape Studies

Calculations of the detailed shape of the $\mu'(H)$ and $\mu''(H)$ curves have always been an elusive and difficult task because pinning forces have

varied a great deal from sample to sample so the experimental facts did not present a consistent picture. For these very carefully prepared Nb samples a fairly consistent behavior arises but all samples do not give identical μ' and μ'' curves. The susceptibility curves of Figure 37 are typical of a large number of samples and demonstrate the reproducibility of the critical fields for two pure niobium samples but they also demonstrate the amount of nonreproducibility in the shapes of the susceptibility curves. End effects are believed to be the most important cause of the change in the shapes of the curves and should be eliminated[1] if a quantitative study is to be made of the flux pinning. It seems worthwhile, however, to try to qualitatively understand the data in terms of the basic theory of pinning. Clem (51) has considered the effects of both surface and bulk pinning on μ'/μ and μ''/μ ($\mu = dB/dH$) and the results of his work are sketched in Figures 38 and 39. Along the x-axis for each graph are the values of $h_s = H_s^*/h_o = (H_{entry} - H_{exit})/2\ h_o$ which arise from the forces due to image vortices. Along the y-axis (into the page) for each graph are the values of $h_b = H_b^*/h_o = \frac{4\pi R J_c}{c h_o}$, where R is the radius of the specimen and J_c is the critical current, which arise from flux flow resistive losses in the bulk. A typical set of susceptibility curves is shown in Figure 40 with characteristic points A, B, C, D, and E. At point A, $H < H_{c1}$ and μ'/μ and μ''/μ are zero since no flux lines are entering the sample to be pinned. For $H \approx H_{c1}$ vortices start to enter and μ'/μ and μ''/μ increase uniformly (monotonically) but the discontinuity (sudden increase then decrease) in μ at H_{c1} causes sudden increases and decreases

[1] Farrell (50) has succeeded in eliminating end effects in a flux flow experiment by using an ancillary field.

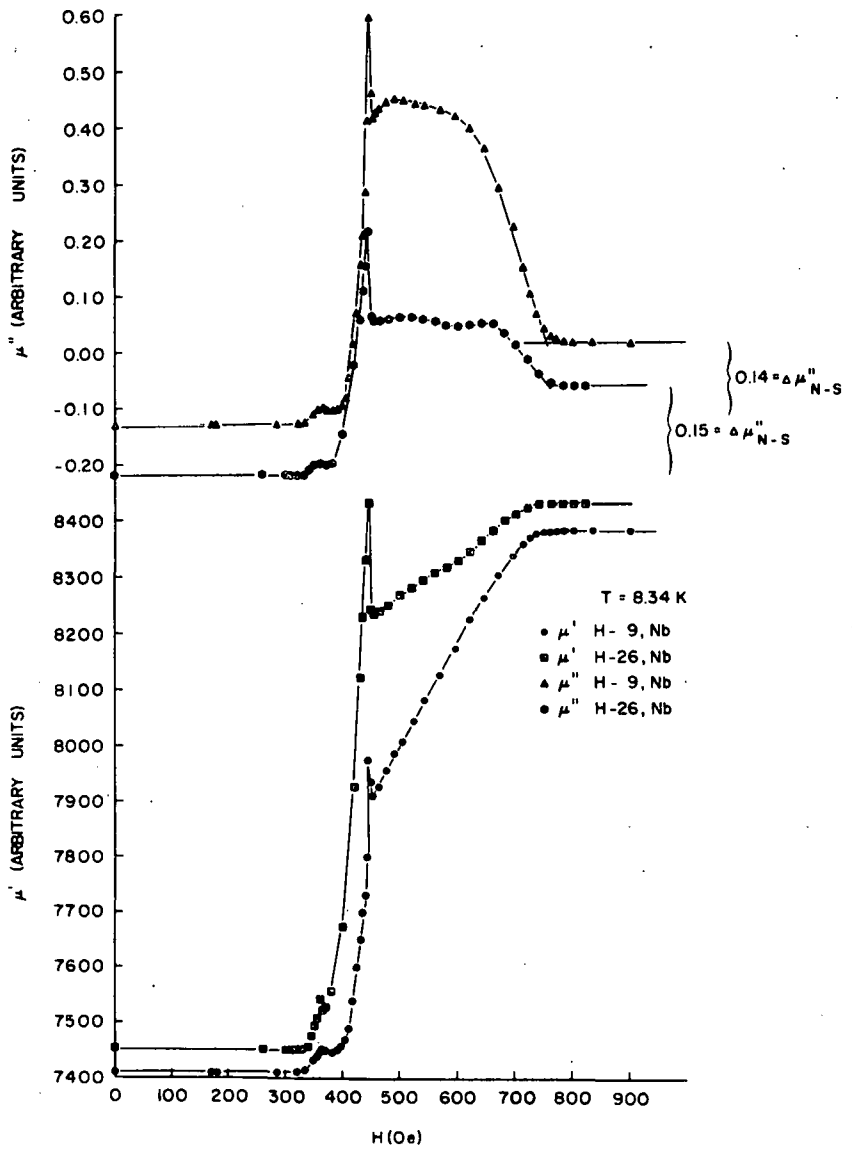

Figure 37. Typical susceptibility curves for the pure niobium samples H-9 and H-26.

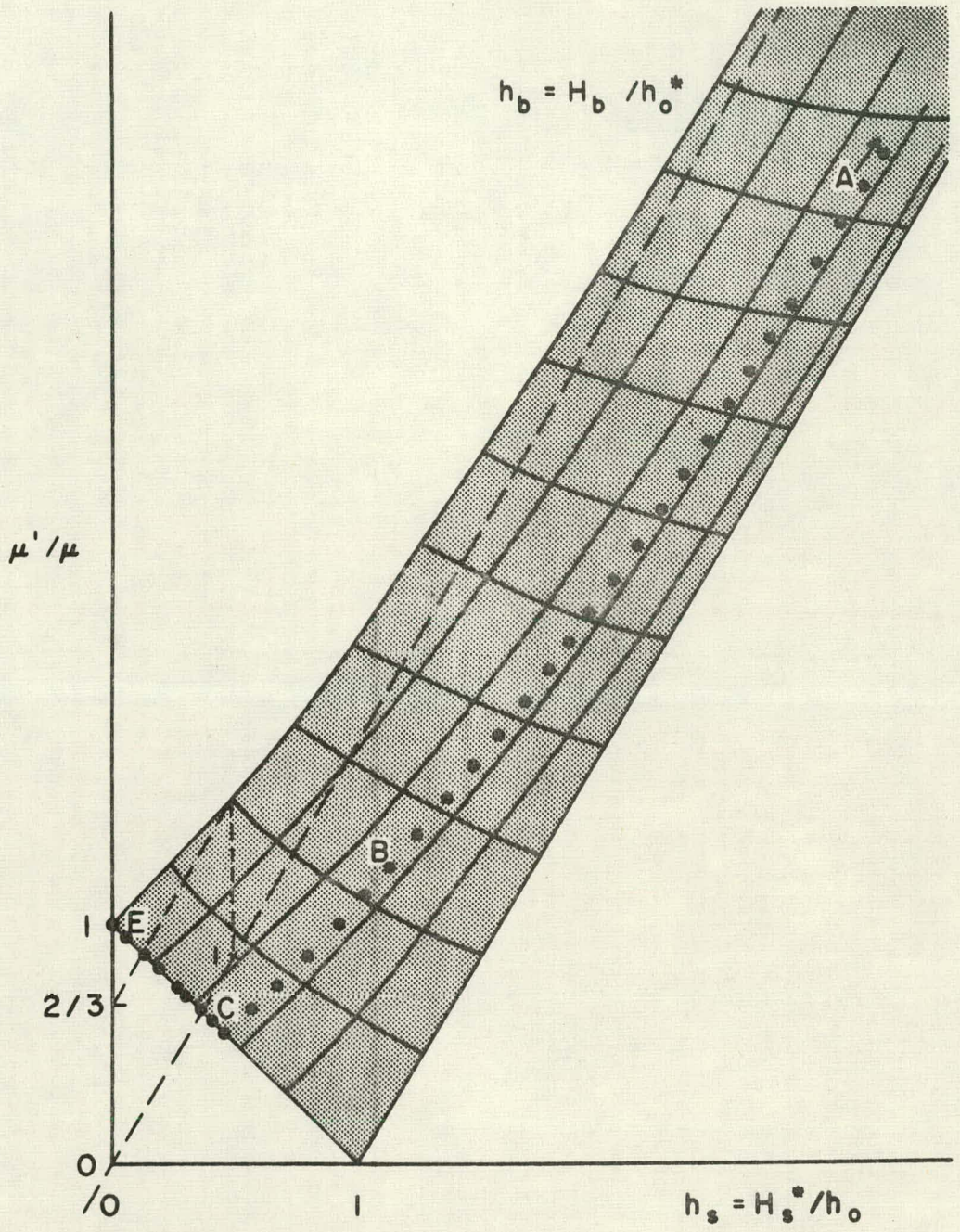

Figure 38. A topological plot of μ'/μ versus h_b and h_s with the characteristic points of the susceptibility curves designated.

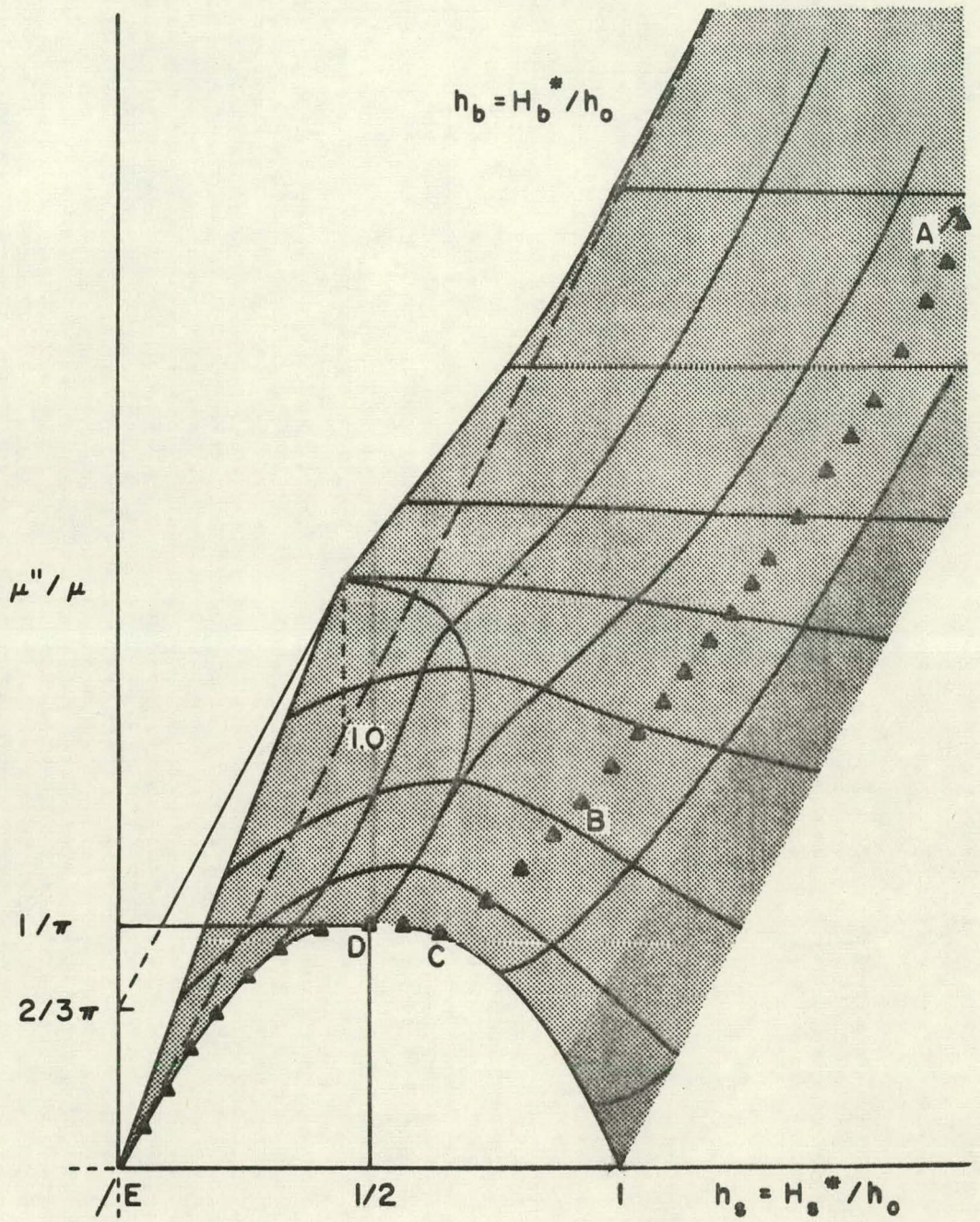

Figure 39. A topological plot of μ''/μ versus h_b and h_s with the characteristic points of the susceptibility curves designated.

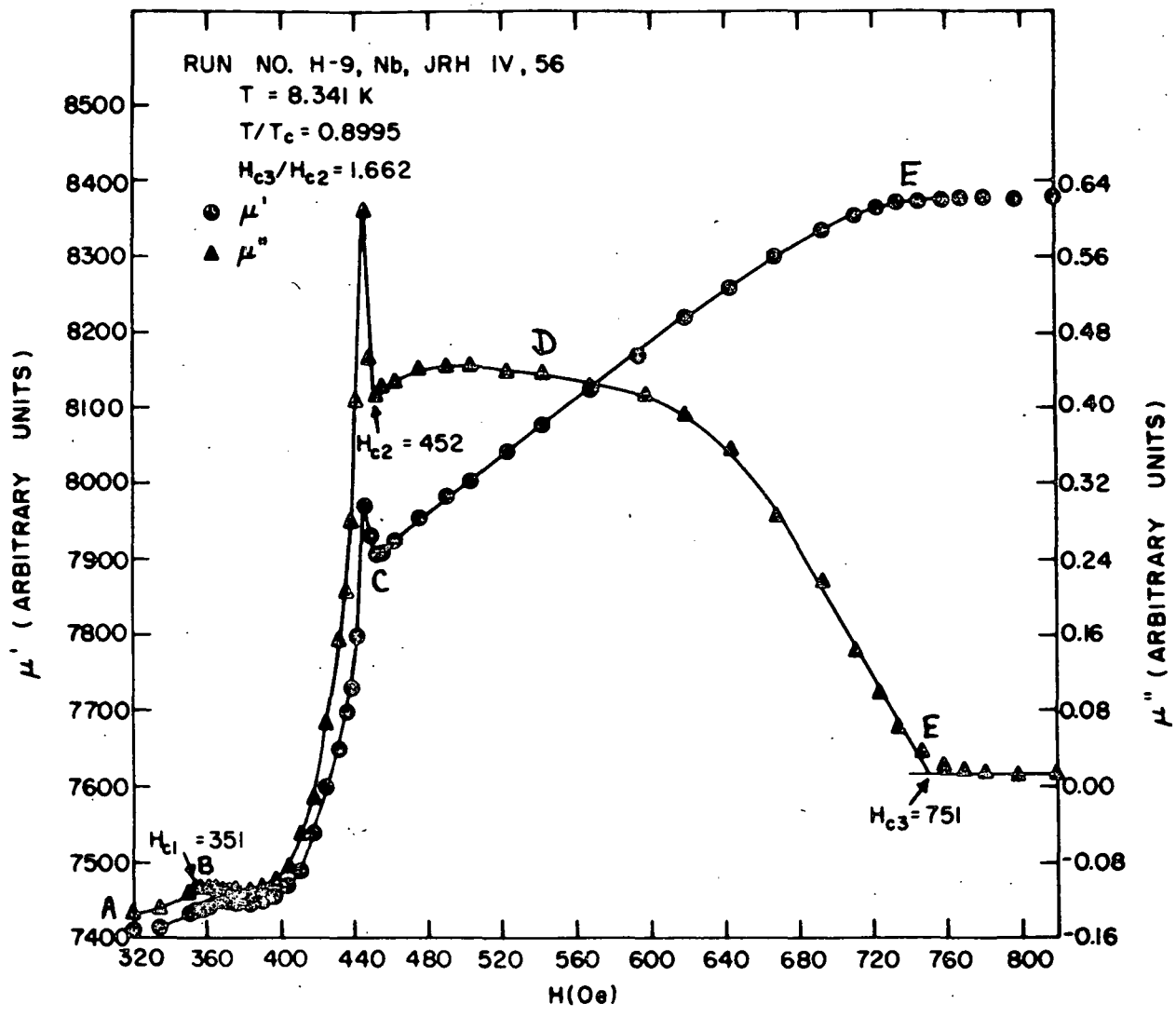

Figure 40. $\mu'(H)$ and $\mu''(H)$ at t = 0.900 with the characteristic flux pinning points A, B, C, D, and E as discussed in the text.

in μ' and μ'' around point B. As H_a is increased still further ($H_{c1} < H_a < H_{c2}$) μ'/μ and μ''/μ increase monotonically. In this region of the applied field μ slowly decreases and hence doesn't affect the general shape of μ' and μ'' much as they monotonically increase. For $H \approx H_{c2}$ μ undergoes another discontinuity (sudden decrease) which causes sudden decreases in μ' and μ'' (point C). For $H_{c2} < H_a < H_{c3}$ there is no bulk pinning and μ'/μ increases linearly to 1 (any nonlinearity in μ' could be due to changes in μ). In this region of the applied field μ''/μ increases to a peak at point D then decreases to zero at H_{c3}. At point E both $(\mu'/\mu-1)$ and μ''/μ equal zero. The reason μ'' does not return completely to zero could be due to eddy currents since $\mu''_{normal} - \mu''_{superconducting}$, $\Delta\mu''_{N-S}$, decreases with increasing Ta content (Figure 41), In much the same way as Γ does (Table II).

Anodization Results

Recent experiments at Karlsruhe and Argonne have indicated a rather novel and important way to prepare surfaces which have a very clean vacuum-insulator interface. The basic idea of the program is to take a Nb sample with a slightly oxidized surface and convert the variety of surface oxides into a tight layer of Nb_2O_5 by anodization (52). Presumably the Nb_2O_5 has a dielectric constant close to 1 and the interface acts in a manner similar to a vacuum-metal interface. A pure niobium sample, H-26, which was prepared in the manner described above, was removed from its glass capsule and electropolished for 20 min at 20 V in a 0.2 normal H_2SO_4 electrolyte. This anodization process forms a layer of Nb_2O_5 about 400 Å thick on the surface of the sample. Susceptibility data were taken

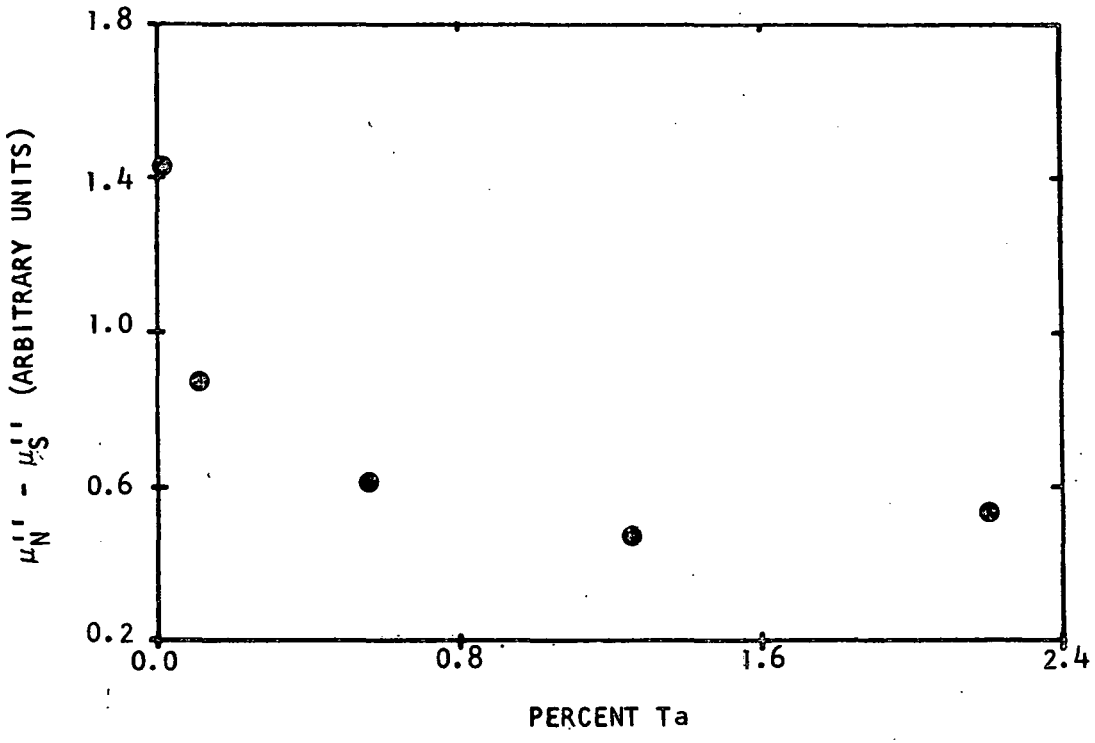

Figure 41. A plot of $\mu_N'' - \mu_S''$ versus the percent Ta contained in the samples.

at several temperatures for this anodized sample and the results of those measurements are compared to the results for the unanodized pure Nb sample, H-9, in Figure 42. The increase in $H_{c3}(T)$ and $H_{c3}(T)/H_{c2}(T)$ may be interpreted as a smaller perturbation of the electron-phonon interaction at the surface and/or a smaller slope of the order parameter at the surface (Figure 42). It appears that the insulating layer of Nb_2O_5 causes the new metallic surface to behave as if it were purer than the metallic surface which existed before the anodization. That is, H_{c3}/H_{c2} versus T/T_c moves toward the clean limit curve of Hu and Korenman (Equation 47).

Frequency Dependence of H_{c3}/H_{c2}

In all of these measurements of surface superconductivity the basic detection mechanism has been set at 31.9 Hz so the measurements are bound to reflect the dynamic response of the vortices to a time varying field. In a way 31.9 Hz might be considered to be static on the time scale of most superconducting phenomena (10^{-10} sec) but extended entities such as vortices might have important time delay phenomena. Hence we set out to look at the frequency dependence of μ', μ'', and the phase boundaries, H_{c1}, H_{c2} and H_{c3} in the low frequency limit.

Using the same type of susceptibility measurements as discussed before H_{c3}/H_{c2} was determined as a function of the frequency, f, at several temperatures. H_{c3} was determined from the μ' curves since eddy current effects ($\Delta\mu''_{N-S}$ is roughly proportional to the square of the frequency) drastically changed the shape of the μ'' curves and made the determination of H_{c3} from the μ'' curves difficult because there was so much variation in behavior from the low frequencies to the high frequencies. H_{c1} and H_{c2} remained

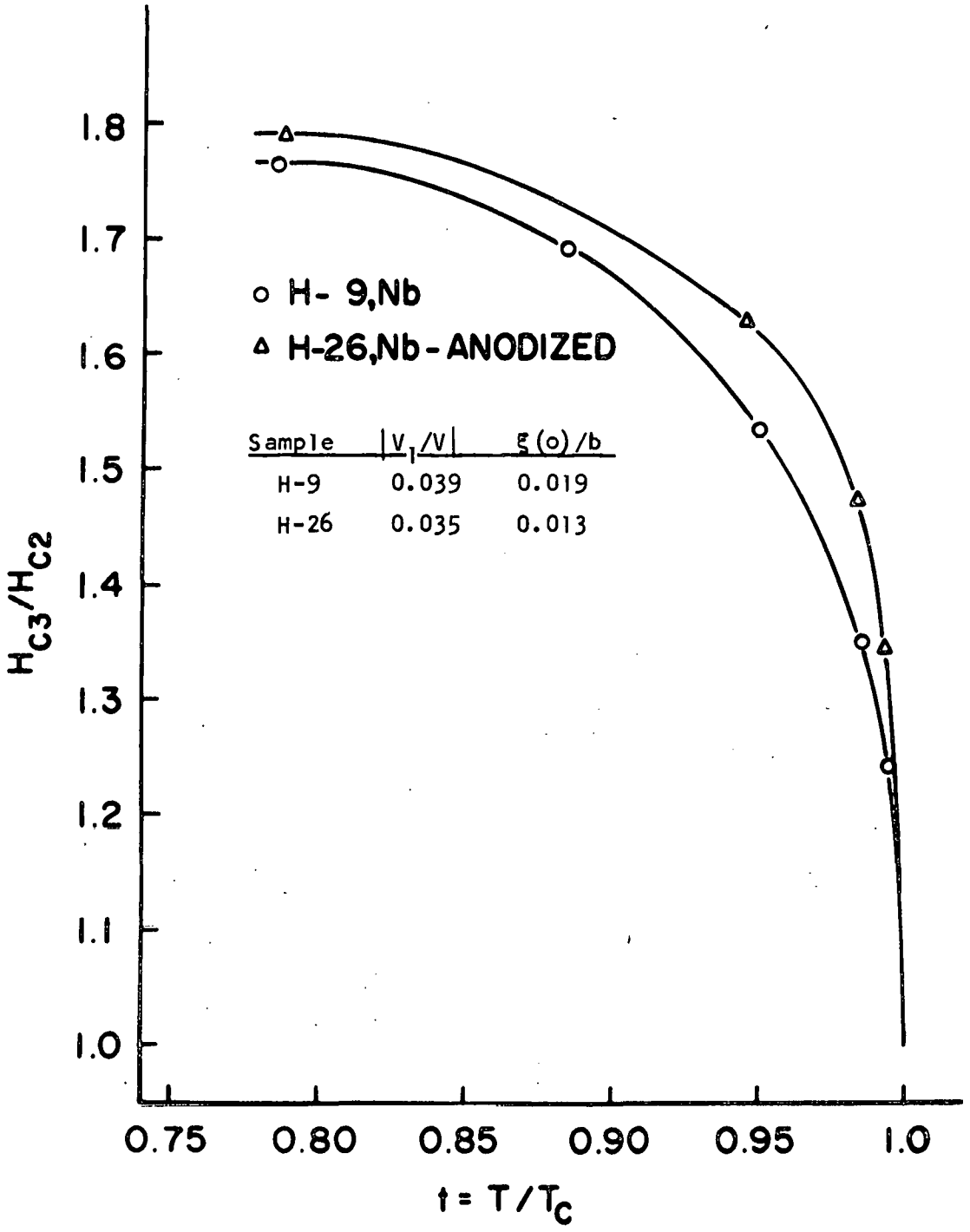

Figure 42. H_{c3}/H_{c2} versus t for the anodized niobium sample, H-26, and the nonanodized niobium sample, H-9.

independent of frequency, but H_{c3} increased somewhat with increasing frequency.

Data obtained from the frequency dependent studies are listed in Table V and a typical graph of $\log_{10} f$ versus H_{c3}/H_{c2} is shown in Figure 43. The results for pure Nb can be summarized as follows:

$$\frac{H_{c3}}{H_{c2}}[T,f] = 0.034 \log_{10} f + \frac{H_{c3}}{H_{c2}}[T,\ f = 1\ \text{Hz}] .$$

It is not clear what causes H_{c3}/H_{c2} to increase as the frequency is increased. The change has the wrong sign to be caused by heating. Ordinarily one would expect an increased energy dissipation at higher frequencies and this is observed in the μ'' curves. This increased dissipation however apparently does not measurably increase the temperature of the surface.

If the data are cast in terms of changes in b, then increasing the frequency decreases the slope of the order parameter and in the case of pure Nb (11 Hz < f < 1100 Hz)

$$\frac{\xi(0)}{b} = 0.043 - 0.009 \log_{10} f, \qquad (60)$$

where $\xi(T) = \xi(0)\epsilon^{-1/2}$.

The frequency dependence data also could be further analyzed to determine the change in interaction strength near the surface as a function of frequency. Z' remains unchanged since

$$\delta h(f,t) = \delta h(t) + \delta h(f) .$$

Table V. Tabulation of the frequency dependence data

f(Hz)	H_{c2}(Oe)	H_{c3}(Oe)	T(K)	$\Delta\mu'_{N-S}$	$\Delta\mu''_{N-S}$
8	534	864	8.207	960	0.049
70	534	885	8.207	934	0.492
160	534	892	8.207	880	2.94
700	532	896	8.210	571	23.40
1600	533	901	8.209	344	113.1
7500	535	906	8.204	190	---
11	214.2	319.4	8.811	970	0.046
110	212.5	323.9	8.812	931	1.08
1100	213.3	332.3	8.812	442	41.65
11000	212.5	332.0	8.812	180	---
11	60.7	78.8	9.138	970	0.046
110	59.9	81.0	9.139	931	1.08
1100	61.2	82.4	9.139	442	41.65
11000	59.8	81.2	9.139	180	---
11	1024	1750	7.284	970	0.046
110	1022	1773	7.288	931	1.08
1100	1019	1802	7.293	442	41.65
11000	1016	1806	7.298	180	---
11	22.6	25.3	9.222	970	0.046
110	21.0	24.4	9.227	931	1.08
1100	21.0	25.0	9.227	442	41.65
11000	21.0	25.0	9.227	180	---

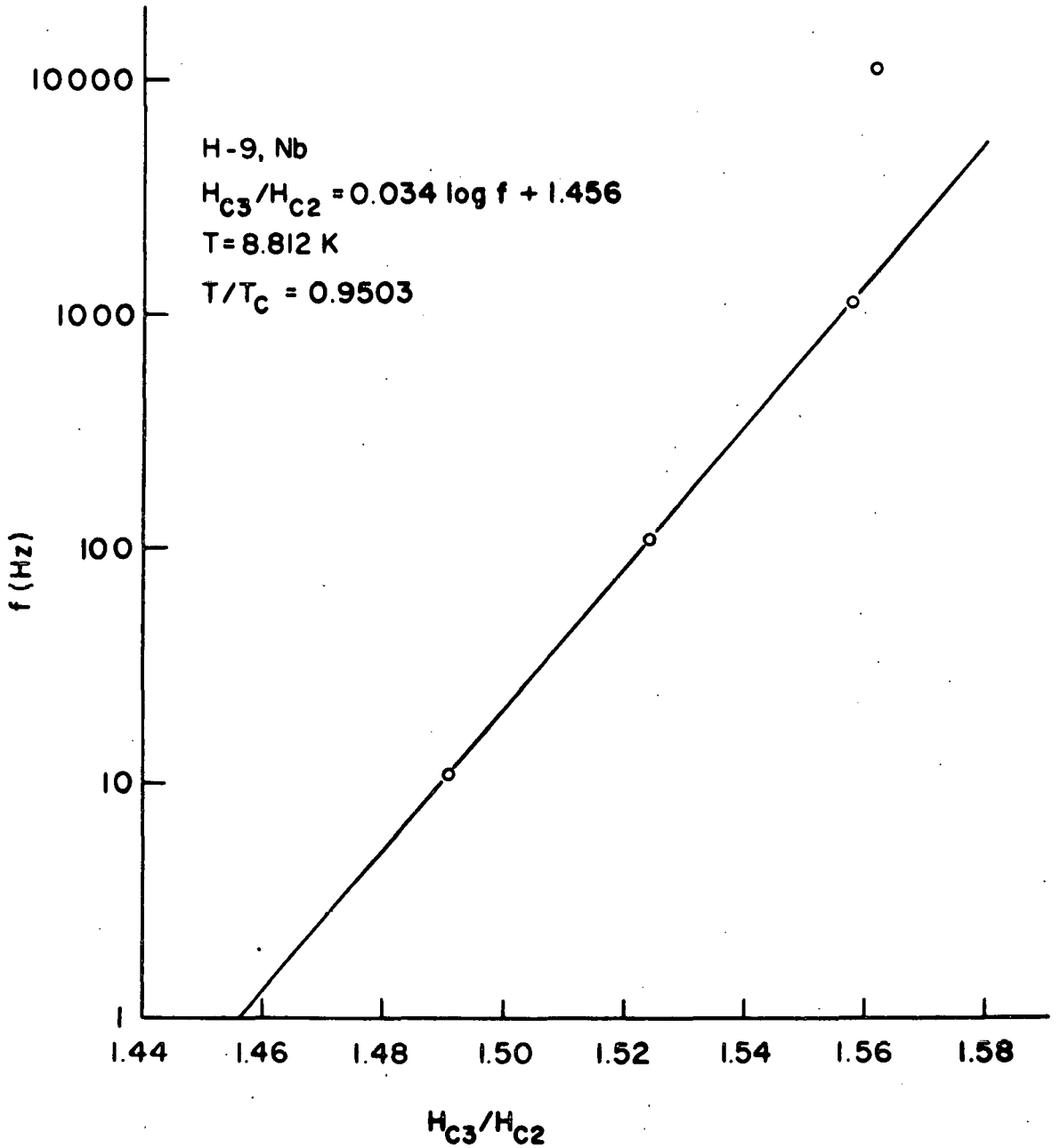

Figure 43. A typical plot of the frequency on a logarithmic scale versus H_{c3}/H_{c2} for pure niobium at a reduced temperature of 0.950.

It appears that $\delta h(t=0)$ decreases for increasing frequency implying that $|V_1/V|$ decreases with increasing frequency. The data was not complete enough to quantitatively determine $|V_1/V|$ and $D/\xi(0)$. Thus, following the previous discussion, increasing the frequency increases the "effective" coherence length thus decreasing the effect of the drop of the magnitude of the interaction strength at the surface and that the higher frequencies increase the distance over which the interaction changes on the macroscopic scale. Unfortunately, at present we do not understand why the effective perturbation at the surface should appear to diminish with increasing frequency.

Comment on End Effects

A small, but important, experimental detail remains concerning the reproducibility of the susceptibility data from sample to sample. Finnemore et al. (35) found that the shapes of the μ' and μ'' curves for pure Nb varied a great deal from sample to sample and there is good evidence now that at least part of this arose from end effects. In Figure 44 is a set of μ' and μ'' curves taken for sample H-9, Nb which was only partially inserted into the measuring coil. This set of curves closely resembles the set of μ' and μ'' curves obtained by Finnemore et al. (35) for sample 53-3, Nb. Hence, it appears that Finnemore et al. (35) obtained curves of different shapes from sample to sample because of end effects; that is, the length of the sample 53-3, Nb was probably much less than the length of the measuring coil.

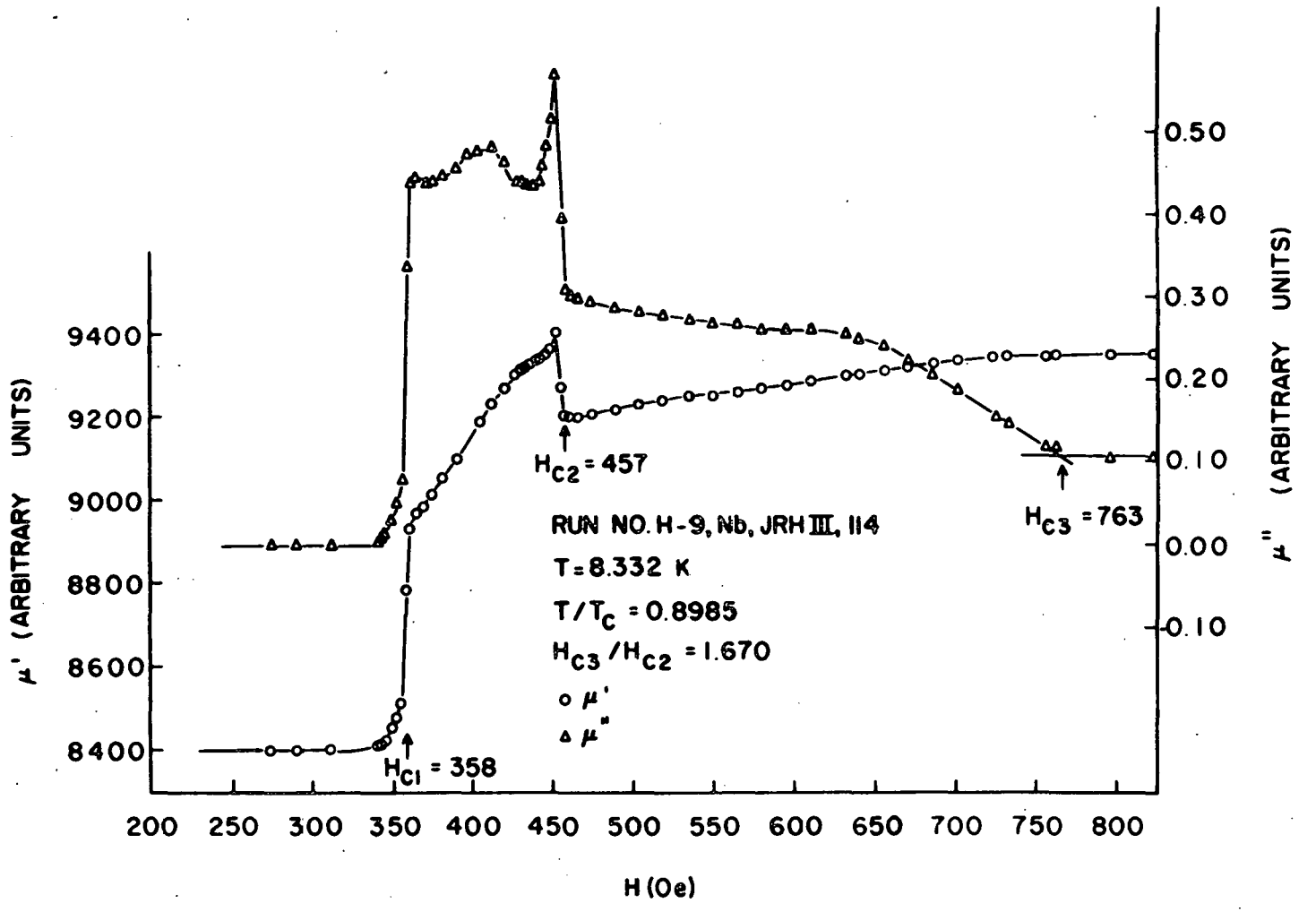

Figure 44. A typical set of susceptibility curves demonstrating the effect of having the sample partially inserted into the measuring coil.

Transition Temperature Measurements

Cappelletti and Rollins (53) have suggested that for a sample which has a reversible magnetization a peak effect should be observable in a susceptibility measurement (μ' versus T) for a low amplitude applied field (small h_o) in the presence of a static field. They have further postulated that this peak will disappear if the residual static magnetic field is identically zero and that the peak will become smaller if h_o is increased. In taking the ac susceptibility data for T_c, μ' was plotted versus T in "zero" static field as in Figure 45. The peak which decreased with increasing h_o is an indication that the residual magnetic field was not identically zero. As mentioned before, the earth's field was cancelled within 0.01 Oe or less using a set of Helmholtz coils and it was not until completion of the experiment that Cappelletti and Rollins ideas came to our attention. Hence, in subsequent ac susceptibility measurements one should be aware that the peak effect may be used to rather sensitively null out the residual magnetic field and it might be a quick way to check samples for reversibility.

The results of the ac susceptibility measurements in "zero" static field are shown in Table VI. The transition temperatures were taken as the temperatures corresponding to $\frac{T_{NOR} - T_{SUP}}{2} \approx T\left(\frac{\mu'_{NOR} - \mu'_{SUP}}{2}\right)$.

Comments on Sample H-23, Nb-20000 ppm Ta

In addition to the samples previously discussed, susceptibility data were obtained for a Nb sample (H-23) with 20000 ppm Ta which was prepared in a separate arc melting process. Several anomalous results occurred for this sample which indicate that susceptibility measurements should be taken

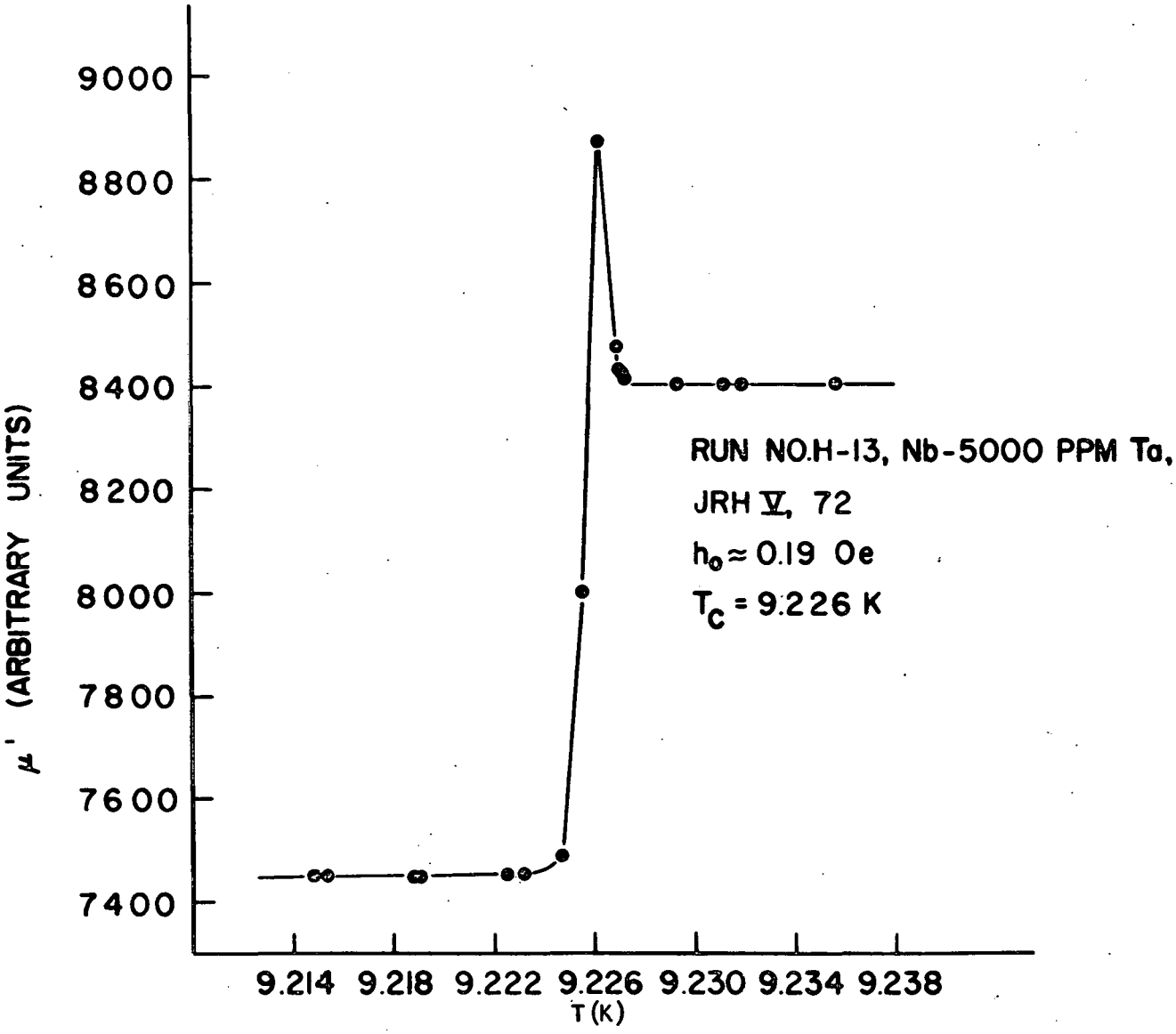

Figure 45. A plot of μ' versus T for sample H-13 in "zer" static applied field.

Table VI. Transition temperatures of the samples

Sample	T_c(K)
H-9,Nb	9.273
H-19,Nb-1000 ppm Ta	9.259
H-13,Nb-5000 ppm Ta	9.226
H-11,Nb-10000 ppm Ta	9.079
H-23,Nb-20000 ppm Ta	9.042

on a similarly prepared sample to check the reproducibility of the data obtained for a Nb sample doped with 20000 ppm Ta. The difference in μ'' between the normal and superconducting states ($= \Delta\mu''_{N-S}$) is shown in Figure 41 for all samples. $\Delta\mu''_{N-S}$, which is a measure of the residual conductivity of the normal state and which is a function of h_o, f, and the volume of the sample, is unexpectedly greater for H-23 than for H-11,Nb-10000 ppm Ta. The critical field curves for H-23 do not follow the general trend set by the other samples as the Ta content is increased (Figures 30, 31, and 37). In fact, if we consider $\kappa_1 = \frac{H_{c2}}{\sqrt{2}H_c}$ and $H_c \approx \sqrt{H_{c1}H_{c2}}$ then $\kappa \approx \sqrt{H_{c2}/2H_{c1}}$ which implies $\kappa_{20\ K} < \kappa_{10\ K}$ in agreement with the $\Delta\mu''_{N-S}$ result. The most startling anomaly, however, was the plot of H_{c3}/H_{c2} versus T/T_c (Figure 46) for H-23. It is not clear, at this time, what caused the anomalous results for this sample and until a similar sample is prepared and the critical fields curves are determined we must consider the results of the measurements on this sample as questionable.

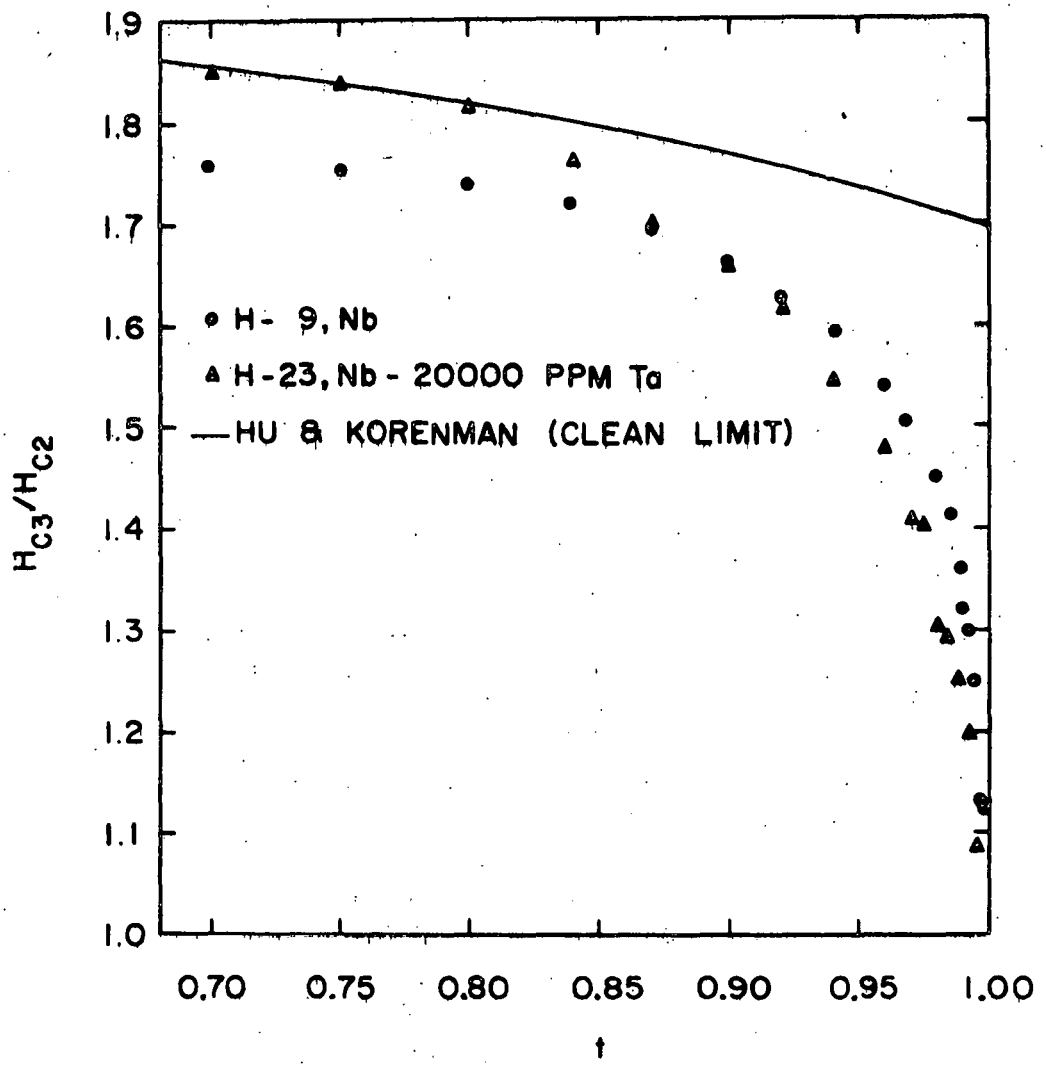

Figure 46. The anomalous behavior of H_{c3}/H_{c2} for sample H-23, Nb-20000 ppm Ta.

BIBLIOGRAPHY

1. H. K. Onnes, Commun. Kamerlingh Onnes Lab. Univ. Leiden, Suppl. 34B, 55 (1913).

2. P. Drude, Annalen der Physik 1, 566 (1900); 3, 369 (1900).

3. D. Shoenberg, Superconductivity, B. H. Flowers and J. M. Ziman, ed. Cambridge Monographs on Physics, pp. 14-16, The Syndics of the Cambridge Univ. Press, New York, N.Y. 1962.

4. W. Meissner and R. Ochsenfeld, Naturwissen 21, 787 (1933).

5. C. J. Gorter and H. B. G. Casimir, Physica 1, 306 (1934).

6. F. London and H. London, Proc. Roy. Soc. A149, 71 (1935); Physica 2, 341 (1935).

7. D. Shoenberg, Proc. Roy. Soc. A175, 49 (1940).

8. A. B. Pippard, Proc. Roy. Soc. A216, 547 (1953).

9. J. Bardeen, L. N. Cooper, and J. R. Schrieffer, Phys. Rev. 108, 1175 (1957).

10. D. K. Finnemore, Ames Lab. A.E.C., Ames, Iowa. Private Communication. 1972.

11. L. W. Shubnikov, V. I. Khotkevich, J. D. Shepelev, and J. N. Rjabinin, Zh. Eksperim. i Teor. Fiz. 7, 221 (1937).

12. W. H. Kleiner, L. N. Roth, and S. H. Autler, Phys. Rev. 133A, 1226 (1964).

13. H. Träuble and U. Essmann, J. Appl. Phys. 39, 4052 (1968).

14. D. Saint-James and P. G. de Gennes, Phys. Letters 7, 306 (1963).

15. C. F. Hempstead and Y. B. Kim, Phys. Rev. Letters 12, 145 (1964).

16. V. L. Ginzburg and L. D. Landau, Zh. Eksperim. i Teor. Fiz. 20, 1064 (1950).

17. L. P. Gor'kov, Zh. Eksperim. i Teor. Fiz. 36, 1918 (1959); Soviet Phys. JETP 9, 1364 (1959).

18. L. P. Gor'kov, Zh. Eksperim. i Teor. Fiz. 36, 1407 (1959); Soviet Phys. JETP 10, 998 (1960).

19. P. G. de Gennes, Rev. Mod. Phys. 36, 225 (1964).

20. A. A. Abrikosov, Dokl. Akad. Nauk. SSSR 86, 489 (1962).

21. D. Saint-James, E. J. Thomas, and G. Sarma, Type II Superconductivity. D. ter Haar, ed. International Series of Monographs in Natural Philosophy 17, pp. 81-121, Oxford, England, Pergamon Press Ltd. 1969.

22. P. G. de Gennes, Superconductivity of Metals and Alloys. D. Pines, ed. Frontiers in Physics, pp. 171-201, New York, N.Y., W. A. Benjamin Inc. 1966.

23. B. Serin, Contribution to Type II Superconductors Conference, Cleveland, Ohio. 1964.

24. G. Ebneth and L. Tewordt, Z. Physik 185, 421 (1965).

25. G. Lüders, Z. Physik 202, 8 (1967).

26. C. R. Hu and V. Korenman, Phys. Rev. 178, 684 (1969).

27. C. R. Hu and V. Korenman, Phys. Rev. 185, 672 (1969).

28. J. E. Ostenson and D. K. Finnemore, Phys. Rev. Letters 22, 188 (1969).

29. C. R. Hu, Phys. Rev. 187, 574 (1969).

30. L. N. Cooper, Amer. J. Phys. 28, 91 (1960).

31. J. E. Ostenson, J. R. Hopkins, and D. K. Finnemore, Physica 55, 502 (1971).

32. W. de Sorbo, Phys. Rev. 130, 2177 (1963).

33. W. de Sorbo, Phys. Rev. 132, 107 (1963).

34. W. de Sorbo, Phys. Rev. 134A, 1119 (1964).

35. D. K. Finnemore, T. F. Stromberg, and C. A. Swenson, Phys. Rev. 149, 231 (1966).

36. E. Fromm and H. Jehn, Vacuum 19, 191 (1969).

37. T. Hurlen, J. Kjollesdal, J. Markali, and N. Norman, Tech. Note No. 1, Contract No. AF61 (052)-90, April. (1959).

38. J. M. Dickey, H. H. Farrell, O. F. Kammerer, and M. Strongin, Phys. Letters 32A, 483 (1970).

39. T. F. Stromberg, Unpublished Ph.D. Thesis, Iowa State University Library, Ames, Iowa. 1965.

40. D. T. Peterson, Ames Lab. A.E.C., Ames, Iowa. Sample history data. Private Communication. 1971.

41. D. T. Peterson, F. A. Schmidt, and J. D. Verhoeven, Trans. AIME 236, 1311 (1966).

42. A. Ikushima and T. Mizusaki, J. Phys. Chem. Solids 30, 873 (1959).

43. J. R. Carlson, Unpublished Ph.D. Thesis, University of Illinois Library, Urbana, Illinois. 1968.

44. R. W. Rollins and J. Silcox, Phys. Rev. 155, 404 (1969).

45. J. R. Clem, Ames Lab. A.E.C., Ames, Iowa. Private Communication. 1972.

46. T. Ogasawara, Unpublished Ph.D. Thesis, Nihon University Library No. NUP-B-67-8 (1967).

47. H. J. Fink and W. C. H. Joiner, Phys. Rev. Letters 23, 120 (1969).

48. B. B. Goodman, IBM J. Res. Develop. 6, 63 (1962); Phys. Rev. Letters 6, 597 (1961).

49. M. D. Maloney, F. de la Cruz, and M. Cardona, Phys. Rev. B2, 2512 (1970).

50. D. E. Farrell, Phys. Rev. Letters 28, 154 (1972).

51. J. R. Clem, Ames Lab. A.E.C., Ames, Iowa. Private Communication. 1972.

52. Argonne Natl. Lab. A.E.C., Argonne, Illinois. Private Communication. 1972.

53. R. Cappelletti and R. Rollins, Ohio University, Akron, Ohio. Private Communication. 1972.

54. H. Träuble and U. Essmann, Phys. Stat. Sol. 25, 373 (1968).

55. U. Krageloh, U. Kumpf, and A. Seeger, Proceedings of the Twelfth International Conference on Low Temperature Physics, Kyoto 1970, ed. E. Kanda, Academic Press of Japan, Tokyo, p. 473 (1971).

56. A. Seeger, Comments Solid State Phys. 3, 97 (1970).

57. J. Schelten, H. Ullmaier, and W. Schmatz, Phys. Stat. Sol. B48, 619 (1971).

58. D. K. Finnemore, J. R. Clem, and T. F. Stromberg, Phys. Rev., to be published August (1972).

59. A. E. Jacobs, Phys. Rev. B4, 3029 (1971).

60. J. E. Ostenson, Unpublished M.S. Thesis, Iowa State University Library, Ames, Iowa. 1969.

61. D. K. Finnemore, Ames Lab. A.E.C., Ames, Iowa. Private Communication. 1972.

ACKNOWLEDGMENTS

The author wishes to express his gratitude to Dr. D. K. Finnemore for his active interest and guidance throughout the course of this investigation and for his advice concerning the preparation of the manuscript. He also wishes to thank Dr. C. A. Swenson and Dr. J. R. Clem for their instruction and helpful suggestions.

The work of Dr. D. T. Peterson and members of his metallurgy group in helping to prepare the samples is appreciated.

APPENDIX I: TABULATION OF THE CRITICAL FIELDS DATA AND SOME TYPICAL SUSCEPTIBILITY DATA

Tables VII-XI contain the critical fields data for the samples discussed in this work. Table XII contains the susceptibility data for the runs used for the figures in the text.

Table VII. Critical fields data for sample H-9,Nb

T(K)	H_{c1}(Oe)	H_{c2}(Oe)	H_{c3}(Oe)
9.252	8.0	9.8	11.0
9.238	12.9	17.5	19.8
9.219	21.8	24.3	30.35
9.197	29.8	34.3	44.55
9.177	38.2	43.1	57.0
9.173	38.7	43.5	59.2
9.130	56.4	64.1	90.6
9.084	74.4	86.2	125.2
8.978	114.2	133.0	200.2
8.899	145.0	172.7	266.2
8.722	211	257	410
8.530	281	351	571
8.341	351	452	751
8.068	443	594	1006
7.782	545	750	1291
7.407	665	955	1661
6.953	830	1214	2131
6.483		1475	2595
6.031		1737	3068
5.561		2000	3547
5.100		2250	4010

Table VIII. Critical fields data for sample H-19,Nb-1000 ppm Ta

T(K)	H_{c1}(Oe)	H_{c2}(Oe)	H_{c3}(Oe)
9.238	6.95	11.70	13.12
9.222	13.9	19.02	22.2
9.201	22.7	28.6	35.0
9.186	28.7	35.2	45.0
9.165	37.1	45.1	60.3
9.121	52.9	63.5	88.3
9.070	73.6	87.9	127.0
9.023	89.1	109.6	161.8
8.983	105.5	130.5	196
8.889	141	176	270
8.797	176	222	348
8.702	210	269	427
8.522	276	362	589
8.331	342	464	768
8.055	437	612	1030
7.775	530	768	1309

Table IX. Critical fields data for sample H-13, Nb-5000 ppm Ta

T(K)	H_{c1}(Oe)	H_{c2}(Oe)	H_{c3}(Oe)
9.210	5.5	7.50	7.50
9.203	5.8	8.40	8.40
9.184	14.0	18.05	19.50
9.174	17.7	22.8	25.3
9.153	26.1	31.5	37.3
9.147	28.8	36.2	44.4
9.119	41.0	49.0	61.5
9.115	42.0	50.5	64.0
9.083	52.9	67.2	88.0
9.075	53.1	66.0	86.1
9.057	65.5	83.1	113.0
9.042	68.0	87.4	118.6
9.037	69.4	90.4	123.6
8.995	84.4	108.8	155.4
8.994	86.2	111.2	157.5
8.952	102.0	134.0	192.0
8.945	104.0	135.0	196.0
8.858	138	183.5	271.7
8.851	139.5	183.2	270.5
8.762	173	232	354
8.757	175	232	350
8.671	205.5	276.5	424.5
8.581	240	328	508
8.484	273	377	594
8.400	305	426	682
8.298	338	480	775
8.115	402	584	965
8.022	432	634	1046
7.750	520	790	1332
7.380	637	1007	1725
7.377	641	1007	1719
6.915	780	1287	2215
6.911	777	1280	2211
6.460	905	1560	2720
5.993	1005	1850	3220

Table X. Critical fields data for sample H-11,Nb-10000 ppm Ta

T(K)	H_{c1}(Oe)	H_{c2}(Oe)	H_{c3}(Oe)
9.034	15.0	42.8	42.8
9.006	21.7	61.0	61.0
8.989	25.5	73.0	73.4
8.943	38.0	97.0	106.2
8.941	44.8	101.8	112.7
8.908	52.5	120.0	139.0
8.806	85.5	187	242
8.716	114	247	335
8.625	145	306	445
8.536	170	370	548
8.534	170	370	549
8.352	230	510	781
8.169	282	645	1008
7.897	367	850	1361
7.626	445	1057	1720
7.264	540	1338	2225
6.811	645	1690	2822
6.355	760	2050	3442
5.891		2410	4100

Table XI. Critical fields data for sample H-23,Nb-20000 ppm Ta

T(K)	H_{c1}(Oe)	H_{c2}(Oe)	H_{c3}(Oe)
8.999	17.3	34.4	37.3
8.970	20.1	53.5	64.1
8.933	32.8	76.5	95.8
8.898	45.2	97.2	125.7
8.865	51.0	118.5	154.5
8.816	68.0	149.3	209.3
8.776	91	174.0	245.0
8.683	120	234.5	346.5
8.498	180	360	556
8.325	231	471	760
8.137	290	602	997
7.868	367	787	1336
7.596	432	960	1695
7.231	540	1205	2185
6.782	650	1530	2810
6.325	775	1870	3465

Table XII. Tabulation of the susceptibility data for the runs used in the figures of the text

μ'	μ''	H	μ'	μ''	H
H-9, Nb (T=8.332 K)					
8399	-0.005	0.00	9274	0.258	579
8400	-0.005	274	9282	0.258	595
8401	-0.005	290	9291	0.258	610
8402	-0.005	313	9303	0.250	631
8412	0.000	340	9309	0.247	640
8418	0.005	343	9319	0.238	656
8428	0.009	346	9327	0.223	671
8455	0.026	349	9335	0.205	686
8482	0.048	352	9343	0.186	701
8518	0.074	355	9351	0.153	724
8785	0.333	358	9353	0.145	732
8935	0.431	361	9356	0.120	756
8970	0.439	364	9357	0.118	762
8985	0.433	369	9358	0.106	796
9017	0.435	374	9358	0.106	822
9055	0.441	381			
9100	0.448	389	H-9, Nb (T=9.252 K)		
9155	0.467	396			
9196	0.469	404	7405	-0.132	0.00
9237	0.474	412	7407	-0.132	2.59
9275	0.457	419	7409	-0.132	3.66
9305	0.435	427	7411	-0.130	4.42
9314	0.433	430	7416	-0.130	5.34
9322	0.431	433	7421	-0.128	5.95
9331	0.429	436	7425	-0.127	6.40
9340	0.435	439	7434	-0.125	7.01
9343	0.452	442	7438	-0.125	7.17
9351	0.474	445	7444	-0.123	7.32
9365	0.508	448	7448	-0.122	7.47
9405	0.562	451	7450	-0.122	7.62
9275	0.392	454	7452	-0.122	7.78
9205	0.306	457	7462	-0.120	7.93
9203	0.298	460	7560	-0.061	8.08
9205	0.298	465	7600	-0.020	8.23
9211	0.292	473	7750	-0.009	8.54
9221	0.284	488	8100	+0.909	8.69
9232	0.280	503	8600	2.000	8.84
9243	0.276	518	8830	1.724	8.99
9251	0.270	534	8900	1.538	9.15
9257	0.267	549	8850	1.111	9.30
9266	0.264	564	8700	0.909	9.45

Table XII (Continued)

μ'	μ''	H
8500	0.476	9.60
8377	0.062	9.76
8375	0.034	9.91
8374	0.025	10.06
8374	0.024	10.21
8373	0.018	10.52
8372	0.012	10.98
8372	0.011	11.59
8372	0.011	12.35
8372	0.011	13.57
H-9, Nb (T=8.978 K)		
7397	-0.133	0.0
7398	-0.133	65.1
7400	-0.133	84.0
7400	-0.133	91.9
7403	-0.133	100.0
7411	-0.130	107.8
7421	-0.123	109.9
7426	-0.122	110.8
7433	-0.118	111.6
7442	-0.110	112.4
7454	-0.102	113.1
7480	-0.076	113.9
7525	-0.031	114.8
7595	0.039	115.6
7590	0.023	116.3
7610	0.025	117.1
7625	0.053	118.0
7650	0.071	118.8
7670	0.091	119.5
7680	0.100	120.3
7705	0.122	121.0
7715	0.136	121.8
7744	0.163	122.7
7763	0.184	123.5
7777	0.203	124.2
7813	0.250	125.0
7826	0.274	125.8
7821	0.270	126.5
7841	0.323	127.3
7951	0.500	129.0
8163	0.714	130.6
8063	0.455	132.2
8000	0.347	133.7
8013	0.351	135.2
8026	0.353	136.9
8052	0.364	139.9
8076	0.370	143.2
8098	0.373	146.2
8118	0.377	149.4
8138	0.380	152.5
8167	0.385	157.2
8201	0.385	161.9
8235	0.375	166.6
8265	0.351	171.0
8293	0.310	175.8
8316	0.265	180.3
8336	0.209	184.9
8353	0.150	189.5
8364	0.088	194.1
8370	0.036	198.6
8372	0.012	203.2
8372	0.012	207.8
8372	0.012	212.4
8372	0.012	216.9
H-9, Nb (T=8.341 K)		
7410	-0.132	0.0
7410	-0.132	171
7410	-0.132	178
7411	-0.130	285
7412	-0.130	320
7414	-0.128	335
7434	-0.112	351
7438	-0.106	354
7441	-0.106	357
7444	-0.105	361
7453	-0.104	365
7451	-0.105	368
7449	-0.107	372
7448	-0.108	375
7448	-0.108	383
7451	-0.105	390
7457	-0.097	397
7470	-0.083	404

Table XII (Continued)

μ'	μ''	H
7491	-0.050	411
7539	0.009	418
7600	0.068	425
7650	0.153	432
7701	0.205	436
7730	0.282	439
7800	0.408	442
7973	0.588	446
7933	0.454	449
7907	0.413	453
7909	0.422	456
7926	0.427	463
7954	0.439	476
7984	0.444	491
8006	0.444	504
8042	0.437	524
8078	0.435	543
8126	0.424	569
8170	0.413	595
8220	0.392	620
8261	0.355	645
8299	0.286	669
8334	0.215	694
8355	0.144	712
8365	0.097	724
8372	0.061	735
8374	0.035	747
8376	0.022	759
8377	0.015	770
8377	0.013	782
8377	0.011	799
8377	0.011	833
8377	0.011	898

H-9, Nb (T=7.407 K)

7410	-0.132	0.0
7410	-0.131	640
7412	-0.129	656
7415	-0.127	668
7420	-0.123	683
7416	-0.124	695
7416	-0.124	710
7415	-0.125	724
7415	-0.125	747
7415	-0.124	765
7415	-0.125	796
7416	-0.124	829
7421	-0.119	855
7434	-0.104	877
7449	-0.090	890
7465	-0.068	902
7475	-0.049	915
7476	-0.024	927
7505	0.045	938
7547	0.120	944
7600	0.238	950
7642	0.294	956
7642	0.290	962
7647	0.294	973
7675	0.333	997
7710	0.355	1021
7795	0.428	1088
7900	0.476	1156
7975	0.512	1217
8050	0.512	1284
8120	0.500	1349
8187	0.465	1412
8257	0.385	1476
8315	0.274	1537
8358	0.137	1601
8368	0.076	1633
8372	0.045	1665
8375	0.029	1695
8376	0.021	1729
8376	0.018	1759
8376	0.018	1791
8376	0.018	1823

H-13, Nb-5000 ppm Ta (T=8.945 K)

7466	-0.127	0.0
7465	-0.127	86.9
7466	-0.127	97.6
7468	-0.127	98.3
7469	-0.127	99.1
7470	-0.127	99.9

Table XII (Continued)

μ'	μ''	H	μ'	μ''	H
7472	-0.126	100.6	8480	0.132	134.5
7479	-0.124	101.4	8400	0.099	134.9
7489	-0.121	102.1	8362	0.069	135.3
7516	-0.105	102.9	8353	0.066	135.1
7542	-0.100	103.7	8352	0.066	136.4
7561	-0.094	104.4	8353	0.066	137.2
7610	-0.086	105.2	8354	0.062	138.7
7640	-0.076	106.0	8359	0.062	140.3
7620	-0.086	106.7	8367	0.059	143.3
7620	-0.086	107.5	8373	0.057	146.4
7637	-0.076	108.2	8378	0.055	149.4
7647	-0.071	109.0	8381	0.052	152.5
7667	-0.062	109.8	8385	0.049	155.5
7683	-0.055	110.5	8391	0.042	158.5
7712	-0.045	112.1	8396	0.033	162.2
7755	-0.028	113.6	8400	0.026	164.6
7775	-0.016	115.1	8404	0.018	167.8
7815	0.005	116.6	8408	0.009	170.7
7857	0.022	118.1	8410	0.000	173.8
7890	0.040	119.7	8413	-0.010	176.8
7935	0.062	121.2	8415	-0.020	179.9
8025	0.103	122.7	8417	-0.028	182.9
8080	0.134	123.5	8419	-0.037	186.0
8120	0.147	123.9	8420	-0.045	189.0
8155	0.159	124.2	8421	-0.052	192.1
8185	0.167	124.6	8422	-0.059	195.1
8210	0.175	125.0	8422	-0.064	198.2
8230	0.182	125.4	8422	-0.066	201.2
8262	0.192	125.8	8422	-0.066	204.3
8280	0.200	126.2	8422	-0.066	210.4
8305	0.208	126.5	8422	-0.066	216.5
8330	0.222	127.3			
8382	0.241	128.1	H-13, Nb-5000 ppm Ta		
8430	0.267	128.8	(T=8.298 K)		
8475	0.294	129.6			
8530	0.320	130.3	7466	-0.127	0.0
8565	0.341	131.1	7466	-0.126	322
8625	0.377	131.9	7479	-0.121	332
8655	0.400	132.2	7497	-0.110	338
8685	0.417	132.6	7527	-0.112	341
8715	0.435	133.0	7541	-0.112	345
8770	0.455	133.4	7539	-0.112	348
8790	0.435	133.8	7540	-0.112	351
8725	0.370	134.2	7559	-0.110	355

Table XII (Continued)

μ'	μ''	H	μ'	μ''	H
7575	-0.106	361	7470	-0.124	620
7592	-0.097	369	7476	-0.119	628
7634	-0.086	378	7490	-0.112	636
7685	-0.071	389	7502	-0.109	643
7736	-0.059	401	7516	-0.109	651
7797	-0.037	415	7527	-0.109	659
7927	0.005	430	7527	-0.109	666
8097	0.038	444	7532	-0.108	675
8243	0.064	456	7540	-0.105	686
8374	0.149	466	7552	-0.101	698
8426	0.191	470	7572	-0.092	712
8464	0.225	473	7586	-0.086	727
8404	0.154	476	7607	-0.081	744
8310	0.090	479	7627	-0.074	762
8310	0.083	482	7648	-0.064	782
8311	0.083	485	7669	-0.055	803
8316	0.079	492	7693	-0.044	826
8326	0.074	508	7744	-0.028	851
8335	0.066	523	7795	-0.009	877
8343	0.062	538	7878	0.017	912
8352	0.059	553	7968	0.038	936
8359	0.055	569	8047	0.074	959
8366	0.051	584	8132	0.256	982
8373	0.049	599	8244	0.263	989
8380	0.045	614	8345	0.220	997
8387	0.039	630	8300	0.161	1005
8393	0.029	645	8289	0.141	1012
8399	0.023	660	8290	0.137	1020
8405	0.012	675	8292	0.135	1028
8408	0.000	691	8298	0.132	1043
8411	-0.015	706	8308	0.122	1073
8416	-0.026	721	8318	0.112	1108
8419	-0.037	736	8328	0.103	1139
8420	-0.050	752	8336	0.094	1172
8421	-0.060	767	8344	0.084	1206
8421	-0.064	782	8350	0.076	1238
8421	-0.066	797	8356	0.069	1270
8421	-0.066	813	8362	0.064	1303
8421	-0.066	843	8368	0.060	1335
			8375	0.053	1366
H-13, Nb-5000 ppm Ta (T=7.377 K)			8381	0.047	1399
			8387	0.041	1432
			8393	0.031	1464
7466	-0.127	0.0	8399	0.023	1497
7465	-0.127	559	8405	0.011	1529

Table XII (Continued)

μ'	μ''	H
8410	0.000	1560
8413	-0.014	1592
8416	-0.026	1622
8418	-0.039	1654
8420	-0.052	1685
8420	-0.062	1717
8420	-0.066	1747
8420	-0.066	1810
H-11, Nb-10000 ppm Ta (T=8.806 K)		
7532	-0.118	0.00
7531	-0.118	62.5
7532	-0.118	74.7
7537	-0.116	79.1
7541	-0.116	80.8
7552	-0.114	83.8
7563	-0.110	85.4
7572	-0.109	86.9
7580	-0.106	88.4
7590	-0.102	89.9
7597	-0.101	91.5
7598	-0.101	93.0
7600	-0.100	94.5
7600	-0.099	97.6
7613	-0.098	100.6
7660	-0.083	105.2
7703	-0.069	109.8
7768	-0.045	114.3
7815	-0.028	118.9
7915	0.009	126.5
8003	0.050	134.2
8081	0.083	141.8
8158	0.121	149.4
8262	0.189	157.0
8389	0.233	164.6
8432	0.233	167.7
8457	0.227	169.2
8475	0.215	170.7
8495	0.206	172.3
8510	0.192	173.8
8525	0.177	175.3
8538	0.160	176.8
8541	0.140	178.4
8535	0.118	179.9
8523	0.104	181.4
8502	0.089	182.9
8481	0.069	184.5
8431	0.032	186.0
8395	0.016	187.5
8395	0.010	189.0
8396	0.005	192.1
8399	0.000	195.1
8401	-0.005	198.2
8404	-0.014	202.8
8406	-0.023	207.3
8409	-0.029	211.9
8410	-0.036	216.5
8412	-0.045	222.6
8414	-0.052	228.7
8415	-0.059	236.3
8416	-0.067	243.9
8416	-0.071	251.5
8416	-0.071	259.2
8416	-0.071	266.8
8416	-0.071	282.0
H-11, Nb-10000 ppm Ta (T=8.169 K)		
7531	-0.111	0.0
7530	-0.111	170.3
7530	-0.111	205.0
7529	-0.111	248.0
7531	-0.111	259.3
7534	-0.110	266.8
7536	-0.110	274.4
7539	-0.109	282.0
7548	-0.106	294.8
7550	-0.107	304.9
7547	-0.108	312.5
7548	-0.108	320.1
7551	-0.108	327.8
7557	-0.108	336.0
7567	-0.106	345.1
7574	-0.103	350.8
7588	-0.100	359.9
7601	-0.096	368.5

Table XII (Continued)

μ'	μ''	H
7616	-0.094	376.1
7630	-0.090	383.3
7663	-0.081	399.3
7713	-0.066	412.4
7749	-0.059	427.2
7787	-0.047	443.0
7827	-0.038	456.7
7859	-0.031	472.0
7888	-0.026	486.2
7916	-0.020	500.3
7945	-0.016	515.6
7975	-0.011	531.7
8003	-0.005	545.9
8048	0.0	563.8
8077	0.009	576.3
8127	0.026	590.4
8196	0.066	605.2
8242	0.094	612.8
8286	0.118	619.1
8304	0.119	625.7
8312	0.107	629.3
8317	0.092	631.9
8327	0.080	635.6
8327	0.062	638.9
8327	0.043	642.0
8328	0.036	645.3
8329	0.033	648.7
8331	0.031	655.2
8335	0.029	664.8
8341	0.026	680.1
8345	0.023	693.8
8352	0.022	711.2
8358	0.020	729.5
8366	0.020	750.8
8374	0.017	773.1
8380	0.013	793.5
8387	0.005	815.3
8390	0.000	833.3
8395	-0.005	852.8
8399	-0.012	872.0
8403	-0.019	892.0
8406	-0.026	912.0
8409	-0.036	933.1
8411	-0.044	953.1
8413	-0.052	974.9
8414	-0.059	993.1
8414	-0.064	1013.0
8415	-0.066	1033.5
8415	-0.066	1060.3
8415	-0.066	1091.5
8415	-0.066	1132.9

H-11, Nb-10000 ppm Ta (T=6.355 K)

μ'	μ''	H
7527	-0.099	0.0
7526	-0.099	610
7526	-0.099	662
7525	-0.099	698
7525	-0.098	732
7526	-0.098	766
7528	-0.095	802
7528	-0.095	838
7528	-0.095	874
7529	-0.095	909
7531	-0.095	942
7534	-0.093	976
7539	-0.091	1009
7542	-0.086	1038
7549	-0.083	1078
7560	-0.076	1111
7570	-0.071	1146
7579	-0.066	1181
7610	-0.048	1247
7630	-0.036	1315
7660	-0.025	1381
7690	-0.012	1447
7710	-0.005	1511
7740	0.000	1576
7760	0.005	1640
7785	0.009	1704
7810	0.011	1767
7845	0.034	1832
7865	0.062	1864
7890	0.098	1896
7905	0.161	1928
1943	0.180	1944
7995	0.225	1960
8115	0.238	1976
8180	0.204	1991

Table XII (Continued)

μ'	μ''	H
8230	0.172	2008
8275	0.154	2026
8290	0.133	2041
8300	0.123	2058
8305	0.119	2073
8310	0.114	2105
8315	0.103	2151
8325	0.093	2213
8330	0.083	2273
8340	0.074	2336
8345	0.071	2398
8355	0.066	2459
8360	0.060	2523
8365	0.054	2584
8375	0.046	2680
8385	0.033	2773
8390	0.025	2872
8395	0.014	2964
8400	-0.005	3063
8402	-0.011	3156
8404	-0.028	3259
8406	-0.040	3357
8408	-0.052	3456
8408	-0.056	3557
8408	-0.056	3659
8408	-0.056	3735
8408	-0.056	3811
8408	-0.056	3887

H-23, Nb-20000 ppm Ta
(T=8.325 K)

μ'	μ''	H
7426	-0.128	0.0
7426	-0.128	100.0
7426	-0.128	150.0
7425	-0.127	175.0
7424	-0.127	200.0
7424	-0.127	210.0
7425	-0.127	220.0
7434	-0.127	230
7448	-0.124	240
7437	-0.125	250
7440	-0.125	260
7469	-0.123	275
7550	-0.104	300
7612	-0.086	325
7670	-0.076	350
7738	-0.064	375
7849	-0.033	400
8008	-0.016	425
8123	0.005	440
8212	0.034	450
8322	0.084	460
8412	0.125	465
8311	0.050	470
8298	0.042	475
8301	0.042	480
8313	0.040	500
8332	0.040	525
8348	0.047	550
8367	0.047	575
8383	0.041	600
8396	0.028	625
8407	0.009	650
8415	-0.012	675
8420	-0.030	700
8425	-0.050	725
8427	-0.066	750
8428	-0.076	775
8428	-0.076	800
8428	-0.076	825
8428	-0.076	875
8426	-0.055	735
8416	-0.020	685
8400	0.017	635
8374	0.040	585
8341	0.040	535
8310	0.040	485
8151	-0.032	435
8053	-0.032	385
7989	-0.023	335
7919	-0.046	285
7887	-0.055	265
7869	-0.060	255
7857	-0.060	245
7855	-0.052	235
7730	-0.062	225
7542	-0.101	215
7457	-0.115	205
7430	-0.125	190

Table XII (Continued)

μ'	μ''	H
7427	-0.128	0.0
7426	-0.128	600
7426	-0.128	656
7426	-0.128	700
7426	-0.128	750
7441	-0.118	800
7432	-0.128	855
7430	-0.125	900
7430	-0.125	950
7434	-0.125	1000
7453	-0.116	1050
7472	-0.105	1100
7486	-0.095	1150
7504	-0.084	1200
7527	-0.074	1300
7566	-0.052	1400
7595	-0.038	1500
7626	-0.028	1600
7661	-0.018	1700
7685	-0.005	1750
7697	0.005	1775
7708	0.024	1800
7725	0.068	1825
7785	0.187	1850
8120	0.164	1875
8160	0.164	1900
8189	0.154	1925
8210	0.150	1950
8245	0.120	2050
8265	0.099	2150
8280	0.088	2250
8295	0.071	2350
8310	0.064	2450
8325	0.058	2550
8340	0.054	2650
8355	0.050	2750
8370	0.040	2850
8385	0.021	2950
8395	0.009	3050
8400	-0.011	3150
8405	-0.032	3250
8410	-0.052	3350
8410	-0.074	3450
8410	-0.076	3550
8410	-0.076	3650
8145	0.101	1860
8105	-0.016	1760
8055	-0.016	1650
7935	-0.028	1294
7905	-0.028	1150
7865	-0.034	1000
7820	-0.026	875
7795	0.0	840
7785	0.020	805
7710	0.052	770
7490	-0.076	735
7429	-0.124	700

APPENDIX II: THE VORTEX LATTICE SPACING AT H_{c1}

Recently Träuble and Essmann (54) have shown the existence of a vortex lattice and triangular vortex domains by a decorating technique. It was originally thought that the triangular vortex network was the result of purely repulsive forces between vortices, but the existence of domains (55,56) and a precipitous drop of the magnetization at H_{c1} (35) are indications that the vortices attract at large distances and repel at close distances. Hence, each vortex may see a potential of the form shown in Figure 47. Neutron diffraction and magnetization measurements (57) have shown that the equilibrium spacing a_o is about 1900 Å for Nb at 4.2 K. Finnemore, Clem, and Stromberg (58) have analyzed the magnetization data of Finnemore et al. (35) to obtain the temperature dependence of the vortex spacing and find that it diverges approximately as $(1-T)^{-1/2}$. Jacobs (59) has stated that in the case of Nb, a low kappa, long mean free path material, a_o should diverge at some temperature less than T_c. The purpose of this experiment was to determine the temperature dependence of a_o more accurately than the previous work, especially in the region of T_c.

The equilibrium spacing a_o as a function of temperature may be obtained from the magnetization curves taken for temperatures between 0 K and T_c. If B_o is the magnetic induction immediately after flux penetration, then

$$a_o = \left[\frac{\phi_o}{B_o \sqrt{3/2}}\right]^{1/2} \tag{61}$$

where ϕ_o is the flux quantum. Figure 48 indicates how B_o is determined for

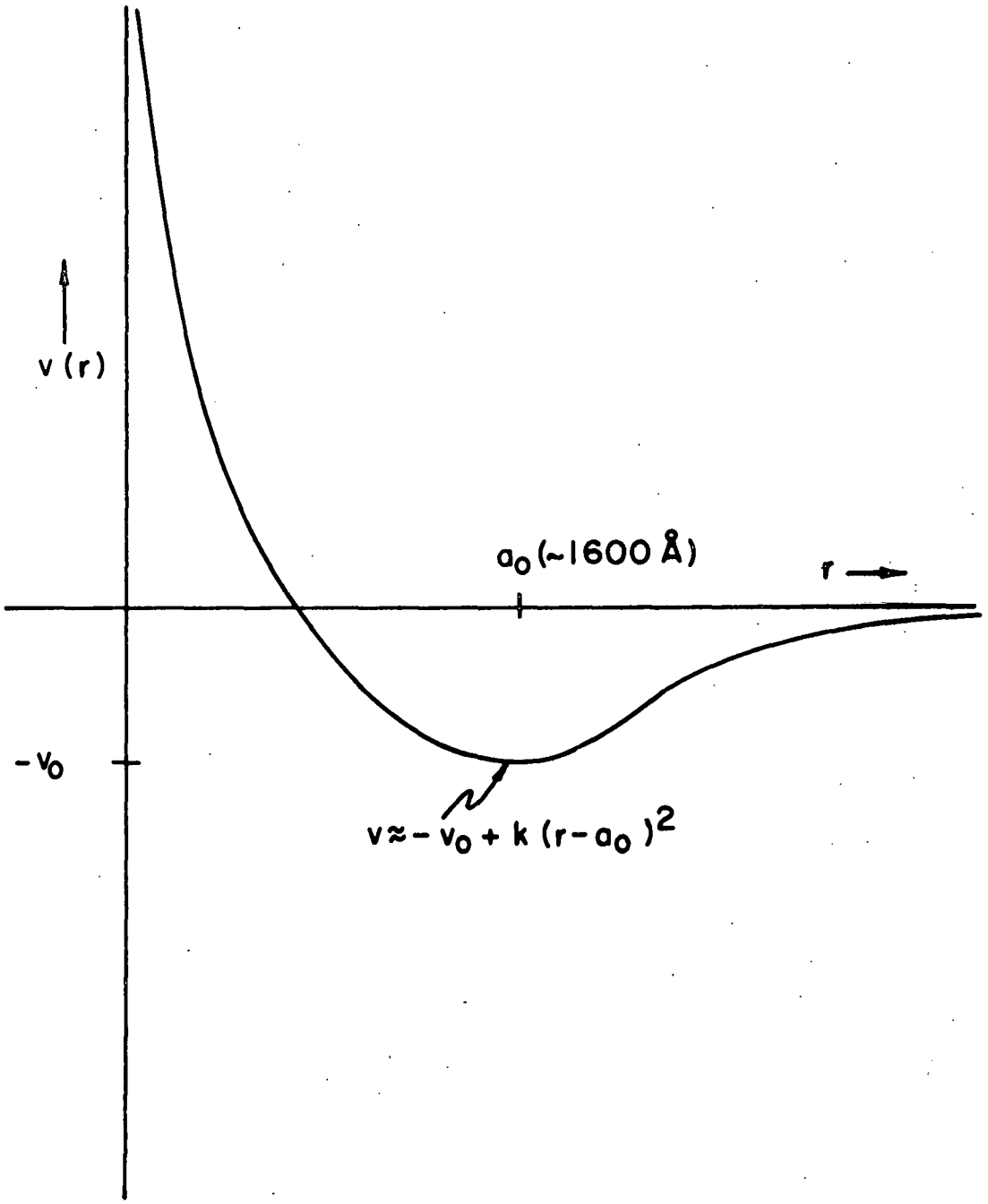

Figure 47. The form of the potential energy of a vortex.

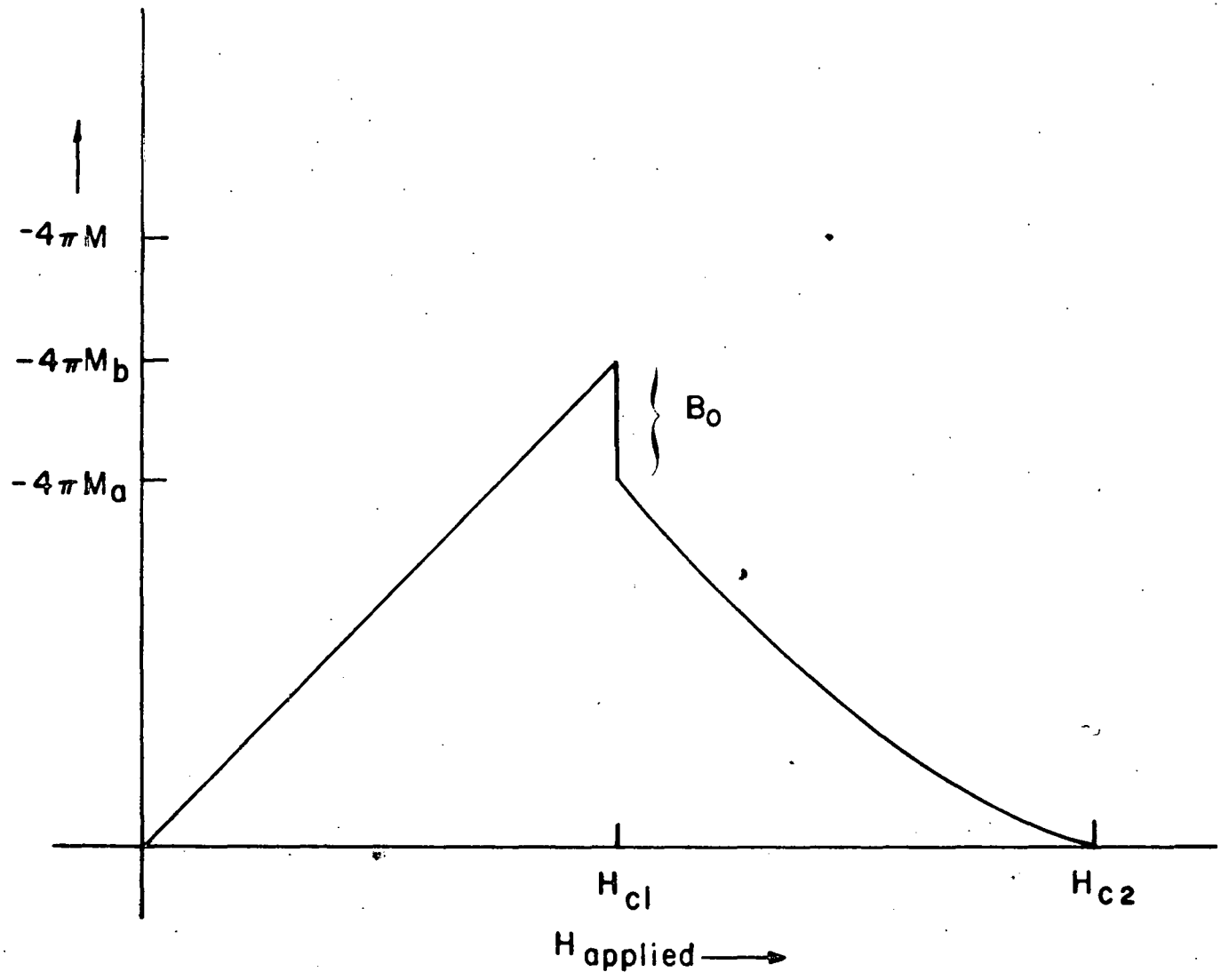

Figure 48. The determination of B_o from a magnetization curve.

one magnetization curve at some arbitrary temperature.

Magnetization curves were obtained for the pure niobium sample, H-9 using the simple experiment arrangement described below. The sample was inserted into the center coil of a compensated, astatically wound, measuring coil (Figure 49). The sample-coil system was suspended inside a double can cryostat originally built by Ostenson (60). For each temperature, H was increased monotonically in stepwise increments and the deflections of the galvanometer, connected in series with astatically wound coils, were recorded. Under those circumstances the galvanometer responded more or less as a fluxmeter. It is not difficult to show that the deflection of the galvanometer (due to the sample) is directly proportional to the change in sample magnetization. It follows that

$$M(H) \propto \sum_{H=0}^{H=H} \text{deflections.} \qquad (62)$$

Due to the fact that the entire cryostat and dewar system were metallic, deflections of the galvanometer were caused which were not related to the magnetization of the sample. These deflections were recorded as background and subtracted from the deflections when the superconducting sample was being studied. Unfortunately, the background deflections were sometimes larger than the deflections due to the sample (that is, the signal to noise ratio was less than one) and were not reproducible.

Although no attempt was made to correct the discrepancies in this magnetization work so that quantitative results could be obtained, the data do indicate, at least qualitatively, that the vortex lattice spacing increases with increasing temperature since B_o decreases as T approaches T_c

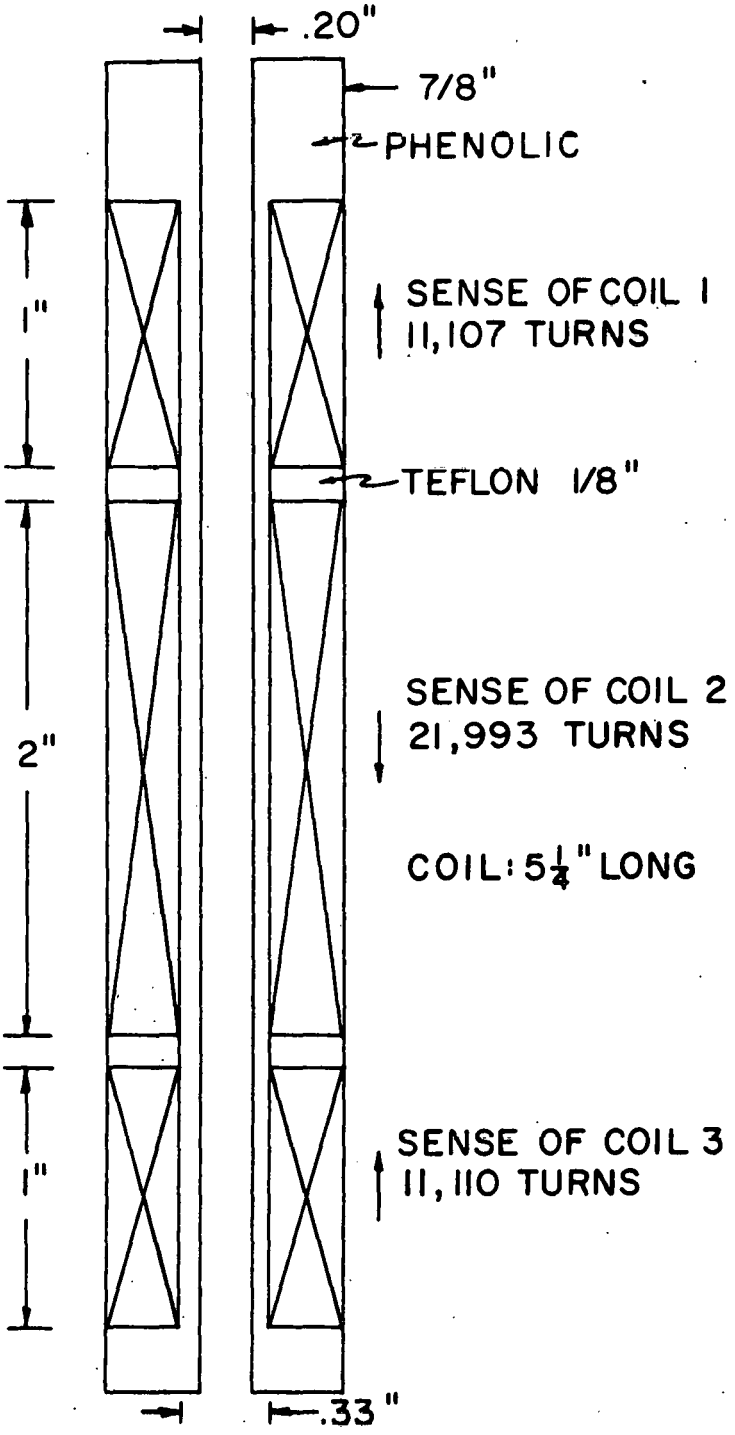

Figure 49. The coil used for the magnetization measurements.

(Figure 50). The data obtained here are in general agreement with the data obtained by Finnemore et al. (35,58). Plans are currently underway (61) to take the same type of measurements described here in a magnetically clean system to determine whether a_o diverges at some temperature less than T_c as postulated by Jacobs (59).

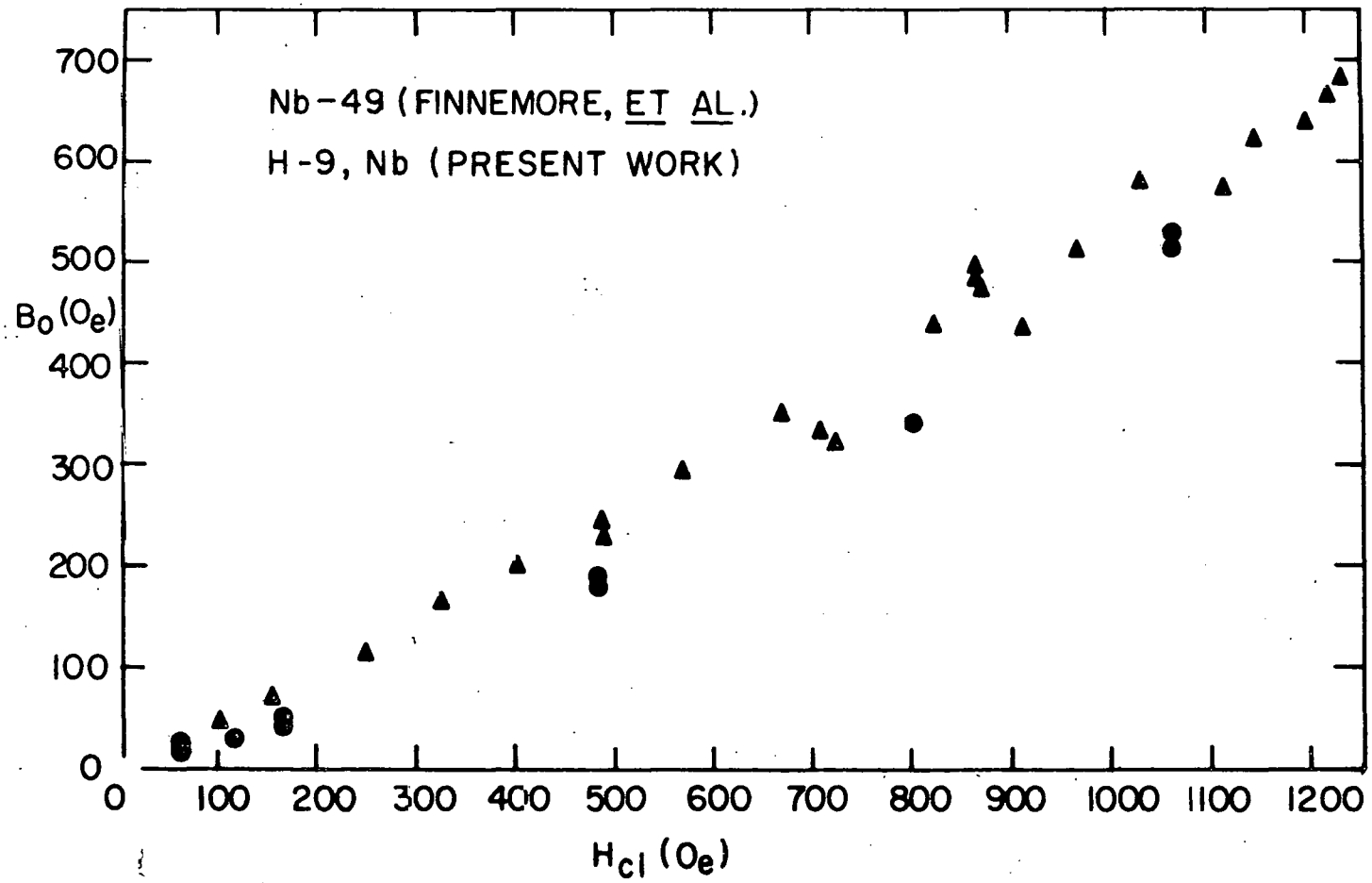

Figure 50. A plot of B_o versus H_{cl} for pure niobium.